The Detection of Local Overheating in

LIQUID METAL COOLED FAST NEUTRON REACTORS

T. J. LEDWIDGE

C.Eng., B.Sc., M.I.E.E., A.Inst.P.

A Thesis submitted to the University Aston in Birmingham
for the Degree of Doctor of Philosophy

July 1969

SUMMARY

This thesis presents a theoretical and experimental study of special instrumentation systems proposed for the protection of sodium cooled fast neutron reactors.

The growth and future potential of the fast reactor project is reviewed and the reasons why its protection represents a special instrumentation problem outlined.

Various possible methods by which mal-function may be detected are examined. One such method, namely the detection and recognition of acoustic noise in a sodium cooled nuclear environment is believed to be have been originated by the author. The development of these systems has necessitated the introduction of novel means of detecting signals from the reactor environment.

A large experimental programme was carried out to assess the transducers and collate the information produced during simulated fault conditions. This investigation included both "out of pile" and "in pile" experiments, electrical heaters being used to simulate nuclear heating. The "in pile" experiment was carried out in the Dounreay Fast Reactor

As a result of this programme a system was designed for the D.F.R.

The design of such a system takes into account the theory of the measurement and correlation of random noise. Theoretical and experimental work is presented which examines the conditions to be satisfied in order that spectral correlation analysis is statistically significant.

The prototype system has operated successfully in the D.F.R. for a few months and two recent non-crucial failures of experimental nuclear fuel elements tend to validate the system in that the installed instrumentation detected and correctly identified the source of the mal-function.

ACKNOWLEDGEMENTS

The author would like to thank the United Kingdom Atomic Energy Authority and particularly the Management of the Dounreay Establishment for providing the necessary facilities enabling the work described in this thesis to be carried out.

Grateful thanks are due to Dr. D. Karo, formally Reader and now Advisor in the department of electrical engineering, University of Aston in Birmingham for suggesting the possibility of pursuing a course of research for a higher degree, and encouragement during the course of the research.

To Mr. A.E. Noble who acted as the University Supervisor in the later stages of the work acknowledgement is due.

Mr. F.J. Barclay, Project Manager of the Dounreay Fast Breeder Reactor provided a continuous stimulus as the External Supervisor during the whole course of this work, the author would particularly acknowledge the help and guidance received from this source.

Many colleagues in the Engineering Development Group at the Dounreay Establishment contributed significantly by helpful discussion and criticism. Although too numerous to mention individually the author's thanks to them is no less sincere.

CONTENTS

CHAPTER 1

INTRODUCTION

1.1 An Appreciation of the Current State of Nuclear Power Development

The genesis of a nuclear power programme, whatever its detailed technical features, is dependent upon the existence in uranium of 0.7% of the only naturally occurring fissile isotope 235 U. Natural uranium is used directly in graphite or heavy water moderated thermal neutron reactors. Alternatively, if a diffusion plant is available, thermal reactors using enriched uranium can be designed which, at the cost of the diffusion operation, impose less onerous restriction upon the use of neutron absorbing materials, having desirable properties such as high temperature strength and corrosion resistance.

The economic importance of conserving natural uranium depends upon its price as determined by demand and supply, that is by the size of the nuclear power programme and the cost of mining and refining known deposits of ore.

The pressure of a nuclear power programme on uranium supplies is a function of the combined nuclear and thermal performance of the reactors, and of the efficiency of the diffusion and fuel reprocessing plants (if used).

The cost of electricity is additionally affected by reactor development cost, capital cost, flexibility of siting as influenced by safety characteristics, and time of construction as influenced by simplicity of arrangement and the like.

Thermal neutron reactors are classified as converters. 238 U is converted in them to fissile 239 Pu. The neutron economy is such that fewer plutonium atoms are produced than are uranium atoms fissioned. The newer forms of thermal neutron reactor are known as "advanced converters". "Advanced" may imply technical features such as improved neutron economy, better thermodynamics, lower capital cost and so forth;

it should, and ultimately must, mean an effective combination of these technical features resulting in lower cost electrical energy.

In fast neutron reactors, the neutron economy is superior and it is both possible and economic to breed plutonium. If as is widely expected cheaper electricity becomes available from fast breeders than from competing systems, the satisfaction will have been obtained of conserving natural uranium supplies, and of ensuring both short and long term supplies of cheap energy.

Fast neutron reactor cores must however be primed with large (relative to thermal reactors) quantities of fissile material. Since in equilibrium operation fast reactors will eventually supply themselves with self generated plutonium it is natural to consider starting with plutonium generated in thermal reactors. The technically feasible alternative of priming the fast reactors with 235 U turns out to be economically unattractive. The fast breeder and thermal convertor therefore, constitute an interdependent dual system.

Surveys (1.1, 1.2, 1.3, 1.4) of the overall possibilities in nuclear power development tend to produce curves of the type shown in Figure 1.1. A judgement is made of the result of competition between nuclear fuels, fossil fuels, and hydroelectric resources and an estimate arrived at of the likely size of nuclear power programme. It is assumed that fast reactors achieve the lowest cost of energy production, which is moreover minimally dependent on fluctuations in uranium price, and that the converter reactors are used as dual product plants making electricity for immediate use and plutonium to prime fast reactors under construction. The fast reactors eventually become self supporting and the use of thermal converters declines.

A version of Figure 1.1 applying to the world as a whole might be Figure 1.2. This diagram is intended, not as a forecast, but to show the exuberance and variety of the competition for a share in the market for converter reactors.

In the United Kingdom the thermal converter programme has been based on the Calder Hall type of reactor, and will be based in the future on the Windscale Advanced Gas Cooled Reactor.

The O.E.C.D. Dragon Reactor Experiment and the Steam Generating Heavy Water Reactor are alternative systems which may in the longer term, play a part in the United Kingdom thermal reactor programme.

A major part of the United Kingdom effort is being applied to the development of the sodium cooled fast breeder reactor. The Dounreay Fast Reactor is supporting a major irradiation programme which will provide tried and tested fuel sub-assemblies to make up the core of the Prototype Fast Reactor, now under construction at Dounreay. The same irradiation programme is yielding invaluable information and results to the designers of converter reactors, at a rate which cannot be rivalled by materials testing reactors employing thermal neutrons.

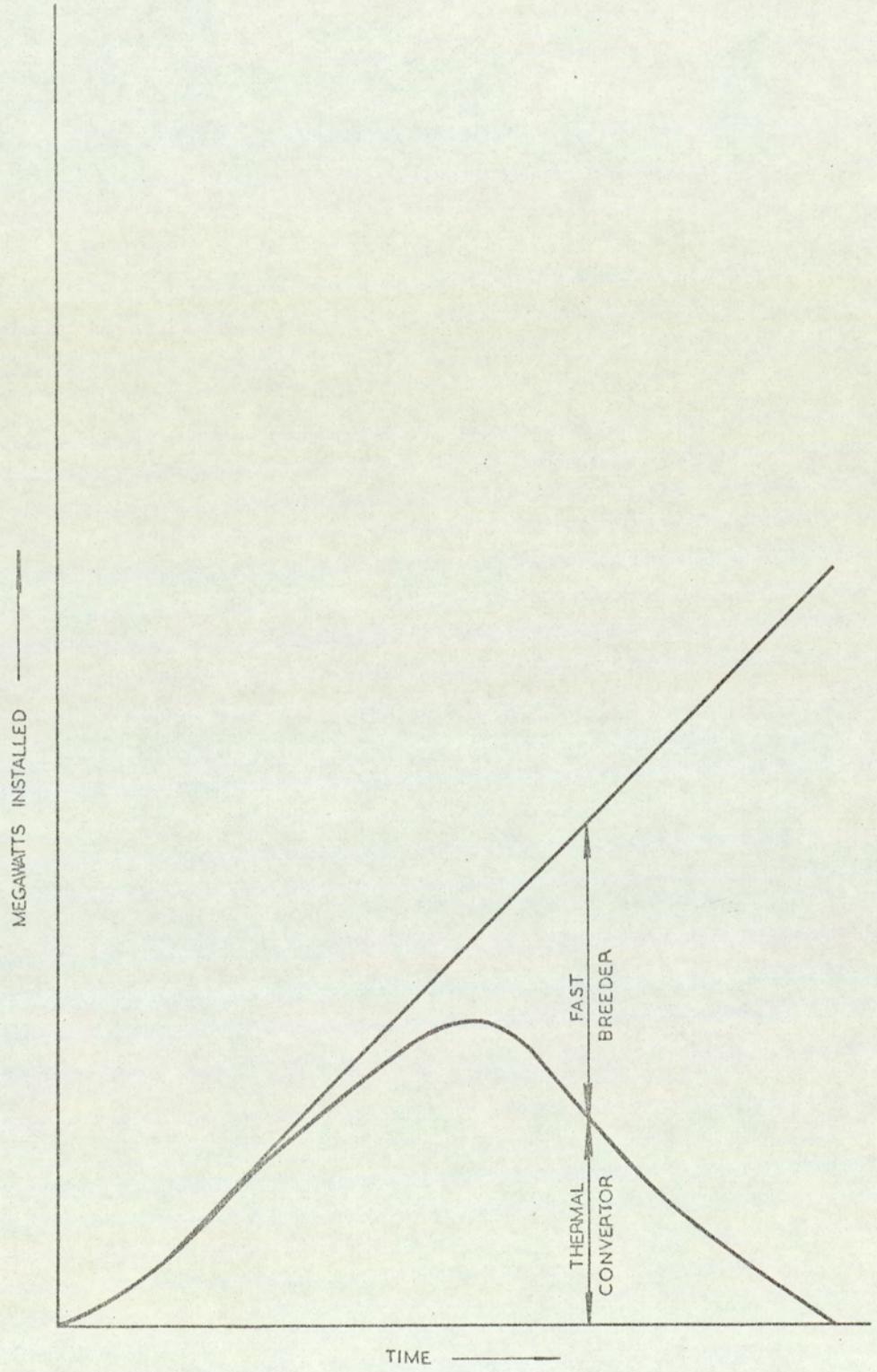

FIG. 1·1 NUCLEAR POWER PROGRAMME OF BREEDERS AND CONVERTORS.

FIG. 1·1.

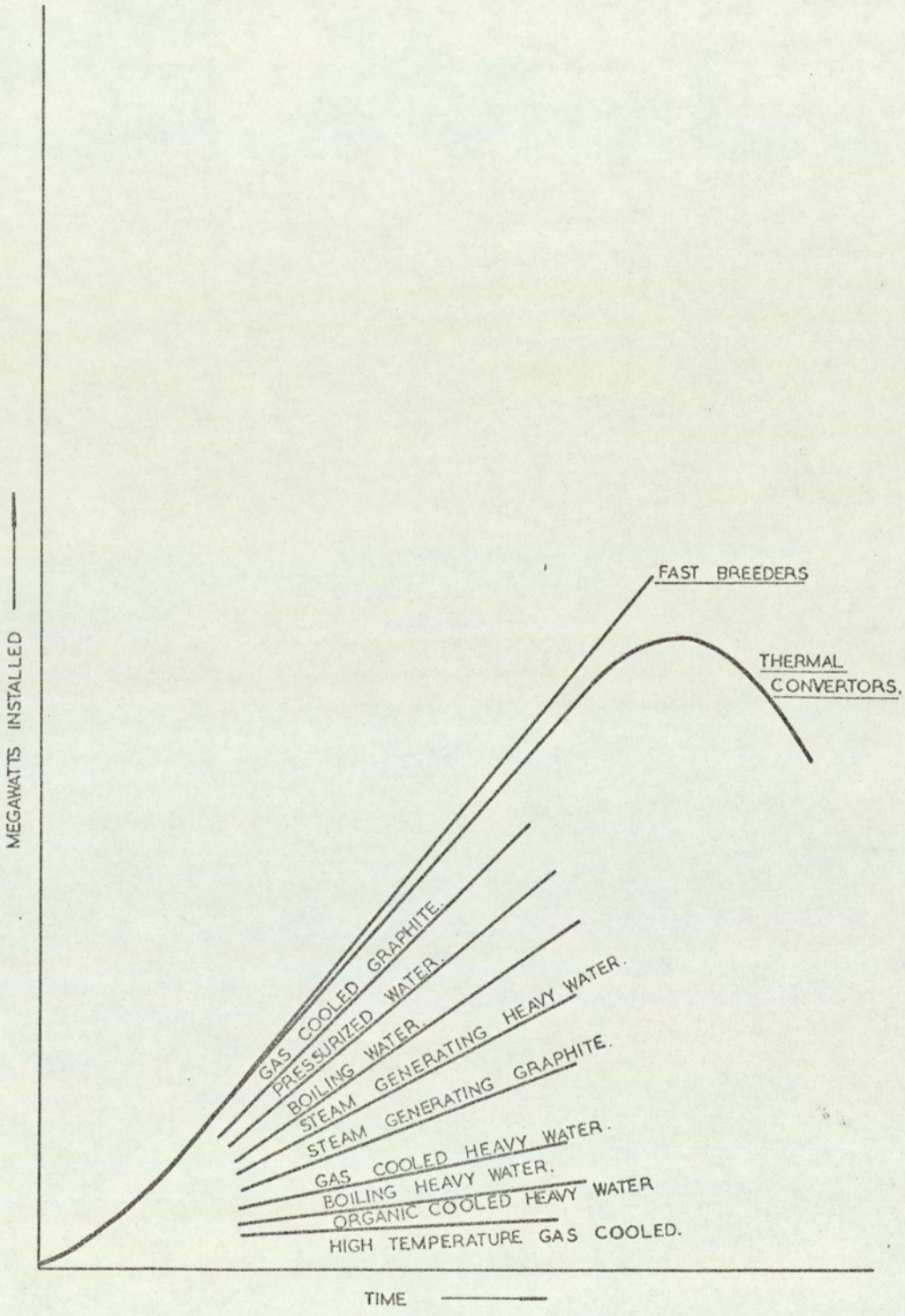

FIG. 1·2 CONSTITUENTS OF THE WORLD NUCLEAR POWER PROGRAMME.

FIG 1·2

CHAPTER 2

DESCRIPTION OF THE UNDERLYING FLUID MECHANICAL PHENOMENA IN LIQUID COOLANTS

2.1 General

Fast reactor cores as envisaged at present will consist of a compact array of closely spaced fuel rod assemblies in wrappers and it is thought that such cores by virtue of their geometry and high power density are, in the absence of precautions not specified herein, especially susceptible to disturbances caused by solid or gaseous matter leading to coolant boiling and then some form of hydrodynamic instability. The underlying fluid mechanical problem is not dissimilar to that found in any equipment in which heat is being put into a number of channels operating in parallel. Reference to the relative power densities in Table 2.1 which compares the power per unit volume in the currently operating and proposed reactor systems, shows that the fast reactor, because of its high fuel inventory, requires for economic performance a very high power density. Hence any overheating is likely to develop on a fast timescale, and a suitable means should be found of detecting quickly mal-operation of such fast reactor cores.

TABLE 2.1

Some comparisons between an advanced thermal reactor and a typical fast reactor design

	Advanced thermal Reactor	Fast Reactor
Specific Power kW/kg	9.5	142
Reactor Power MW	1500	600
Core Volume m^3	500	1
Power density MW/m^3	3	600

There are several possible modes of failure and it is not important to discuss these in detail here. It is sufficient to say that all involve partial or complete flow blockage between pins. This blockage may be caused by solid matter or, more likely in a practical system, by gaseous matter either being released from failed fuel pins or carried into the heat transfer region by the liquid metal coolant. It is fairly clear that if the liquid metal flow, which is taking the heat away from the fuel pins, is either reduced in velocity or replaced by gas then serious temperature excursions both of the fuel pin and the remaining low velocity coolant will occur. Due to the turbulent mixing of the fluid from the exit from the fuel channels it is in principle possible to suggest that such disturbances may be detected by observing the fluctuations in temperature, which we will call temperature noise, at the outlet of such channels and clearly this could well be the first early warning system which we propose to investigate. If, however, we assume that the process proceeds without interruption then at some stage in the development coolant boiling will occur.

2.2 Pressure Drop Characteristics of Heated Channels and Related Parallel Channel Problems including Sonic Effects

It can be said of the majority of operating reactors that their installed safety systems have never been called upon to protect the reactor against an uncontrolled departure from intended conditions. Neverthless, in the interest of ultimate safety, a great deal of effort is expended on analysing the behaviour of reactor cores in accident conditions.

A reactor core consists, almost inevitably, of a multiplicity of parallel channels through which coolant is forced by a common pressure drop. The number of channels is large, and accordingly flow failure in one channel has a negligible effect on core pressure drop.

In a heated, liquid cooled channel, reduction of flow at constant heat input leads to a pressure drop characteristic of the type shown in Figure 2.1. If an accidental flow reduction occurs in a channel operating at design point A, an alternative 'stable' operating condition B may be

reached, in which the flow of boiling liquid gives rise to a pressure drop equal to that obtained with a much higher flow of sub-cooled liquid. The word 'stable' has been used in a restricted hydrodynamic sense and certainly in a sodium cooled reactor the fuel containment condition at 'B' would be intolerable.

The speed at which events would move in changes proceeding from A towards B has occupied the attention of many investigators and attention has focussed, interalia, on the velocity of sound in two phase mixtures, which may set a limit to the speed of ejection of boiling fluid from a parallel sided channel.

The author has with others (2.1) measured the speed of transmission in an air water mixture of a mild shock due to the rupture of a metal diaphragm and has obtained the values plotted on Figure 2.2.

A simple theory for air/water gives the curve on Figure 2.2. The low velocities obtained are qualitatively explicable, in that, in an incompressible fluid, the velocity of sound would be infinite. If compressible voids are introduced into a nearly incompressible liquid the effect is likely to be dramatic, as the curves indeed show.

In France the quantity of gas entrained in flowing sodium has been deduced (2.2) by measuring the velocity of sound in the mixture.

In a boiling liquid the transmission is rendered complex by the possibility of bubble condensation. The condensation of water vapour bubbles by a pressure shock has been demonstrated experimentally in the United States by Karplus (2.3). Whereas sound transmission is usually taken to be isentropic it is clear that waves of significant amplitude in a vaporising liquid are transmitted by a process which is more nearly isothermal than isentropic.

2.3 Nucleate Boiling in Liquid Cooled Reactors

The boiling of a liquid around a heated surface can best be understood by referring to what is known as a boiling curve Figure 2.3 shows heat flux plotted against excess temperature Δt (temperature difference

surface to bulk liquid). In the initial stages of the curve the predominant mode of heat removal is natural convection. As Δt increases a superheated layer forms around the heater and ultimately small vapour bubbles form at nucleation points or sites in the heated surface. As the wall temperature further increases the bubbles break away and a steady output of vapour bubbles streams into the bulk liquid. This section of bulk curve is known as the nucleate boiling regime. As the heat flux is still further increased the frequency of bubble production from nucleation sites increases as also does the number of nucleation sites until finally the rate of bubble production is so large that bubble coalescence takes place resulting in the formation of a vapour film. This point is called the departure from nucleate boiling and for practical purposes is synonymous with burn up. The predominant heat transfer is by radiation and with most metal heater materials the temperature of heater rises to above the melting point.

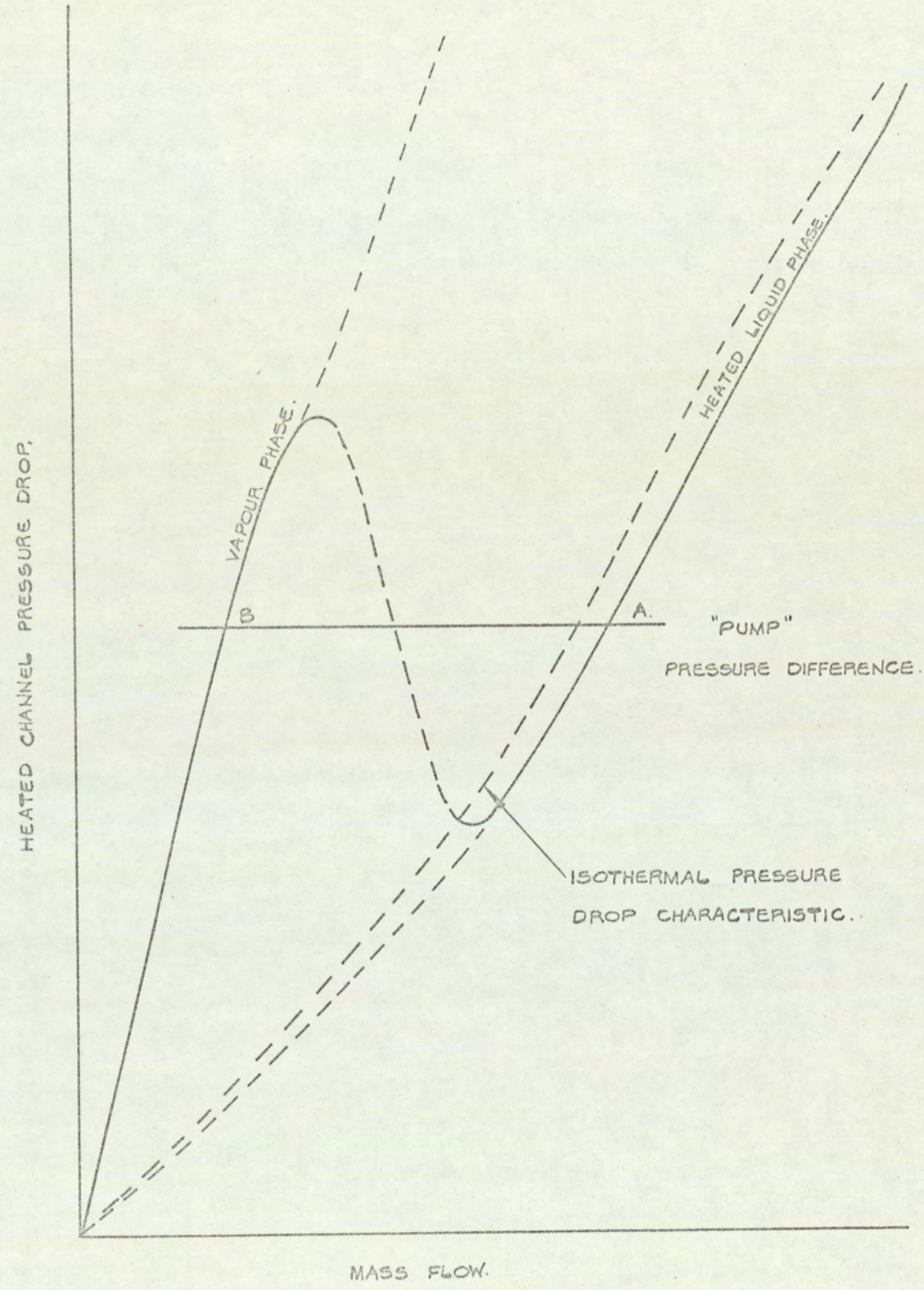

FIG 2·1 HEATER CHANNEL PRESSURE DROP CHARACTERISTIC.

FIG 2·1

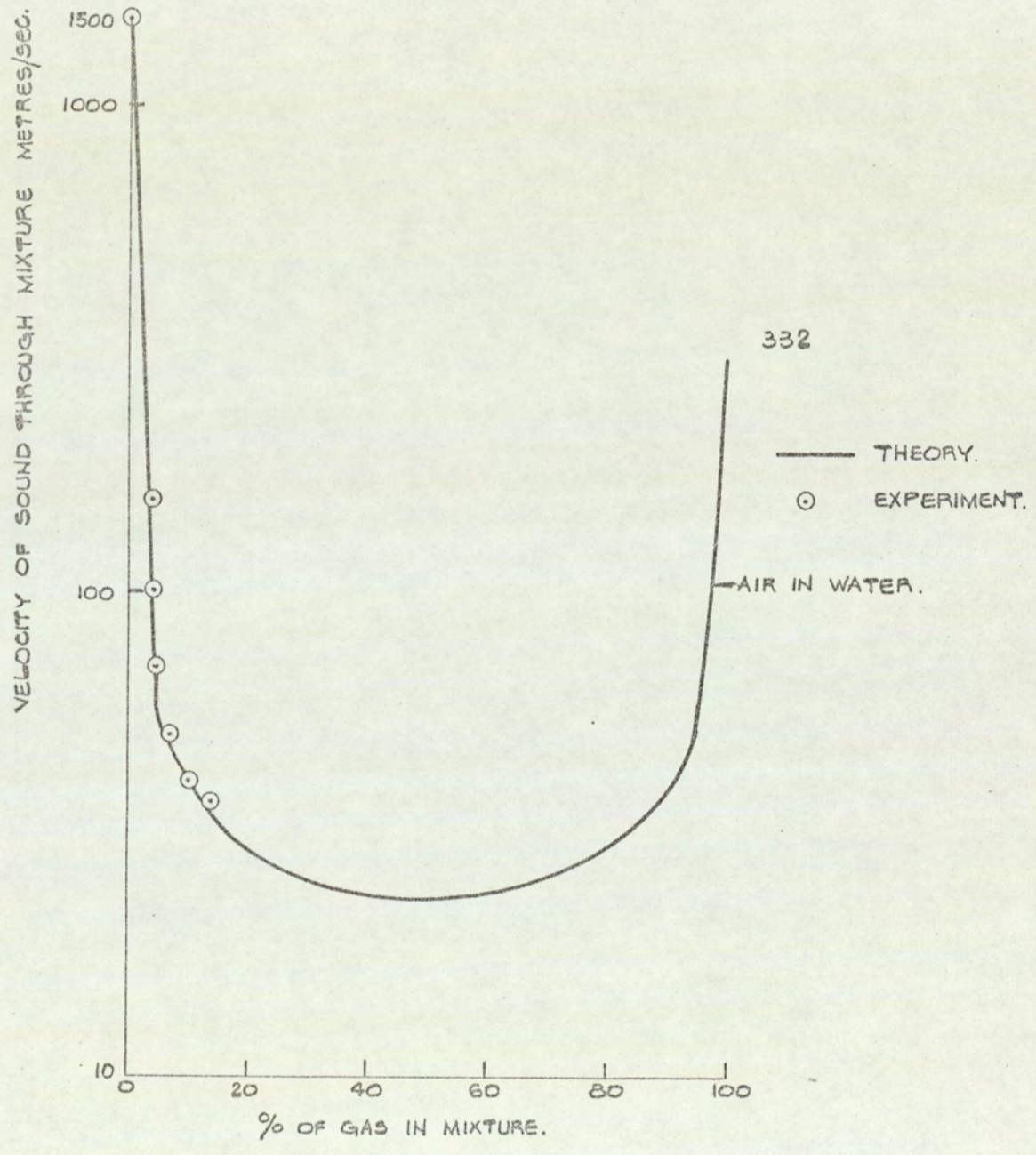

FIG. 2·2 VELOCITY OF SOUND IN A GAS—LIQUID MIXTURE.

FIG 2·2

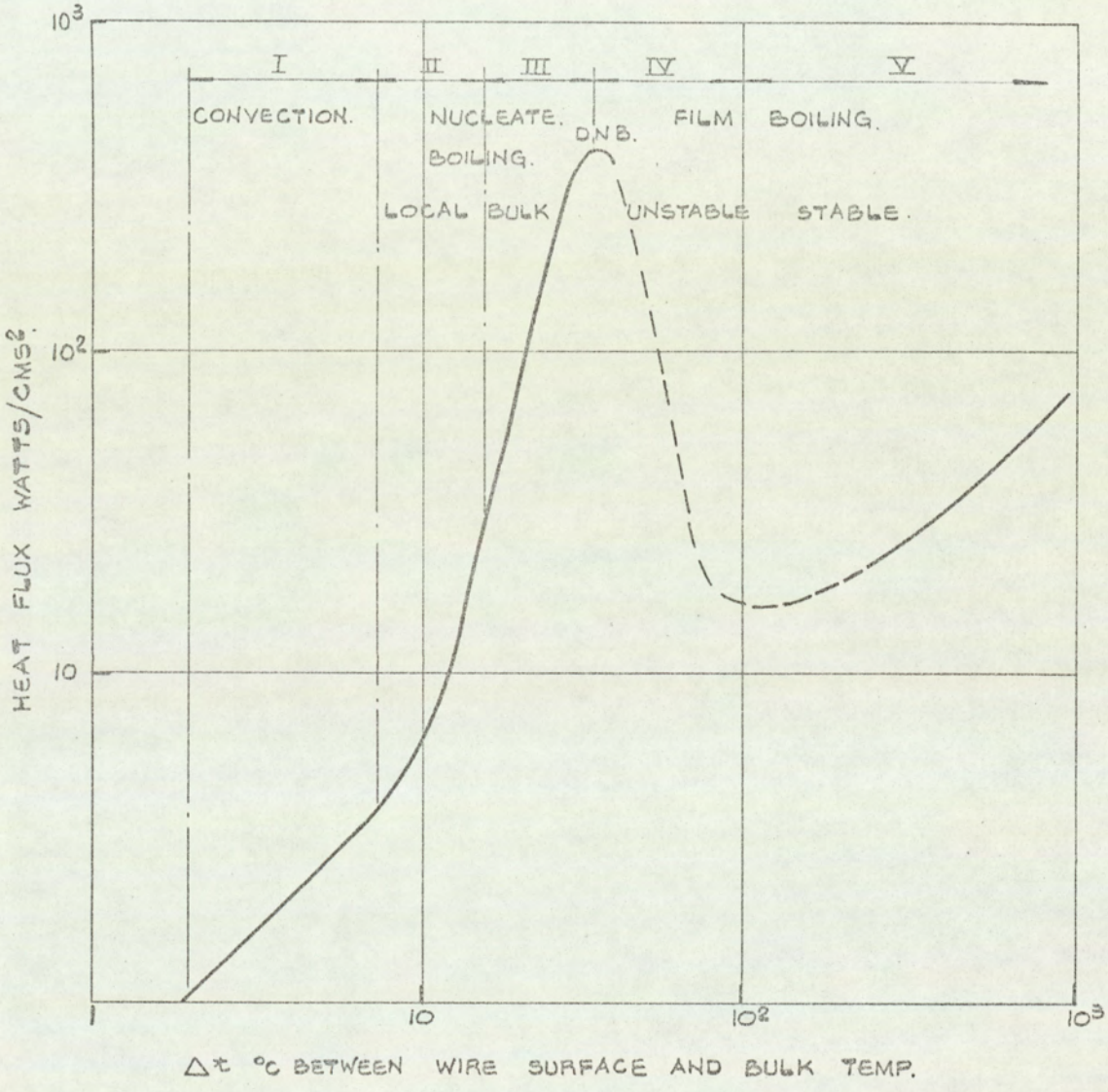

FIG 2·3 BOILING FROM A HORIZONTAL PLATINUM WIRE IN WATER.

FIG 2·3

2.4 Onset of Nucleate Boiling in a Liquid

The temperature of a heated surface producing nucleate boiling bubbles must be in excess of the normal saturation temperature corresponding to the static pressure at the surface. Simple equilibrium theory for the growth of a spherical bubbles radius r, shows that the surface temperature is given by:

$$\theta_w = \frac{\lambda/G}{\log k/ \left(P + \frac{2\sigma}{r} - Pa\right)} \qquad (1)$$

where λ is the latent heat of vapourisation, G the gas constant, P the imposed static pressure, σ the surface tension at the bubble interface and Pa the partial pressure due to dissolved gas in the liquid. k is a constant in the Clausius Clapeyron equation. The normal saturation temperature is given by:

$$\theta \text{ sat} = \frac{\lambda/G}{\log k/P} \qquad (2)$$

The difference between (1) and (2) is termed the superheat necessary to initiate nucleate boiling.

In practice the bubble radius r and the pressure due to dissolved gas will be unknown. However, estimates may be made covering dissolved gas contents between zero and the saturation value of about 0.1 p.p.m. for argon in sodium.

In the experiments described in this thesis, (Chapter 5),it was decided to try to model reactor boiling conditions as closely as possible. To this end indirectly heated standard fuel tube was used as the boiling surface. The first series of experiments was carried out using a horizontal tube configuration, as shown in Figure 2.4. The pin was welded into adaptors in the vessel wall. On several occasions when high values of superheat were present the temperature gradient was such that these welds acted as nucleation points. This fact was established as the wall temperature of the pin did not fall to saturation temperature when boiling

began. For the second series of experiments the rig was designed so that no welds, or rough surfaces, existed to act as nucleation points. It was necessary therefore to have a vertical tube configuration as shown in Figure 2.5. The cover gas used for both experiments was argon.

Claxton (2.4) has argued that nuclear radiations are unlikely to induce nucleation at pressures near one atmosphere. It is suggested therefore that the acoustic behaviour of boiling sodium in reactor conditions can be inferred from these experiments.

2.5 Differences Between Water and Sodium

The equations above show that the necessary superheat for the initiation of nucleate boiling in sodium is much higher than that required in water for the same bubble size and partial pressure of the dissolved gas. As the solubility of argon is very much lower than that of air in water this intrinsic difference is likely to be amplified.

Mathematical models exist (see section 3.5) which attempt to analyse the growth of a bubble in a superheated layer of liquid and its subsequent collapse in a sub-cooled region. These models, which take into account both heat transfer and hydrodynamic effects, predict that water bubble growth is heat transfer limited whilst sodium bubble growth is inertia limited. During collapse both are inertia limited at large subcooling, the final collapse being "cushioned" by the non-condensible gas within the bubble. Reduced cushioning is likely in a sodium system due to relatively low gas solubility and hence higher frequency acoustic signals are to be expected.

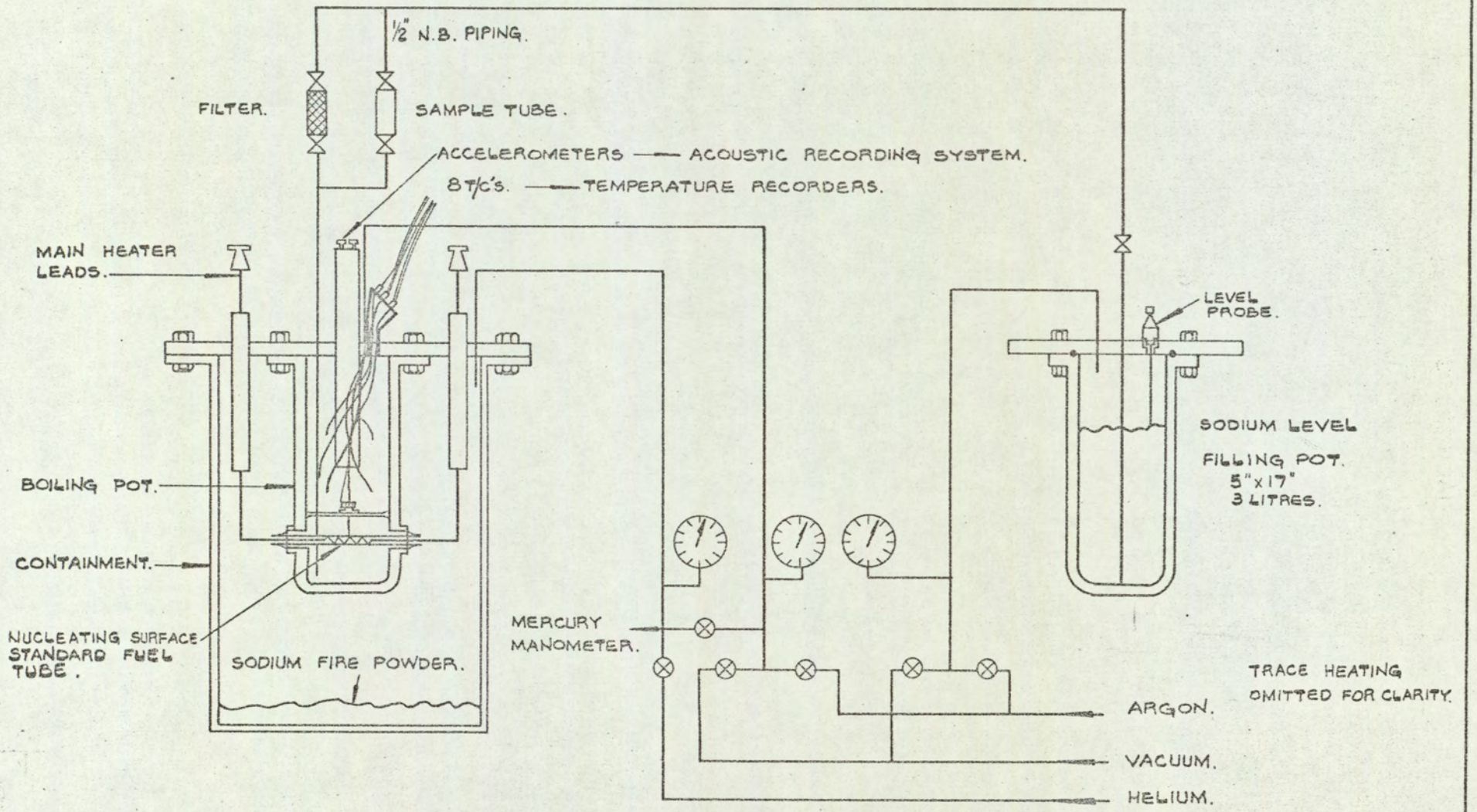

FIG. 2.4 SODIUM BOILING TEST RIG — HORIZONTAL

FIG. 2.4.

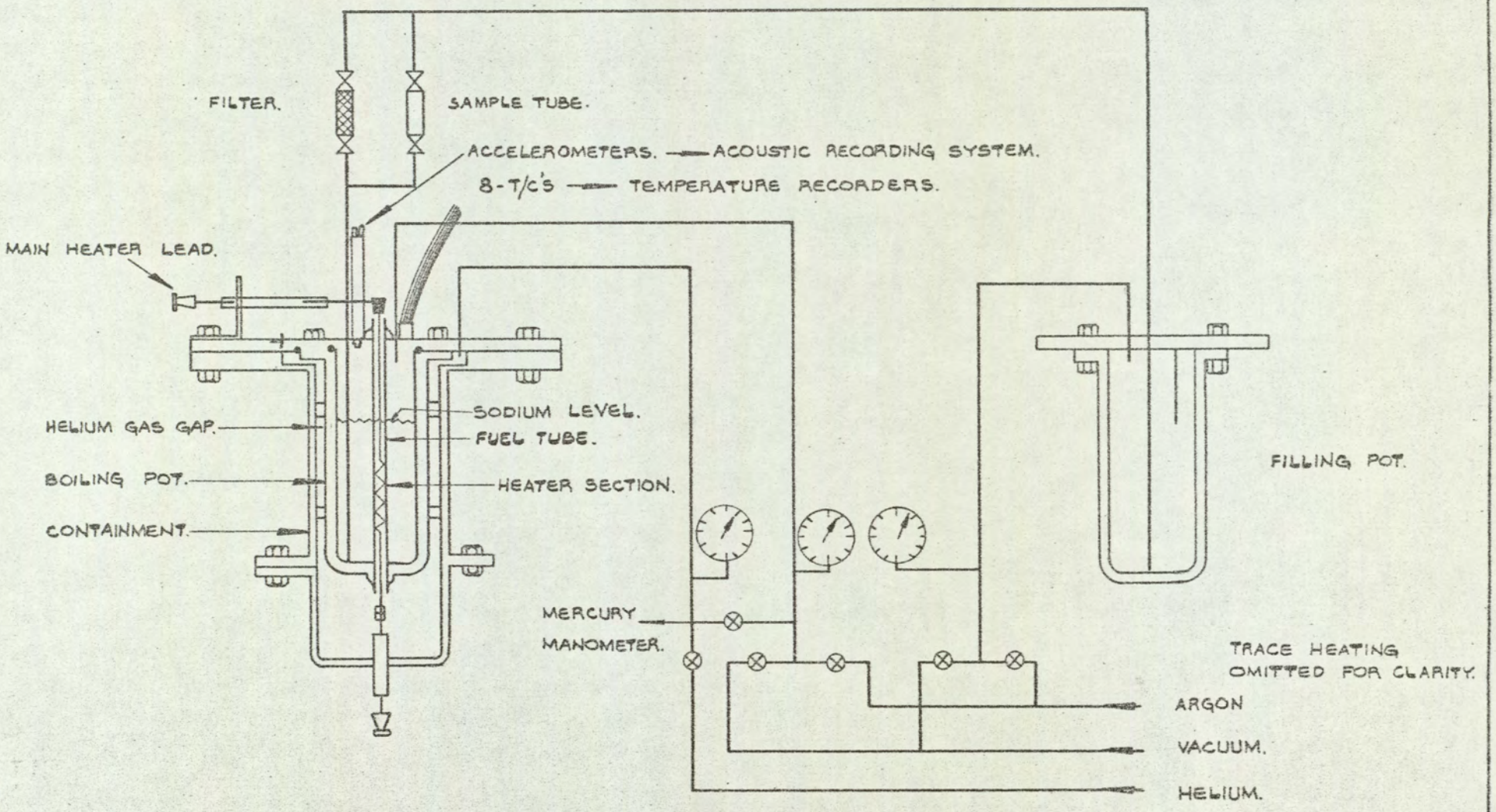

FIG. 2-5 SODIUM BOILING TEST RIG — VERTICAL PIN.

FIG. 2.5

CHAPTER 3

THE CENTRAL PROBLEM OF DETECTING LOCAL OVERHEATING

3.1 Core Instrumentation

The instrumentation of a reactor core is required to show that the power output of the core is being safely removed by the heat transfer system when operating at design conditions and to detect deviations from normal. Departures from intended power level are normally detected by neutron flux monitoring ion chambers. Departures from specified operating conditions of the heat transfer system are relatively difficult to detect because the total flow and average outlet temperature of the reactor are insensitive to local high temperature (local blockage). In any economical reactor design the expensive core must be exploited at high power density. It is impractical to measure the flow and temperature distribution within the compact fuel assemblies and it is necessary therefore to develop alternative detection schemes which will give prompt warning of local fault conditions. If possible this instrumentation should be capable of giving location as well as detection of fault conditions. The large and expensive fissile inventory in a fast reactor results in economic power densities much higher than in thermal reactors. Local flow stagnation is therefore particularly damaging and although filters are incorporated which make blockage with solid material most unlikely its detection is nevertheless important. However gaseous impurities are much more difficult to eliminate and cause pressure drop effects and local reduction in heat transfer.

3.2 Some possible ways of detecting local failure are measurement of Local Flow Velocities in as Many Positions as Possible.

Bearing in mind the environment in which such measurements would have to be made this seems a most difficult line to follow. It would rely on the development of miniature flowmeters capable of operating in high neutron fluxes under liquid sodium at temperatures round about

600°C. The leads to such instruments would be a gross impediment to flow. It is thought that the technological difficulties of such a development are such as to make any investigation along this line quite fruitless.

3.3 Temperature Fluctuations as a Fault Detector

A system which may give a warning before boiling occurs is the detection of the so-called thermal noise (temperature fluctuations) in the coolant stream. The coolant issuing from a sub-assembly containing a blockage will be to some degree stratified into hot and cool streams. At an optimum distance from the exit mixing will result in temperature fluctuations of maximum amplitude. Since the temperature distribution in a healthy element is non-uniform, there will be a steady noise background, relative to which a change must be detected. There is no published information on the existance of temperature fluctuations at relatively high frequencies, above a few Hz, in sodium. In fact very little has been published on the application of random noise analysis to turbulent heat transfer. Corrsin (3.1) initially treated the decay of isotropic temperature fluctuations in isotropic flow and later developed expressions for the spectrum of temperature fluctuations.

A more detailed analysis of the spectrum of convected quantities in low conductivity fluids was carried out by Batchelor (3.2) and by Batchelor, Howells and Townsend (3.3) for large conductivity fluids.

Previous experimental work on the measurement of the space and time dependance of the statistical properties of temperature fluctuations has been limited to work on fluids such as air, water, mercury, ethylene glycol. Tanimoto and Hanratty (3.4) used a modified anemometer to measure temperature fluctuations in a pipe containing turbulent flowing air.

Rust and Sesonske (3.5) investigated experimentally the turbulent temperature fluctuations in mercury and ethylene glycol in a pipe.

They used a fast response thermocouple having a time constant of the order of 10^{-4} secs to measure the fluctuations in a 0.925 inch diameter pipe. The results showed the thermal mixing lengths compared well with the Von Kármáns theoretical predictions. The spectral density results show the existance of measurable fluctuations up to several hundred Hz. The shape of the spectrum follows only partially the theoretical shape predicted by Corrsin and Batchelor. This agreement holds in the region 20 to 60 Hz above which the experimental spectrum falls off much less rapidly than predicted by theory. The authors regard this evidence as tentative and can not be taken as validating the theory.

Further experimental work on the same problem was carried out by Bobkov, Ibragimov and Subbotin (3.6) using water and mercury. Again rapid response thermocouples were used, the outputs of which were amplified with a band pass of 0.15 to 300 Hz. The resulting empirical formula they propose is $f_{max} = \frac{Re^{0.8}\ Pr^{\frac{1}{2}}}{80}$. It is not clear however what is meant by the expression "maximum pulsation frequency".

Temperature measurement in sodium cooled reactors is by mineral insulated chromel-alumel thermocouples sheathed in stainless steel. These are rugged and corrosion resistant, and have adequate sensitivity and response time for normal temperature measurement. When such couples are applied to the detection of thermal noise the band width is limited to below about 1 Hz. In an attempt to increase the effective band width of the noise sensor, work was carried out (see 4.3.b) by the author and colleagues on the development of an eddy current probe. In this probe changes in the impedance of an encapsulated inductance reflect instantaneously resistivity changes corresponding to fluctuations in the coolant temperature. The difficulty is to provide electrical insulation adequate for high temperature in a radiation field.

3.4 Measurement of the acoustic noise produced by bubbles during the nucleate boiling stage.

Vibrating bubbles as a sound source

Gas bubbles in a liquid can under certain circumstances be sources of large amounts of sound energy. The sound of air bubbles formed at a nozzle was first investigated experimentally in 1933 by Minnaert (3.7). He showed that the sound of an oscillating bubble was essentially due to volume pulsations and that it behaved like a simple second order damped system. The frequency of oscillation in this simple mode is given by

$$f_o = \frac{1}{2\pi r}\sqrt{\frac{3\gamma P}{\rho}} \qquad (1)$$

In general however a bubble may oscillate in a variety of modes and it was not until 1956 that Strasberg (3.8) calculated the sound pressure radiated from a bubble oscillating in a number of different modes. It is shown quite clearly in this paper that the only mode of practical importance is the one observed previously by Minnaert, the next highest mode being a factor of 10^6 down in radiated pressure. Some of the various oscillations together with the frequency of oscillation are shown in figure 3.1. It is postulated that a vapour bubble that is produced in the super-heated layer during nucleate boiling will behave in a very similar manner to a gas bubble, in that condensation and evaporation of the vapour in the bubble will be eliminated as long as the bubble remains in the super heat layer.

3.5 Collapsing bubbles as a sound source *

"In recent years, considerable attention has been given to the problem of the growth and collapse of vapour bubbles in a liquid. This has arisen from considerations of nucleate boiling, cavitation damage, and two phase flow phenomena, such as flashing flow in desalination plants (3.9). The problem is extremely intractable, but a great deal of literature now exists on the subject. For a survey of the analytical aspects of vapour

* abstracted from an internal report by G.C. CORNFIELD

bubble dynamics, the reader is referred to the paper by Din-Yu Hsien (3.10). Detailed theoretical treatments, including numerical results, on the growth and collapse of a vapour bubble are given by Zwick and Plesset (3.11), Ivany and Hammitt (3.12) and Florschuety and Chao (3.13). The paper by Florschuety and Chao (3.13) also includes useful experimental data. These papers all contain extensive bibliographies.

The problem which is discussed here initially is the determination of the motion of a vapour bubble which has grown in a super heated region of the fluid and is suddenly transported to a cooler region of the liquid. This implies that the external pressure on the bubble will exceed the saturated vapour pressure in this region, causing the bubble to collapse. As the bubble collapses, vapour will condense at its surface, releasing latent heat. This heat will be conducted away into the surrounding liquid raising the temperature of the bubble wall and thus increasing the vapour pressure inside the bubble. For high sub-coolings, this heat transfer effect will be small until the final stages of collapse, when high pressure and temperature transients of short duration will occur. It is these final transients which give rise to the high frequency end of the acoustic spectrum.

The complete solution to the problem would require the simultaneous solution of the continuity, momentum and energy equations for the liquid and vapour, coupled by the conservation of mass momentum and energy across the bubble surface. In practice, to obtain any solution several simplifications are necessary. The model of bubble collapse which will be developed relies on the following assumptions.

(i) The bubble collapses in a spherically symmetric fashion. Without this assumption, it is doubtful if much theoretical progress can be made. Its validity has been questioned by several experimenters (3.13, 3.14, 3.15), who have seen various examples of unstable collapse, generally in large pressure gradients. (Some experimental work by the author and colleagues at D.E.R.E. on the stability of collapsing vapour bubbles produced by sub-cooled boiling is shown in photographic form in figs. 3.2 and 3.3).

(ii) The liquid is incompressible. For moderate degrees of sub-cooling, the liquid velocities should remain considerably less than the sonic velocity, enabling the liquid to be regarded as incompressible. This is not the case for very high sub-coolings or cavitation bubbles (3.12). The liquid may also be regarded as inviscid (3.12) and for initial radii greater than .01 cm, surface tension effects are negligible.

(iii) The bubble interior is assumed to be uniform. In this case it is necessary that the motion be slow enough for a uniform pressure to be maintained in the bubble. Some variations in the vapour temperature are bound to occur, but it will be assumed that the vapour is compressed isentropically throughout most of its volume. It is further assumed that the vapour obeys the ideal gas law.

(iv) Thermodynamic equilibrium is assumed between the liquid and vapour at the interface. This is permissible as long as the velocity of the vapour relative to the interface is small compared with the speed of sound in the bubble.

(v) Physical parameters such as latent heat, specific heat, thermal conductivity, liquid density etc., are assumed to remain constant during motion. Although temperature dependent forms of these quantities could be included, their variation over the temperature ranges experienced will be small and it is doubtful if the increased complexity would be justified.

The justifications and implications of the above postulates are discussed at great length in the references mentioned above.

BASIC EQUATIONS

Using assumptions (1) and (2) above, the momentum equation for the liquid reduces to

$$\rho \{ R\, d^2R/dt^2 + 1.5\, (dR/dt)^2 \} = p_v - p_o \qquad (1)$$

and the pressure at a point in the liquid is given by

$$p(r) = p_o + R \{ (p_v - p_o)/\rho + 0.5\, (dR/dt)^2 [1-(R/r)^3] \}/r \qquad (2)$$

The heat conduction equation is

$$\rho c \{ \partial\theta/\partial t + (R/r)^2 (\partial R/\partial t)\, \partial\theta/\partial r \} = (1/r^2) \frac{\partial}{\partial r}(r^2 k\, \partial\theta/\partial r) \qquad (3)$$

The energy balance across the bubble wall is somewhat complex, but Florschuety and Chao (3.12) provide an argument that a good approximation is

$$k(\partial\theta/\partial r)_{r=R} = \rho_v \lambda \partial R/\partial t \qquad (4)$$

The vapour pressure is given as a function of the bubble surface temperature by integrating the Clapeyron - Clausius equation using assumptions 5 (iv) and 5(v) above to give

$$p_v(\theta_s) = p_v(\theta_o) \exp \{ -\lambda(1/\theta_s - 1/\theta_o)/G \} \qquad (5)$$

Assuming that the vapour is compressed adiabatically, the vapour temperature is given by

$$\theta_v = \theta_o \{ p_v(\theta_s)/p_v(\theta_o) \}^{(\gamma-1)/\gamma} \qquad (6)$$

In principle equations (1) - (6) can be solved to give the bubble radius and vapour pressures as functions of time. In practice, the problem reduces to two-coupled non-linear partial differential equations, and their solution, even numerically would entail great difficulty.

The only significant step towards solving these equations was made by Plesset and Zwick (3.16). They showed if the temperature variation in the liquid is appreciable only in a thin layer around the bubble surface, then it is possible by a procedure of successive approximations to obtain a solution to equation (3). In practice, they show that the zero - order approximation is quite sufficient in the case of water vapour bubbles. This is equivalent to ignoring terms of the order

$\{(r/R)^3 - 1\}$ in the thin liquid layer, over which temperature variations are appreciable, and leads to the expression

$$T_s = T_o - (D/\pi)^{\frac{1}{2}} \int_o^t \frac{R^2(x)\ (\partial T/\partial r)\ r = R(x)}{\left\{ \int_x^t R^4\ (y)\ dy \right\}^{\frac{1}{2}}} \quad dx \qquad (7)$$

Use of this expression gives good results for the initial stages of collapse, but the assumption of a thin thermal layer breaks down as the bubble radius approaches zero. The high conductivities of liquid metals may also make this assumption less realistic. Unfortunately, it is these final stages of collapse which give rise to the high frequency end of the acoustic spectrum. It would be desirable if other approximations, which do not rely on thin boundary layers, could be used to examine this stage of the collapse. With this aim in mind, it was proposed that rather than try to obtain approximate answers to equations (1) - (6) by means of mathematical simplifications, it would be preferable to use judicious physical intuition, to simplify the physical model and then solve the resulting equations exactly."

The author is greatly indebted to G. C. Cornfield who carried out the mathematical analysis and organised the tremendous amount of computational effort needed to present the theoretical result shown in fig. 3.4

SPECTRAL RESOLUTION

Once the pressure time relationship, given by equations 1-6 has been derived for some point in the liquid, the power density spectrum of the acoustic signal can be found by evaluating the finite Fourier integral of the pressure signal

$$F(f) = \int_o^\tau p(r,t)\ \exp\ (-2\pi i\ ft)\ dt \qquad (8)$$

where τ is the lifetime of the bubble.

It has been shown by Rice (3.17) that if the average number of bubbles generated per second is γ, then the power density is related to F(f) by:

$$P(f) = 2\gamma\left|F(f)\right|^2 \qquad (9)$$

The limiting case of bubble collapse is the one of a theoretically empty spherical cavity subjected to an external pressure. This is a classic problem studied by Rayleigh (3.18). The results of his analysis is compared to the case of vapour bubble collapse in figure 3.5.

A typical experimental acoustic frequency spectrum for sub-cooled nucleate boiling in water is shown in figure 3.6. The shape of the spectrum is dominated by the vessel in which boiling takes place, and the upper cut off by the response of the hydrophone used. The curves do however show the activation of more bubbles as the heat flux is increased.

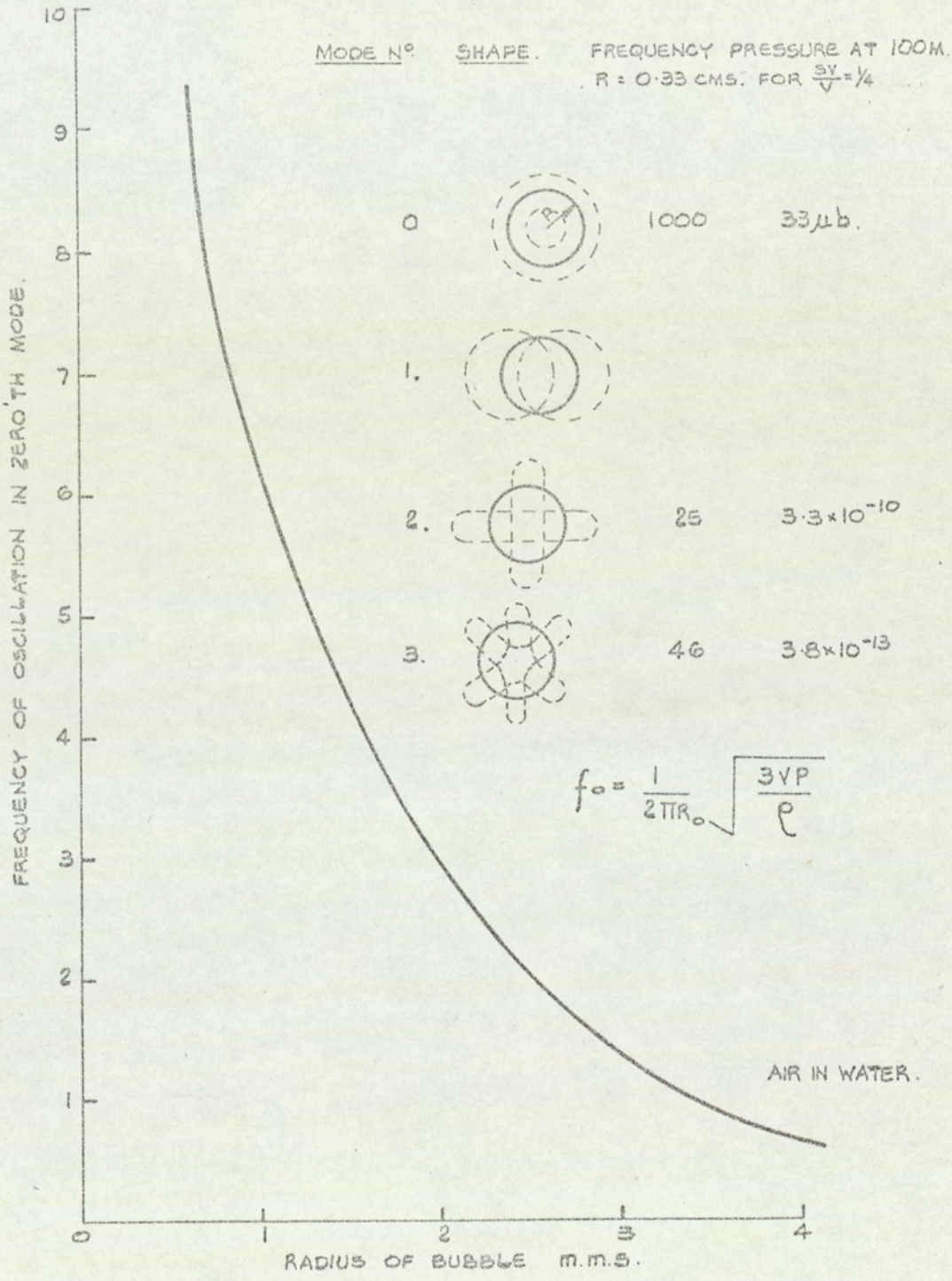

FIG.3·1 VIBRATING GAS BUBBLES AS A SOUND SOURCE REF. 3·7 & 3·8.

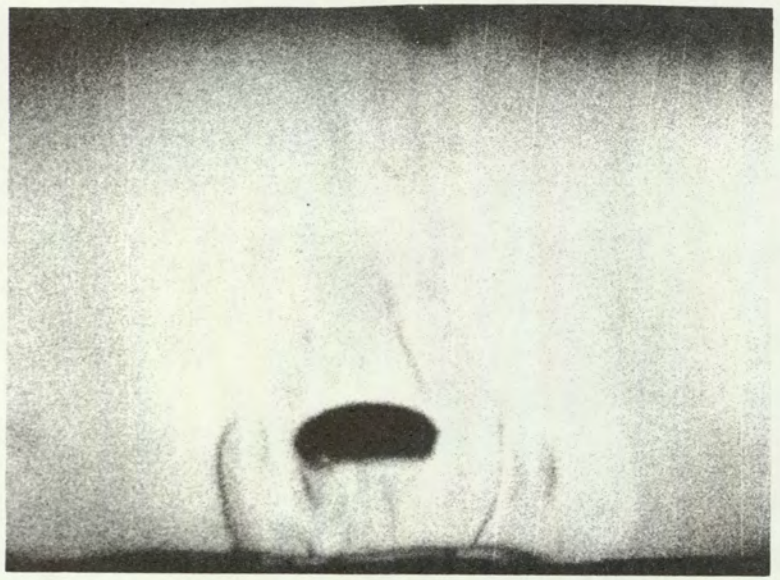

T = 0

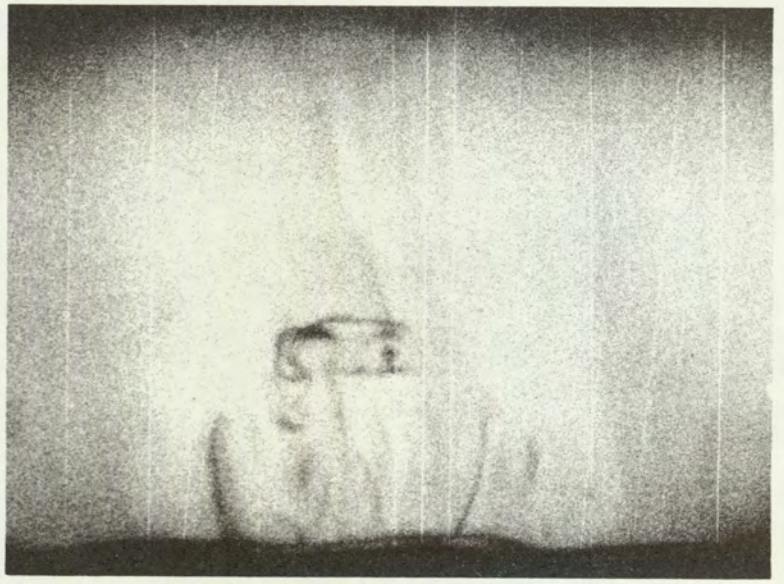

T = 1.5 millisecs

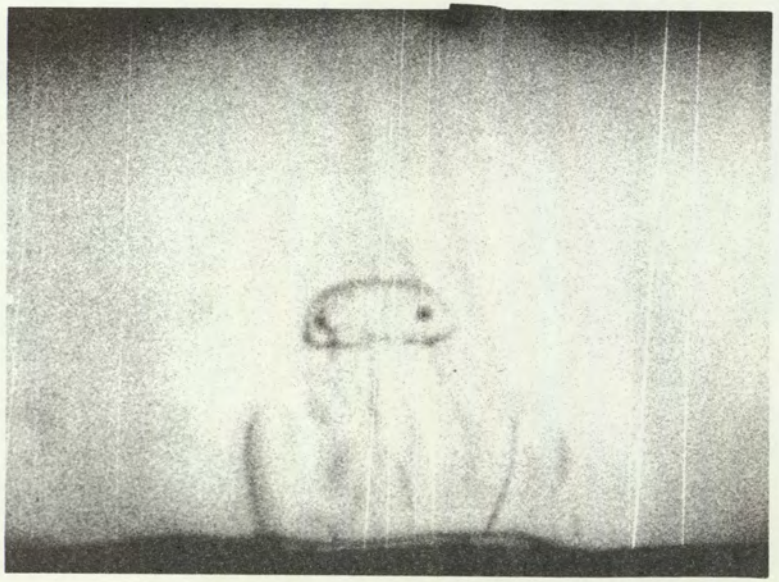

T = 2.2 millisecs

T = 6 millisecs

TORROIDAL COLLAPSE OF A WATER VAPOUR BUBBLE

Figure 3.2

T = 0

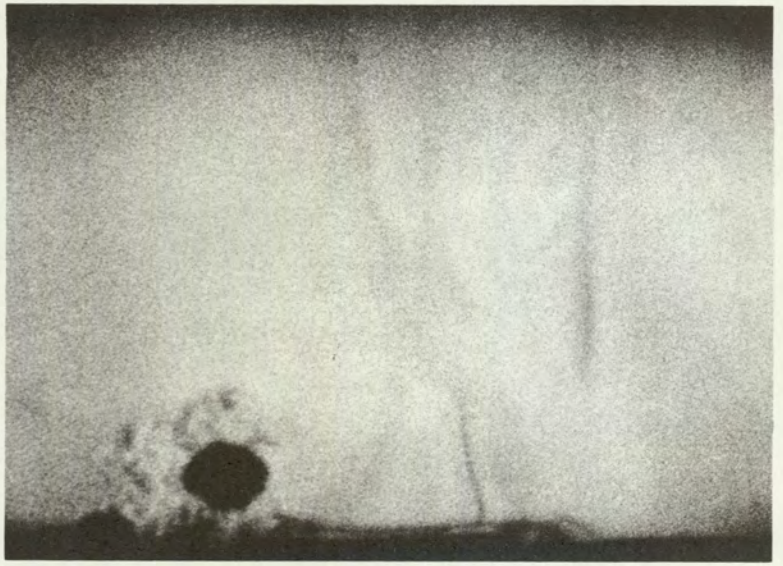

T = 0.17 millisec

T = 0.33 millisec

T = 0.83 millisec

SPHERICAL COLLAPSE OF A WATER VAPOUR BUBBLE

Figure 3.33

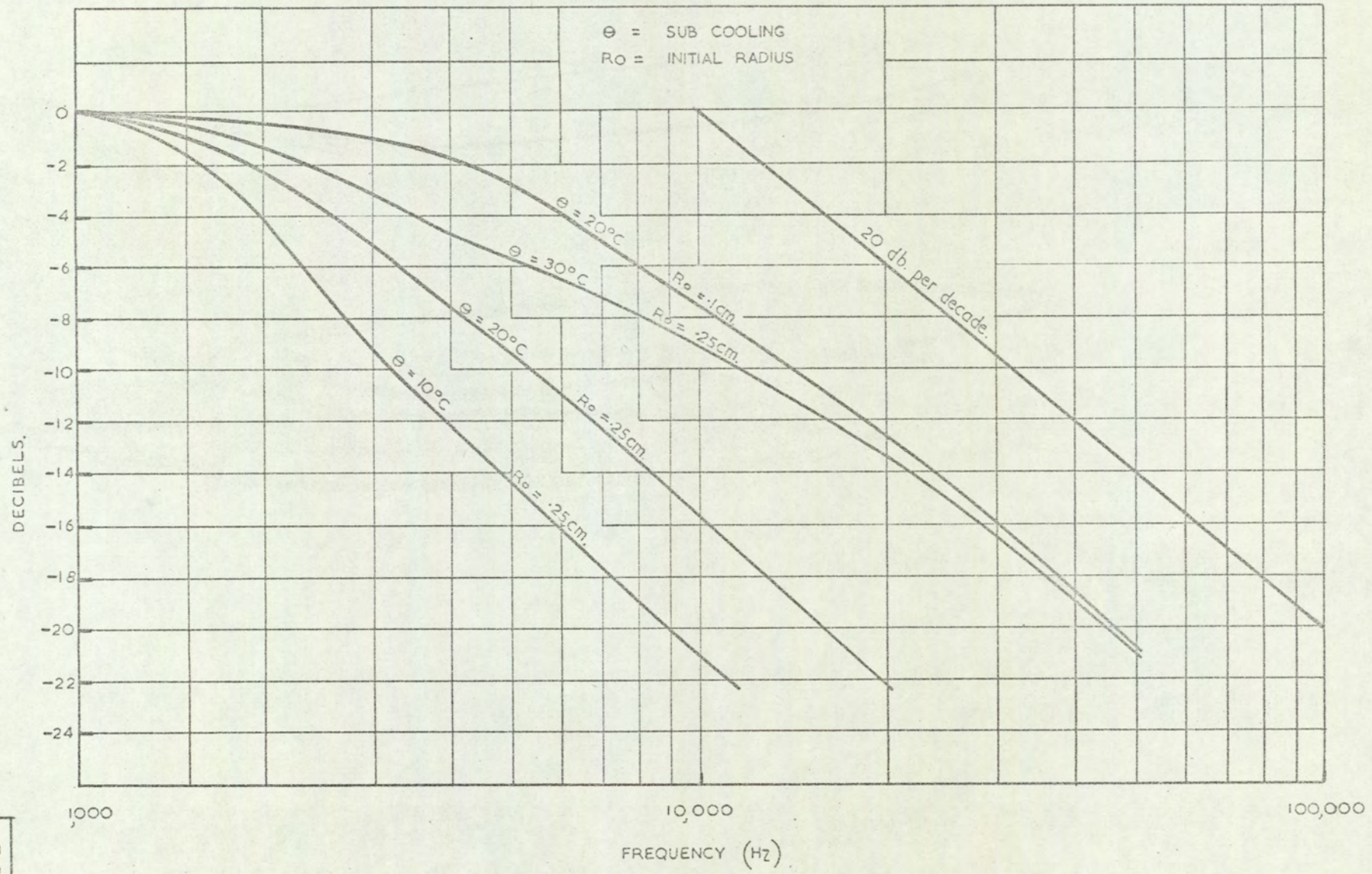

FIG. 3·4

FIG 3·4 THEORETICAL POWER DENSITY SPECTRUM FROM COLLAPSING WATER VAPOUR BUBBLES.

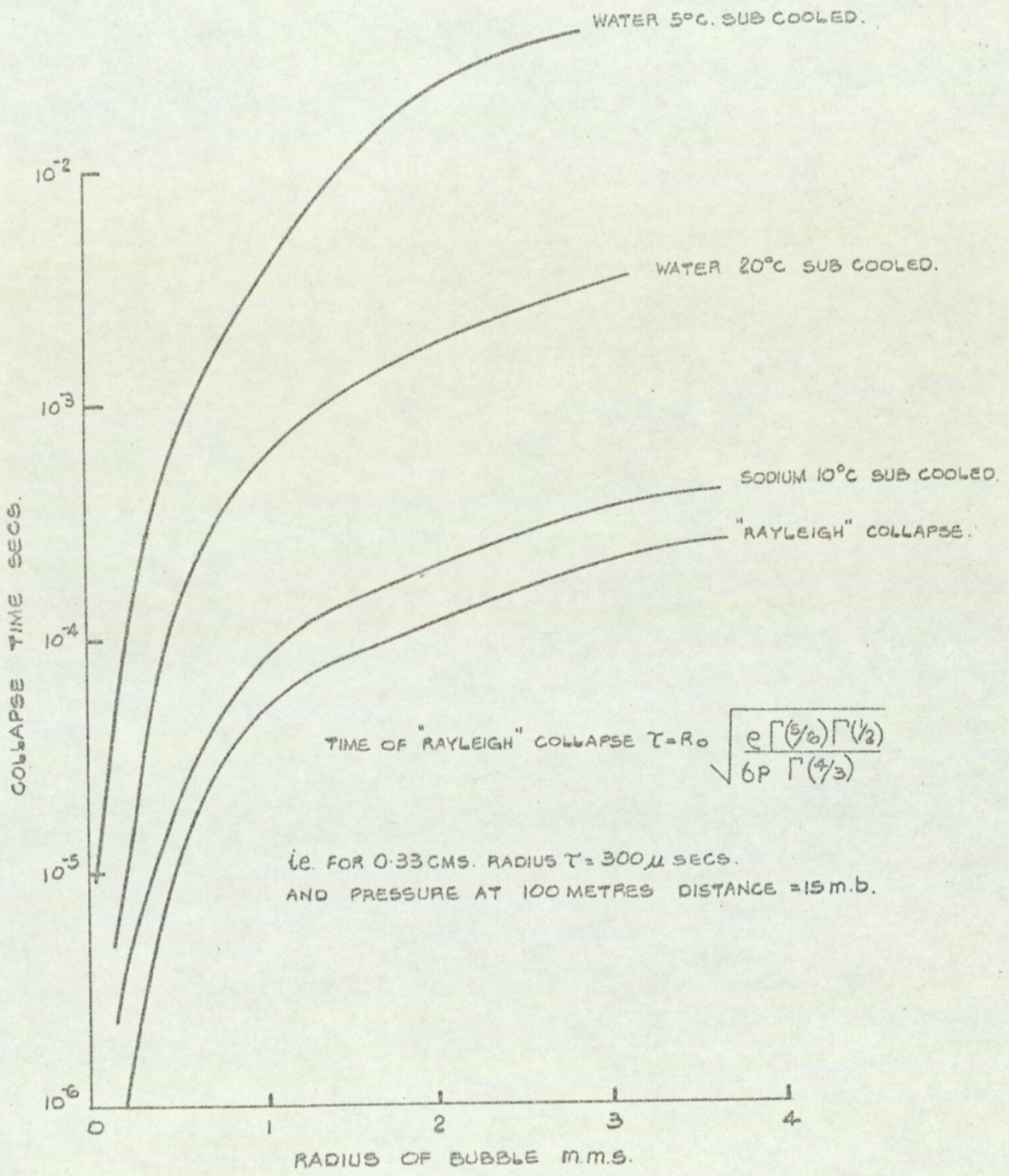

FIG 3·5 COMPARISON OF "RAYLEIGH" COLLAPSE AND VAPOUR BUBBLE COLLAPSE WITH VARIOUS SUB COOLING.

FIG 3·5

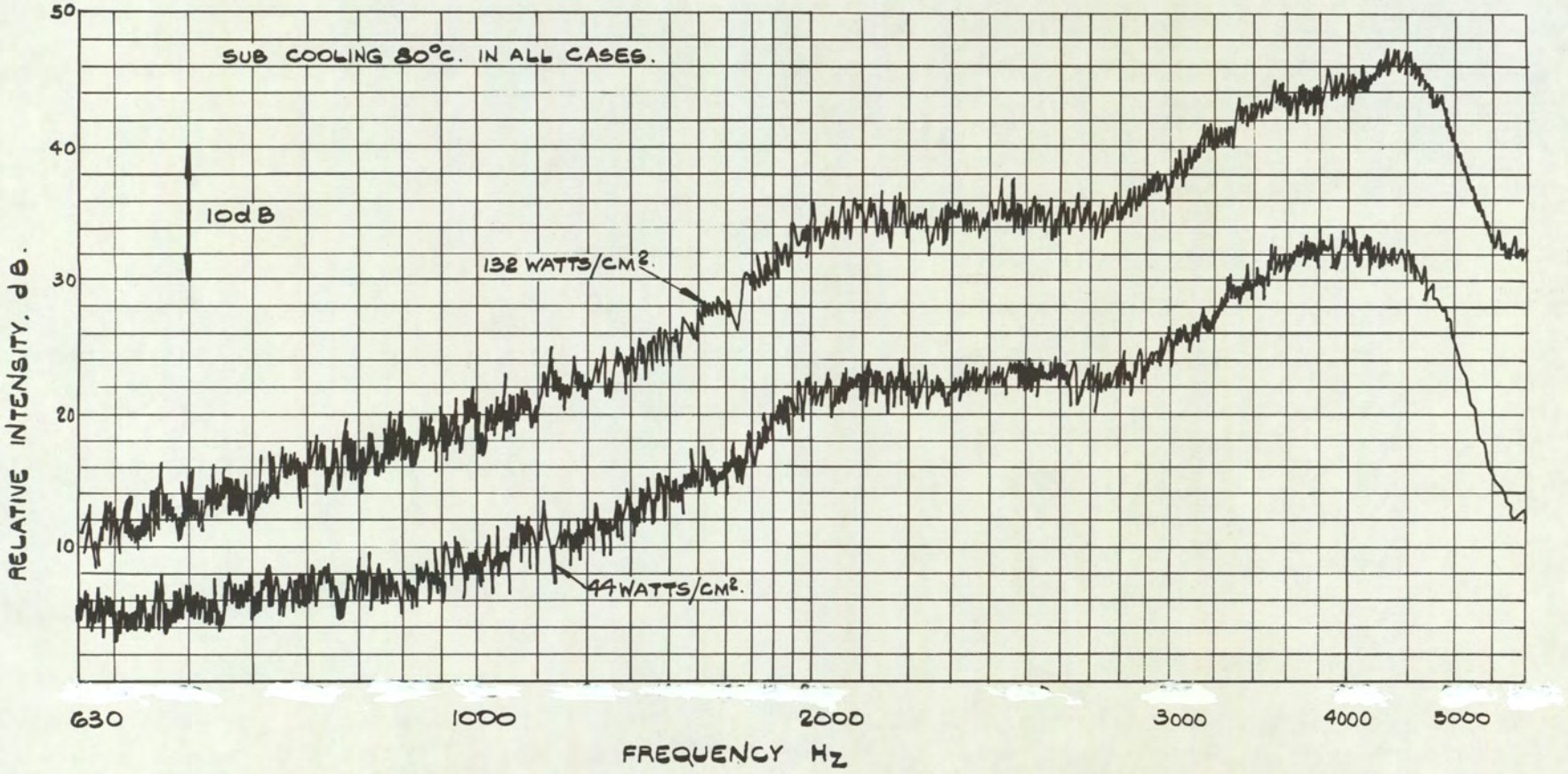

FIG. 3·6 TYPICAL ACOUSTIC FREQUENCY SPECTRA FROM NUCLEATE BOILING IN WATER SHOWING EFFECT OF HEAT FLUX AT CONSTANT SUB-COOLING. USING 5% CONSTANT PERCENTAGE BANDWITH ANALYSER.

FIG 3·6

CHAPTER 4

SYSTEMS AND TRANSDUCERS FOR THE DETECTION OF RANDOM NOISE IN A REACTOR ENVIRONMENT

4.1 Environmental Conditions

Any information detector positioned in the stream of sodium after it has passed through the reactor core will be subject to an extremely destructive environment. The temperature of the sodium will vary up to a maximum of round about 650°C and a neutron flux in the region of 10^{15} neutrons per square cm. per sec.

The corrosion of materials by the alkali metals has been a subject of intermittent but extensive work for the last eighteen years in support of reactor and space programmes. Studies in the U.K. and U.S. have established corrosion rates of various steels at sodium temperatures of up to 725. The main factors affecting corrosion in metals are the ambient temperature, the dissolved oxygen content, and the sodium flow velocity. In general an increase in each one of these parameters increases the corrosion rate. The only common materials compatible with sodium for any period of time are nickel, mild steel and stainless steel of which stainless steel is by far the best at elevated temperatures. To ensure a reasonable life-time the minimum thickness of any device is considered to be about 10 thou. The neutron flux causes damage to all materials and any device can only have a limited lifetime in this environment. The neutron flux in the operating position is higher than previously available in materials testing reactors and the possible lifetime, especially of instruments, can only be extrapolated from limited information which has been obtained at much lower neutron fluxes. Any transducer, used in numbers in the future, would provide unique information concerning the durability of its component parts which would lead to the development of improved materials and transducers.

4.2 Transducers for the Detection of Acoustic Noise

(a) Under Sodium Microphone

The schematic drawing of a proposed under-sodium microphone is shown in Figure 4.1 and it may be seen that the construction is extremely robust consisting essentially of two concentric cylinders. The inner cylinder is insulated with flame sprayed aluminium oxide and undercut over the centre portion to give a necessary gap between the alumina and the outer shell. The operation of the microphone is by the elastic deformation of the outer shell of the device. This deformation is accommodated by providing a gap between the outer shell and the alumina. The advantage of using a microphone of this form is the relative ease by which such a device may be manufactured; a circular symmetry enabling machining operation to be carried out without much trouble. The materials of construction, namely stainless steel and aluminium oxide, are both compatible with the reactor environment mentioned above.

A mathematical theory of the operation of the transducer is given in A1 and shows clearly that the sensitivity of the transducer is linearily related to the pressure and to the square of the diameter of the outer shell. A typical transducer was manufactured and tested under water using a simple substitution technique with reference to a standard hydrophone. The results of this test, showing the comparison between hydrophone and transducer, are shown in Figure 4.2 and are further summarised in Figure 4.3 which shows as a function of frequency the comparison between the theoretical and experimental response and sensitivity. It is noticed from the figures that reasonable agreement exists in the absolute magnitude of sensitivity. For the size of transducer tested the first resonance is at about

5 kHz. As resonant frequencies will be inversely proportional to the diameter of the microphone it is clearly possible to make transducers having a high natural frequency, but examination of the theoretical analysis Appendix I and II shows that the sensitivity will be decreased.

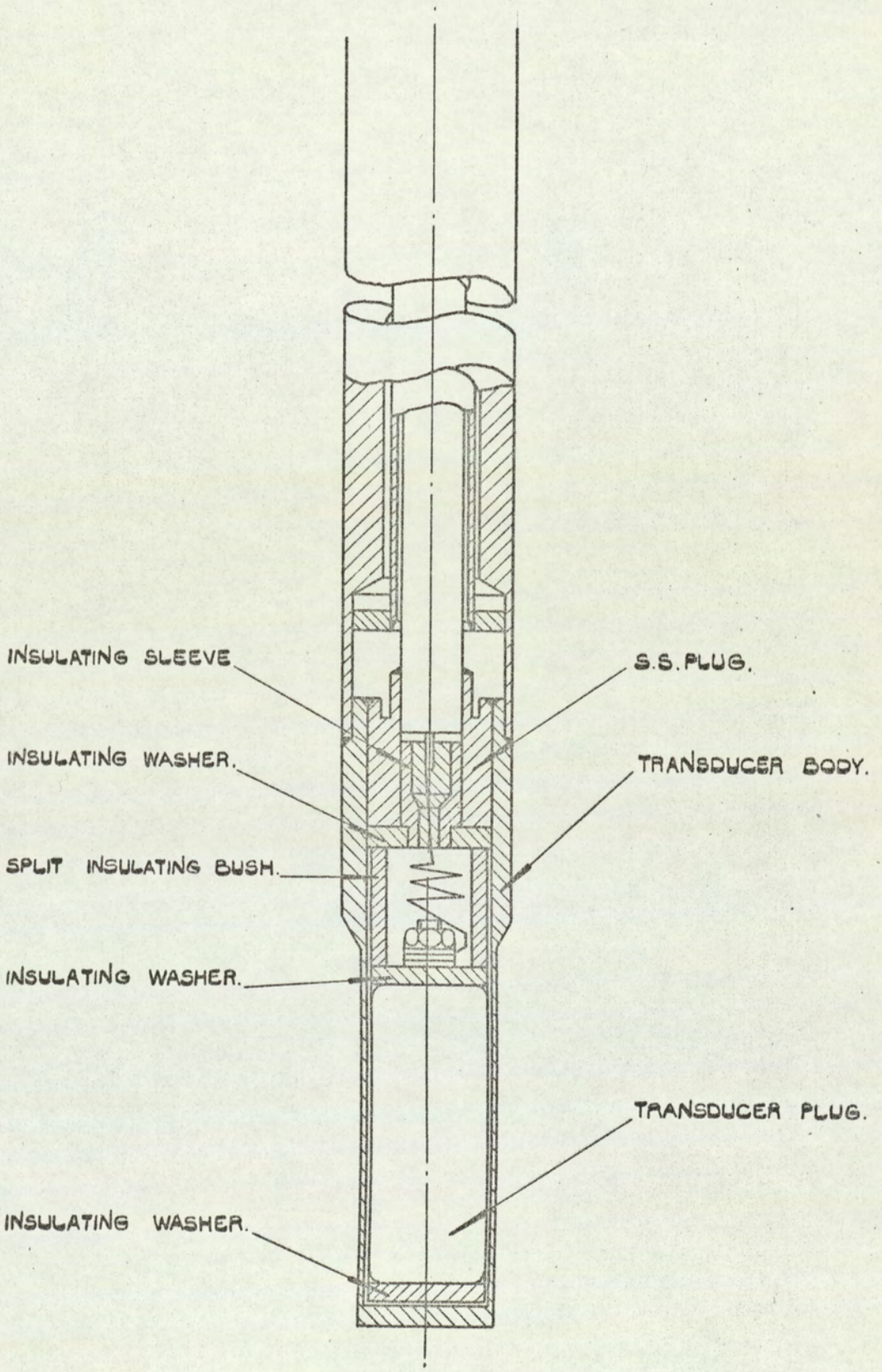

FIG. 4·1. CAPACITANCE TYPE MICROPHONE.

FIG 4·1

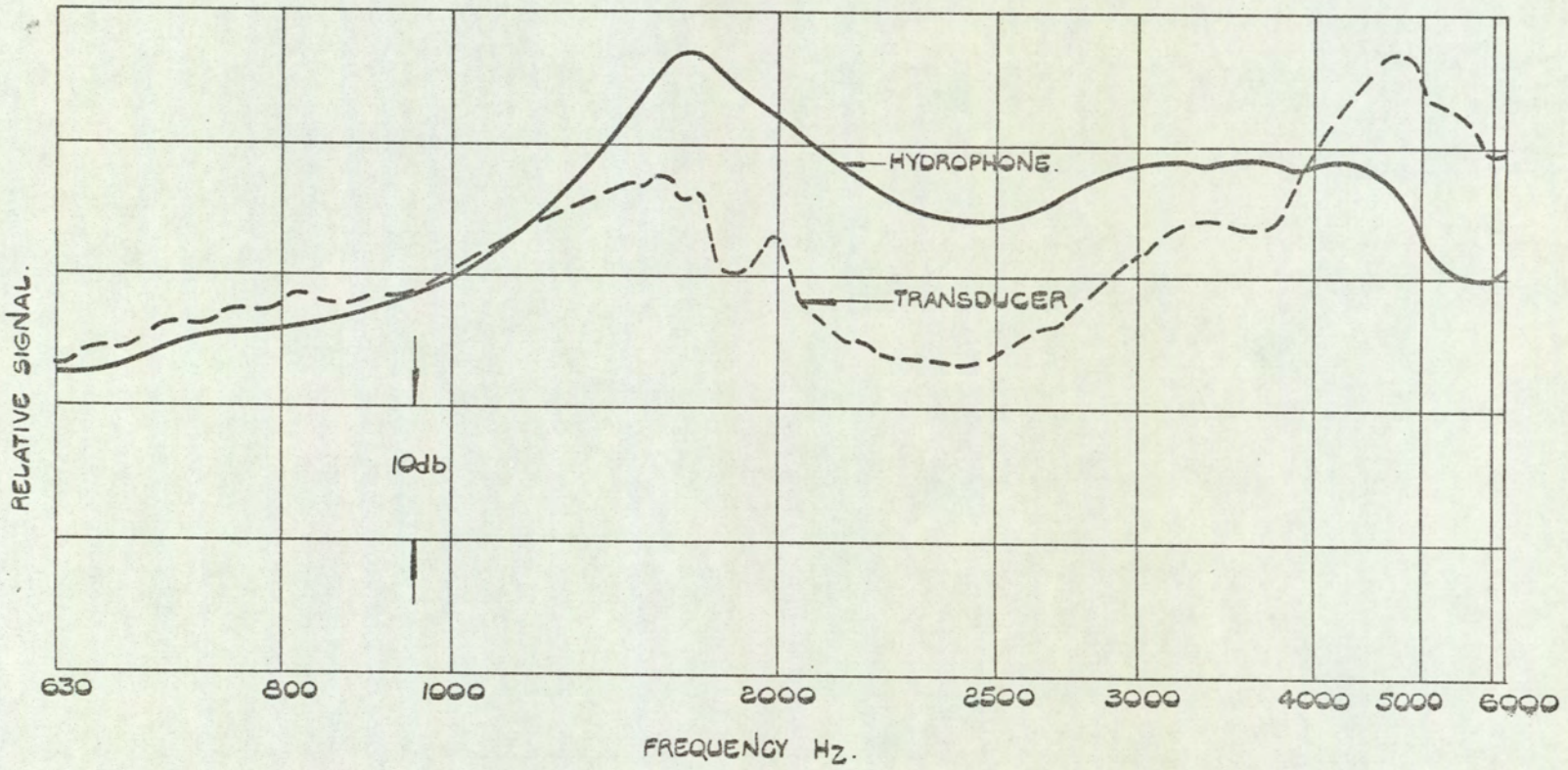

FIG 4.2 TYPICAL EXPERIMENTAL FREQUENCY SPECTRUM RESPONSE OF ONE INCH DIAMETER MICROPHONE.

FIG. 4·2.

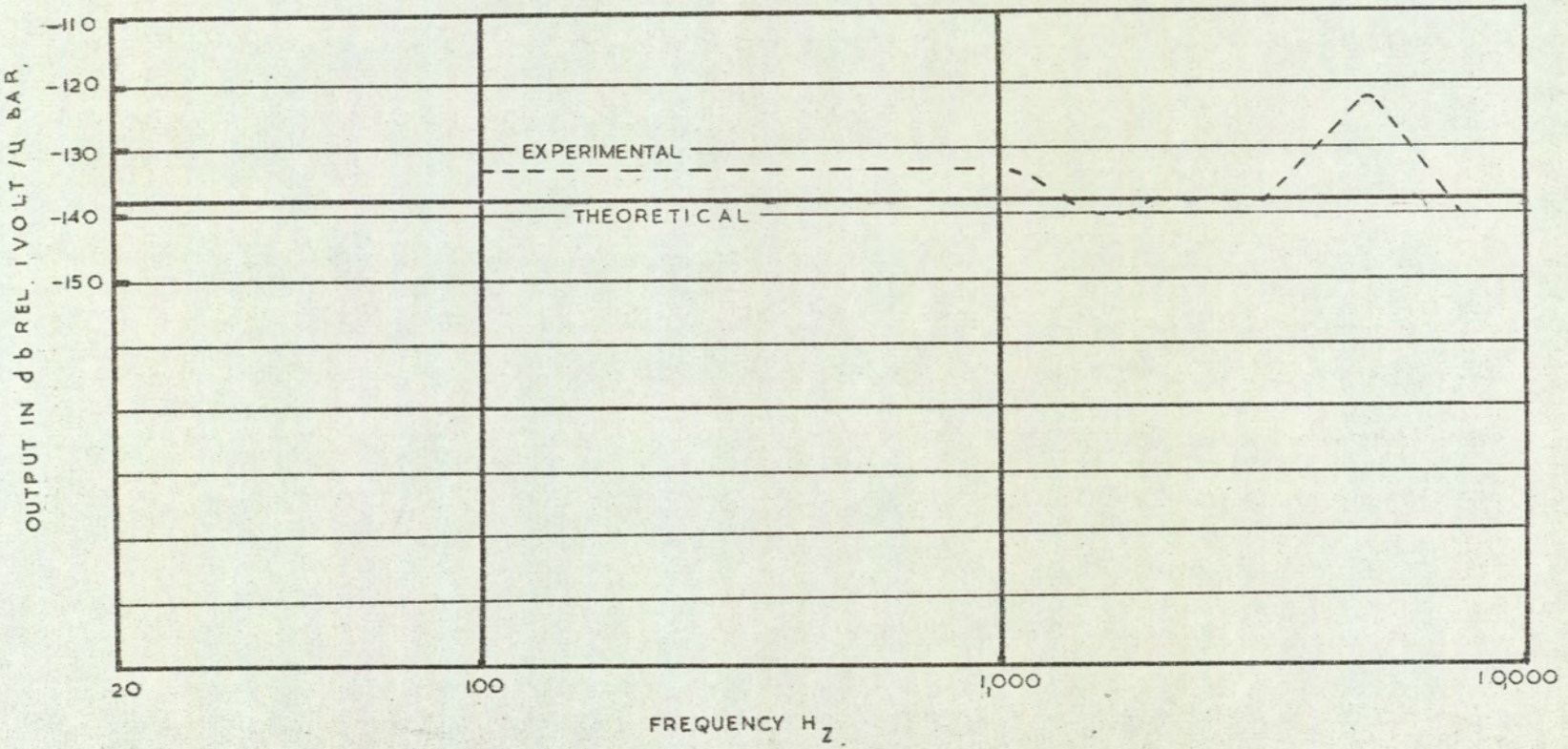

FIG. 4·3 COMPARISON OF THEORETICAL AND EXPERIMENTAL SENSITIVITY OF A 1" DIA. MICROPHONE.

FIG. 4·3.

(b) Acoustic Wave Guides

One system of detecting acoustic energy in hostile environments is conceptually very simple. Into the liquid from which the acoustic information is desired, is inserted a solid steel bar, into which the acoustic energy will couple albeit with some loss of about 10 db. Nevertheless, the energy which is coupled into the rod is guided along its length and can be taken to another part of the system in which the environment is less hostile. In the reactor application, the rods are long vertical rods protruding from a cool low neutron flux region, down through suitable sealing and acoustically insulating regions into the area from which the acoustic information is desired. At the top end of the acoustic wave guide conventional piezo electric accelerometers are mounted and the conversion of the acoustic to electrical energy is accomplished at this point. A diagram of an acoustic wave-guide assembly is shown in Figure 4.4.

Following the scheme by which the under sodium microphone was evaluated typical wave-guides were manufactured and again calibrated under water by a simple substitution technique with reference to a Grulton SSQ-28 hydrophone.

The sensitivity of the hydrophone was -90 db relative to one volt per micro bar. The way in which these acoustic wave-guides have been applied in the Dounreay Fast Reactor is shown in Figure 4.5. This diagram shows how the normal seal plug was modified to carry three acoustic wave-guides protruding into the central region of the reactor.

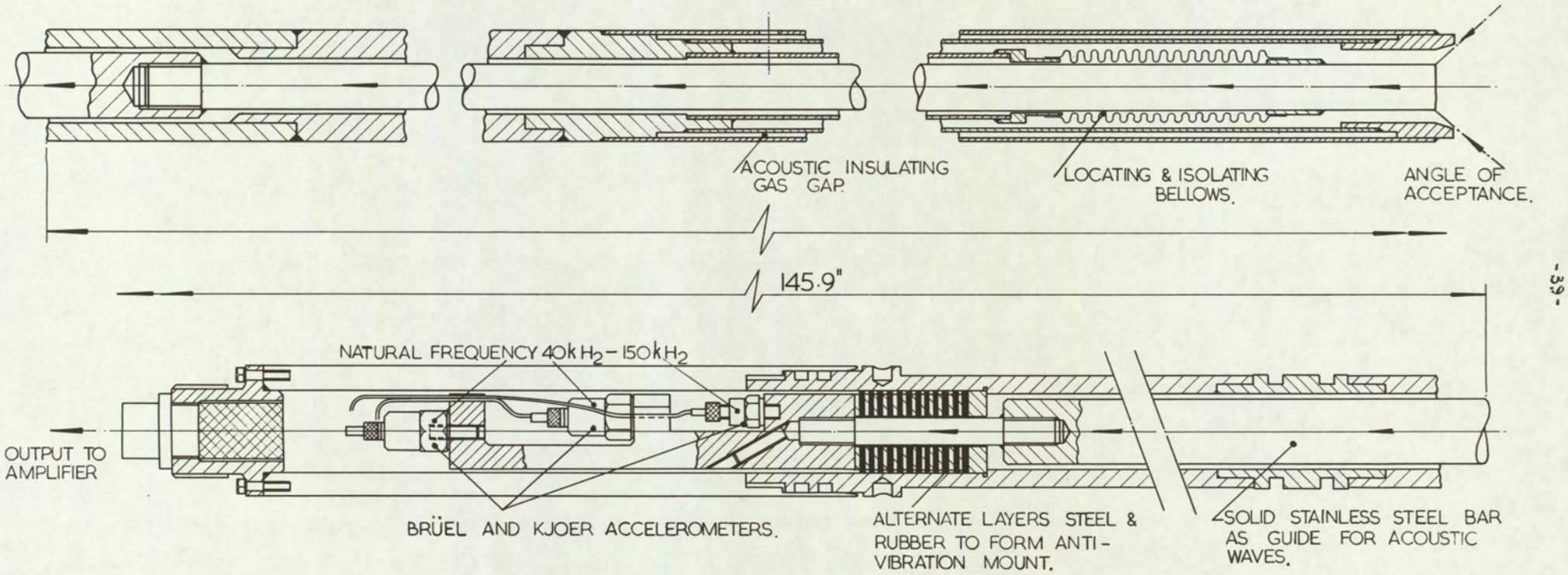

FIG.4·4.WAVEGUIDE—BELLOWS TYPE.

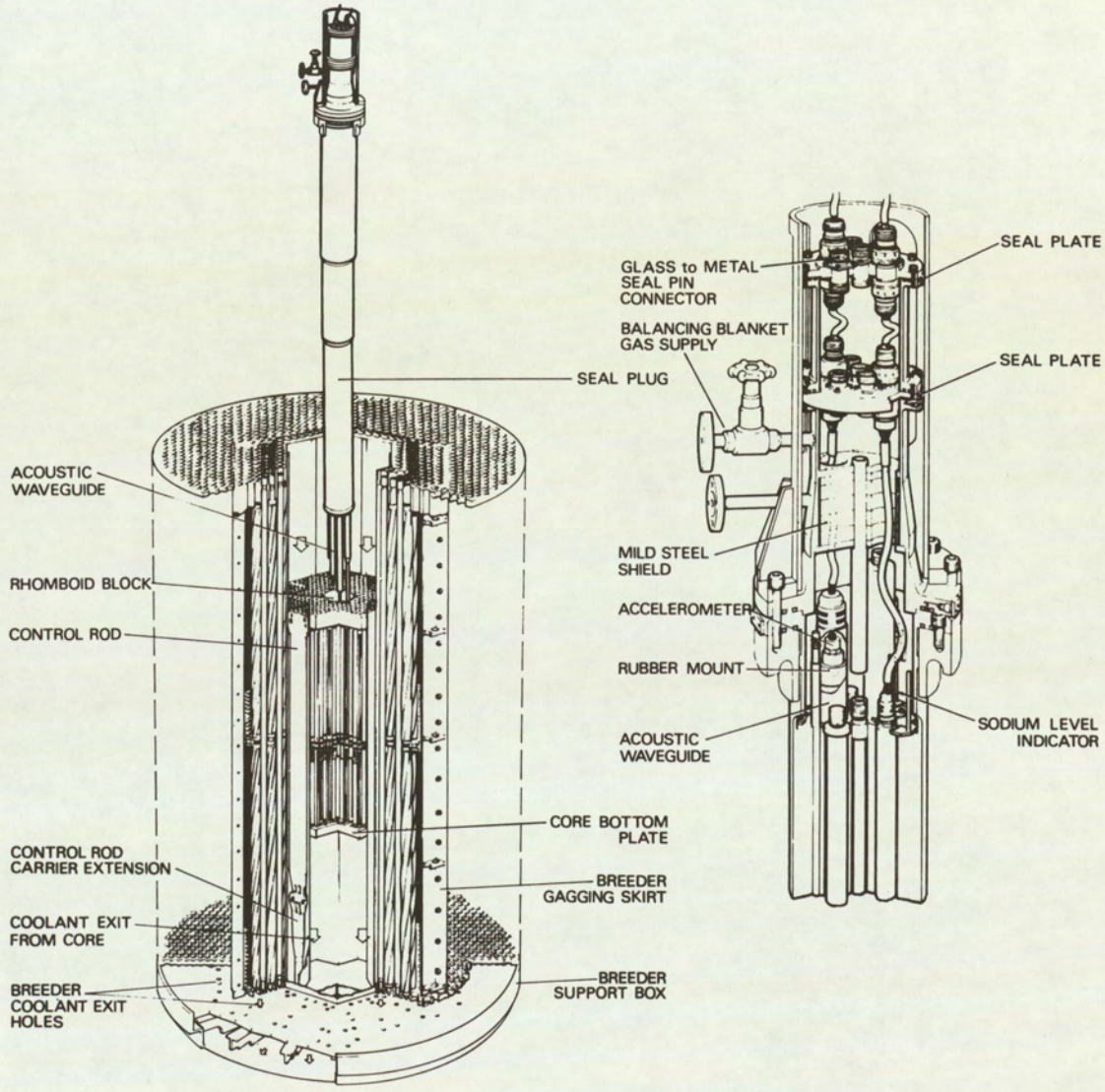

FIG. 4.5

D.F.R. CORE AND BREEDER SHOWING ACOUSTIC WAVEGUIDE INSTALLATION (ELEMENTS OMITTED FOR CLARITY)

4.3 Transducers for the Detection of Temperature Noise

(a) Thermocouples

One method which has been used successfully to detect random noise fluctuation of temperature in the low end of the spectrum is by the use of conventional stainless steel sheathed chromel-alumel thermocouples. Because the thermocouple element itself has necessarily to be sheathed in stainless steel, the resulting thermal time constant associated with this device is finite. Typically a $^{1}/_{8}$th diameter thermocouples, which is of the robust type, normally used in reactor environment, has a time constant of the order of one second. It is clear, therefore, that information on temperature fluctuations will be limited to regions below about one cycle per second. Bachelor and others have shown that temperature fluctuations exist up to very much higher frequencies in the order of 100 Hz. There is a clear incentive to pursue the development of devices which are capable of measuring temperature fluctuations in this high frequency end of the spectrum.

(b) High Temperature Eddy Current Coils for the Detection of Temperature Noise

As the coolant in which the temperature fluctuations exist is liquid sodium, which is a very good conductor, the temperature fluctuation will be accompanied by instantaneous change in the electrical conductivity of the liquid sodium. It is clear, therefore, that measurements of the electric conductivity fluctuations will give an accurate measure of the temperature fluctuations which are causing these conductivity changes. In principle, therefore, if one measures the complex impedence of a simple inductive coil immersed in and coupled electromagnetically with the sodium, then by measuring changes in this impedence it is possible to deduce the temperature fluctuations which are responsible for the impedence fluctuations. The initial work on the development of a suitable transducer has

been carried out by Hughes (4.1). From this initial work a practical system has been developed capable of operating at temperatures up to 600°C in liquid metal cooled reactor environments.

A photograph of two different sized transducer assemblies is shown in Figure 4.6.

The transducers is essentially a short inductance wound from mineral-insulated standard thermocouple cable. Cable diameters of ½ m.m. and 1 m.m. have been used in transducers manufactured at D.E.R.E. The way in which the transducer is applied to a reactor environment is shown in Figure 4.7. The details of the coil connections and the use of the transducer in a bridge configuration is shown in 4.8.

A detailed account of the construction of this probe is given in (4.2) and a summary of its intrinsic sensitivity in (4.3).

Typical results of the response of the probe to gross conductivity changes, caused by air bubbles passing through mercury, are shown in Figure 4.9.

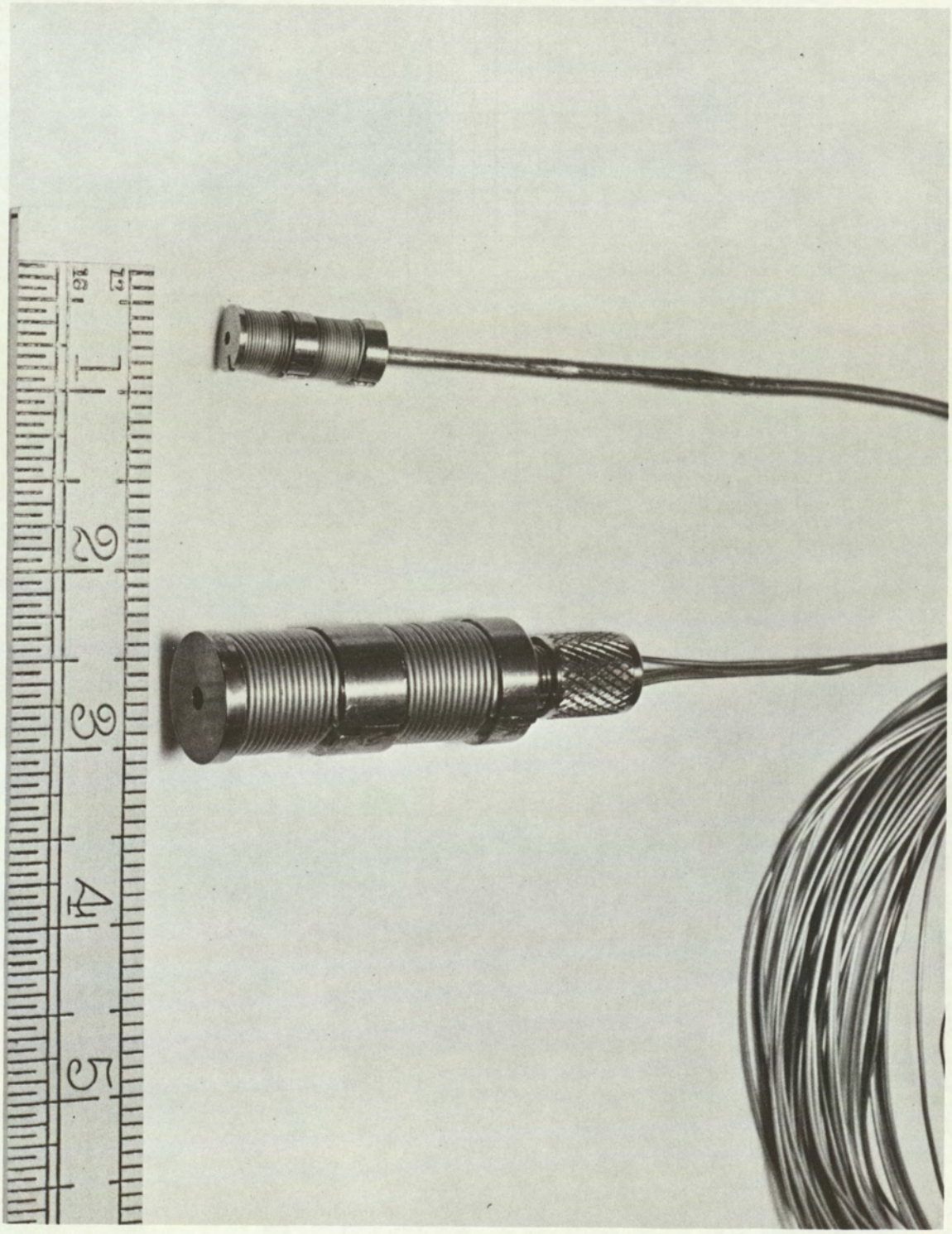

Fig. 4.6 Electrical Conductivity Probes

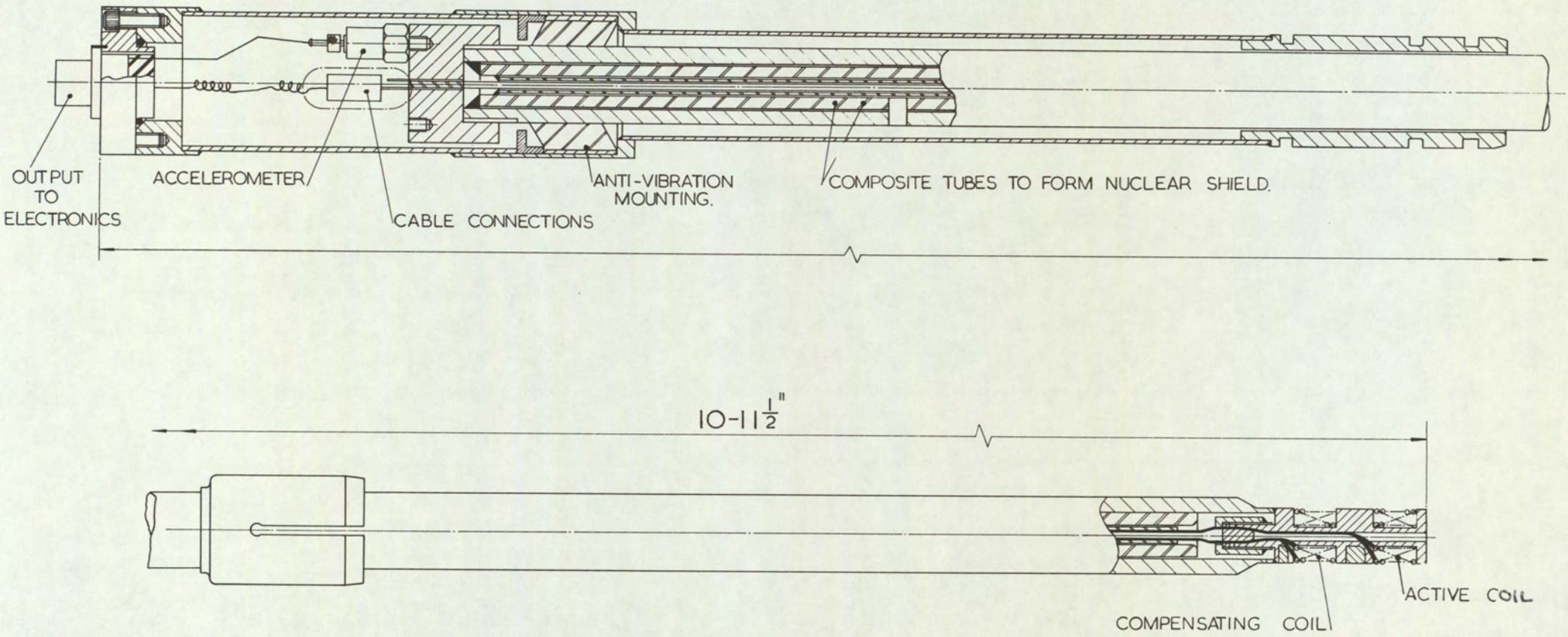

FIG. 4·7. CONDUCTIVITY PROBE WAVEGUIDE.

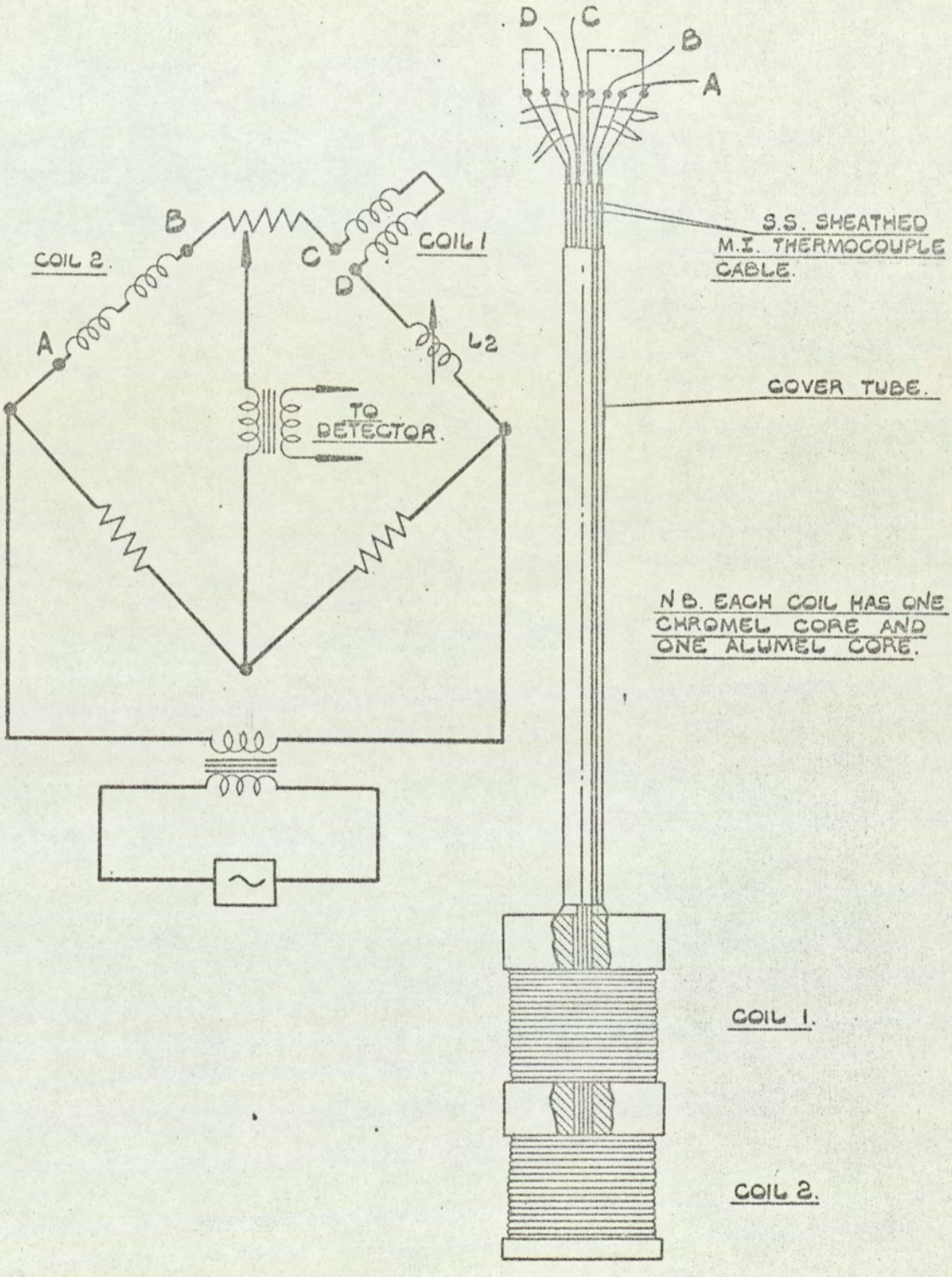

FIG 4.8 HIGH TEMPERATURE EDDY CURRENT PROBE.

FIG 4.8

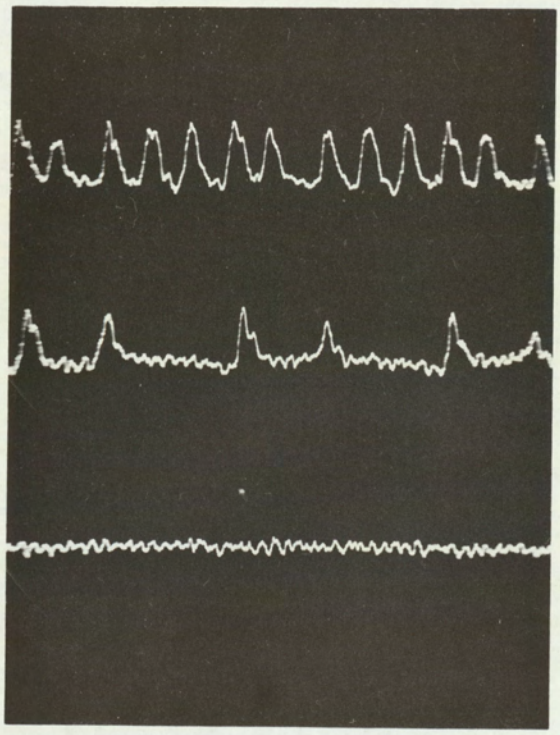

½ mm bubbles approx 2/sec

½ mm bubbles approx 1/sec

System output with no gas

FIG4.9 Gas Bubbles Passing electrical conductivity probe immersed in mercury.

CHAPTER 5

EXPERIMENTS CARRIED OUT TO ASSESS THE TRANSDUCERS AND MEASURE THE INFORMATION GIVEN OFF DURING COOLANT BOILING

5.1 Some Comparisons Between the Static Pool Boiling of Sodium and Water

In order to compare the behaviour of boiling sodium to that of boiling water, on which much more work has been done in the past, a simple static test rig was built in which either water or sodium could be introduced around a standard fuel tube. A brief description of the test rig and the associated instrumentation together with the results obtained is given below.

5.1 a) Description of Test Rigs

Horizontal Tube Installation (Fig 2.4)

After a surface finish check a standard fuel pin was seal welded into adaptors on the wall of the boiling pot. The system was hydraulically tested, degreased and dried out.

Eight one-millimetre chromel-alumel, stainless steel sheathed, mineral insulated thermocouples were used. One thermocouple was firmly pressed against the centre of the upper surface of the tube. The remainder were arranged to show the axial and radial temperature distribution.

The tube heater assembly is shown in Figure 5.1. After the copper end-pieces were screwed into the titanium tube adaptors this assembly was ground into the tube previously welded into the boiling vessel until 0.005 in. diametral clearance was achieved. "Brimor", a high temperature strain gauge cement, was brushed onto the heater and the assembly baked at 150°C. The heater was then pushed into the tube.

The boiling vessel was now lowered into an outer sodium leak containment, which was helium filled to ensure good heat transfer between the heater tube and the outer tube.

Piezo electric accelerometers were screwed to the top of the wave guide, a 1 in. dia. stainless pipe closed at both ends, which extended through the flange into the sodium.

Vertical Pin Installation (Fig 2.5)

This rig was basically the same as the previous case except that the pin now extended from the top flange through the bottom of a boiling vessel, 5 in. diameter x 10 in. deep. The other difference was that all surface finishes were extremely carefully controlled. The boiling vessel finish in the range 10-20μ in. and the pin in the range 30-40u in. Also, the boiling vessel was turned from a stainless steel bar, the only weld in it being the seal weld where the fuel tube went through the bottom of the vessel. As this weld was relatively cool during the experiment it could not act as a nucleation point for boiling. All thermocouples were polished and before assembly all surfaces in contact with the sodium were given an acid-water-solvent treatment.

Three thermocouples were pressed against the 3 in. long heated section of the tube. The remaining thermocouples again measured the bulk liquid metal temperature throughout the vessel.

An outer containment was again fitted for sodium leak and heat transfer reasons as in the previous case.

5.1 b) Instrumentation

(i) Main Heater Power Control

When assembled the main heater has a resistance of 0.02 ohms at 800-900^{o}C, and an ambient temperature insulation resistance of 50 MΩ at 100 volts. Power was supplied from a heavy current transformer with output tappings arranged so that at a heat flux of 160 watts/cm^2 the current was 350A at 7 volts. Power was measured by wattmeter, voltage was taken directly across the heater and current metered via a 100 : 1 current transformer. Control was by means of a variable transformers on the primary side of the heavy current transformer.

(ii) Temperature Recording

Signals from chromel alumel thermocouples were fed directly into two 0-1000°C potentiometric recorders. The chart speed was 24 in/hr and the response time 4.5 secs per full scale deflection. The main heater temperature was displayed on a single pen recorder and the bulk temperatures on a 16 point selector recorder.

(iii) Acoustic System

Of the piezo electric accelerometers secured to the wave guide, two had a natural frequency of 20-25 K c/s and the third a natural frequency of 160 K c/s.

The high frequency accelerometer signal was fed through a frequency analyser and then displayed on a logarithmic chart recorder. In this way the frequency spectrum could be checked for components up to 650 K c/s.

One low frequency accelerometer signal went to an audio amplifier and was used for control purposes.

The other low frequency signal fed a logarithmic analyser and recorder which could plot, on-line, a frequency spectrum from 20 c/s - 20 K c/s. In parallel with this system was a tape recorder which stored the boiling signal when there was insufficient time available for on-line analysis.

(iv) Blanket pressure measurments were made intermittently on a valved mercury manometer (Figure 2.4 and 2.5).

5.1 c) Experimental Technique

Horizontal Tube

The sodium was transferred through the filter to the boiling vessel. Trace heating enabled the bulk temperature to be raised to 550°C. The main heater was then switched on, and the temperature allowed to rise until the pin wall temperature was approximately 30°C below the saturation temperature. The blanket pressure was then reduced to the value using the mercury manometer. The wall temperature continued to increase until boiling occurred.

When boiling was established acoustic and temperature measurements were taken. The blanket pressure was then increased and boiling suppressed when preparations were made for adjustment to the next point on the Pressure/Temperature curve (see Figure 5.2).

Vertical Tube

The procedure was similar, but higher heat losses to the environment slowed down the rate of temperature rise and resulted in longer periods of sub-cooled boiling.

5.1 d) Results

The results are shown in tabular form in Tables I and II and graphically in Figures 5.2 to 5.11.

5.1 e) Discussion of Results

Heat Transfer

The heat transfer properties of the sodium during boiling are shown plotted in Figures 5.2 and 5.3. Both horizontal and vertical systems yielded a natural convection curve which approximately followed the theoretical relationship $\Delta\Theta = k\phi^{4/5}$, and showed a sudden increase in the heat transfer coefficient when boiling began.

Superheat

The experimental and theoretical wall temperatures (θ_w) are shown in Figure 5.4. The theoretical value for θ_w is given by the relationship:

$$\Theta w = \frac{\lambda/G}{\log k/(P + \frac{26}{r} - Pa)} \qquad (1)$$

The extreme values for θ_w, when $P_a = 0$ and P_a = saturation (0.1 ppm) are shown for a cavity radius of 10 μ. The experimental points for θ_w were widely scattered but a range of values are shown for different horizontal pins. The dominant variable appears to be cavity size. This could explain the difference between horizontal and experimental curves as the argon partial pressure seems to indicate a cavity

size of about 10 μ.

The variation of superheat for the horizontal tube is shown in Figure 5.5. For the first series of boiling tests a low superheat curve was yielded, which appeared to be characteristic of all "virgin" horizontal tube tests. The departure from low to high superheat values appears to be only a function of "boiling history" and to have little relation to immersion time.

The superheat varied for the vertical tube in a random manner as shown in Figure 5.6. On two occasions when the pressure was decreased with the wall temperature almost equal to the corresponding saturation temperature, boiling began with zero superheat.

Another interesting phenomenon was observed during the sodium boiling runs which is shown in Figure 5.7. When boiling began, either with zero or with appreciable superheat, the process was quite normal but then on some occasions the boiling would become more and more erratic, until it finally stopped. Then with all parameters remaining constant the boiling would in fact start again and repeat the same pattern. This "stop-start" phenomena had an easily recognisable counterpart in the wall temperature as it went through its various phases. The boiling acoustic signal also changed accordingly and became more spasmodic, as the boiling stopped.

The acoustic noise produced during nucleate boiling is assumed to be caused by bubble growth, collapse or oscillation. It is thought that the oscillatory mode will predominate in the low frequency end of the spectrum whilst the collapse mode will predominate in the higher frequency range. The amount of dissolved gas in the liquid will effect the total sound intensity by attenuation particularly at the higher end of the spectrum and also by "cushioning" the final collapse of the bubble.

Figure 5.8 which compares the relative acoustic spectrum of the

boiling noise of fresh water, degassed water and sodium shows that the amount of dissolved gas in the fresh water seriously reduces the sound output.

Figure 5.9 shows the decrease in the sound ouput at a typical high frequency of about 3 kHz with decreasing sub-cooling. This decrease is probably due to the partial change over from the collapse mode to the oscillatory mode. Because of the very different thermal conductivities of the two liquids, this effect should be signficant over a much larger sub-cooling range with water than with sodium. The rapid decrease that is evident in the water trace at about 11^{o}C sub-cooling is thought to be due to bubble coalescence which is known to take place at the heat fluxes used at this sub-cooling. This figure also illustrates the much more continuous nature of the boiling water noise.

Figure 5.10 represents the smoothed data in the audio frequency band and compares the relative acoustic outputs of water and sodium boiling noise as a function of sub-cooling.

Figure 5.11 shows typical high frequency comparisons of sodium to water boiling noise at constant sub-cooling. The importance of the amount of dissolved gas on the bubble collapse mode of sound production has been mentioned earlier in this thesis. Although the water used was degassed by reducing the blanket pressure to a few m.m. Hg, the dissolved air content would be gross compared to the dissolved argon in the sodium. It is believed that these gas nuclei are responsible for the ultra high frequencies being suppressed in the water experiments.

CONCLUSIONS

The tubes used in these experiments may be thought to have an equivalent active cavity size of about 10 μ.

The magnitude of the superheats observed in this practical situation are acceptable in the sense that the energy release when nucleation takes place can be contained.

The nucleate boiling of sodium is a non-reproduceable phenomenon compared to that of water.

The variation in amount of dissolved argon in these experiments, even from zero to saturation level does not strongly affect the superheat necessary to initiate nucleation. The dissolved argon content is important however in the suppression of very high frequencies when the bubbles are collapsing.

These experiments show that acoustic similarity between water and sodium is good in the audio range provided degassed water is used.

Boiling sodium continues to produce sonic energy up to much higher frequencies than degassed water.

Due to limitations imposed by the heater, only a small part of the superheat/pressure curve has been investigated. Future work therefore will be concentrated in the following unknown areas.

a) Expansion of the superheat/pressure curve to pressures greater than 1 atmosphere by using an electron bombardment heater.

b) Influence of impurity levels in the liquid metal on its boiling characteristics.

c) High frequency spectrum to be investigated more fully.

TEST RESULTS STATIC SODIUM BOILING

TABLE I

Horizontal tube.

Ref. No.	Test No.	Flux w/cm^2	Press m.m.Hg	Sat. Temp. ^oC	Bulk Temp. B^oC	Wall Temp. w^oC	Super Heat ^oC	Sub-Cooling ^oC	$(\theta_w - \theta_B)$ ^oC	Relative Acoustic Intensity
1	16/1	80	103	702	690	730	28	12	40	-
2		80	90	692	700	735	43	- 8	35	-
3		80	135	722	730	765	43	- 8	35	-
4		80	190	750	745	780	30	5	35	-
5		80	290	783	770	810	27	13	40	-
6		80	340	797	790	835	38	7	45	-
7		80	495	833	820	865	32	13	45	-
8	16/2	80	51	650	655	690	40	5	35	25
9		80	95	697	700	740	43	- 3	40	17
10		80	120	713	725	765	52	-12	40	14
11		90	180	746	745	790	44	1	45	15
12		90	270	777	770	810	33	7	40	20
13		115	355	801	780	840	39	21	60	17
14		115	458	824	810	860	36	14	50	26
15	16/3	80	65	670	655	690	20	15	35	-
16		80	110	716	690	730	14	26	40	-
17		80	127	718	720	760	42	- 2	40	-
18		90	190	750	740	785	35	10	45	34
19		90	260	774	765	810	36	19	45	27
20		115	355	801	780	835	34	19	55	39
21		115	448	822	810	860	38	12	50	9
22	16/4	60	60	659	645	680	21	14	35	24
23		80	90	692	695	725	33	- 3	30	25
24		80	140	724	720	755	31	4	35	22
25		90	200	753	745	785	32	8	40	37
26		90	220	761	770	810	49	- 9	40	13
27		115	365	804	795	840	36	9	45	25
28		115	440	821	815	855	34	6	40	9
29		115	58	650	685	700	50	-	-	22
30		115	75	679	710	735	56	-	-	18
31		115	140	725	745	765	40	-	-	15
32		115	200	753	765	785	32	-	-	14
33		115	275	780	785	810	30	-	-	11
34	16/1	150	72	678	675	705	27	3	30	24
35		150	140	724	710	735	11	14	25	45
36		150	160	735	740	770	35	- 5	30	26
37		150	200	753	765	790	37	-12	25	13
38		150	250	771	780	815	44	- 9	35	14
39		150	355	801	805	840	39	- 4	35	11
40		150	400	811	830	860	49	-19	30	15
41	16J	150	100	700	665	705	5	35	40	48
42		150	140	720	710	740	20	10	30	48
43		150	165	739	745	775	36	- 6	30	19
44		150	190	749	755	790	41	- 6	35	21
45		150	280	780	795	825	45	-15	30	16
46	16F	80	66	670	660	690	20	10	30	31
47		80	100	700	700	735	35	0	35	25
48		80	140	724	725	760	36	- 1	25	36
49		90	185	747	745	780	33	2	35	17
50		90	220	761	770	800	39	- 9	30	17
51		115	365	803	790	835	32	13	55	28

Ref. No.	Test No.	Flux w/cm^2	Press m.m.Hg	Sat. Temp. ^oC	Bulk Temp. B^oC	Wall Temp. w^oC	Super Heat ^oC	Sub-Cooling ^oC	$(\theta_w - \theta_B)$ ^oC	Relative Acoustic Intensity
52		115	440	820	815	865	45	10	50	-
53		115	320	793	820	835	42	-27	15	23
54	17	200	98	698	680	725	27	18	45	-
55		200	108	705	685	730	25	20	45	-
56		200	113	708	685	735	27	23	50	-
57		200	148	729	710	760	31	19	50	-
58		200	153	732	710	765	33	12	55	-
59		200	198	753	730	790	37	23	60	-
60		200	208	756	730	785	29	16	55	-
61		200	226	763	765	810	47	- 2	45	-
62		200	283	781	765	830	49	16	65	-
63		200	308	788	775	840	52	13	65	-
64		200	358	802	785	850	48	17	65	-
65		200	358	802	785	850	48	17	65	-
66	18/1	110	115	710	680	725	15	30	45	-
67		110	158	734	709	755	21	25	46	25
68		110	208	756	735	785	29	21	50	20
69		110	258	773	750	805	32	13	45	20
70	18/2	110	128	717	685	735	18	32	50	-
71		110	178	744	735	785	41	9	50	-
72		140	228	763	820	771	8	65	-	-
73		140	341	797	790	850	53	7	60	-
74	18/3	140	108	705	695	750	45	10	55	-
75		140	158	734	730	795	61	4	65	-
76		140	250	772	-	810	38	-	-	-
77		140	328	794	795	865	71	- 1	70	-
78	18/4	140	88	691	655	720	29	36	65	42
79		140	138	718	710	780	62	8	70	31
80		140	188	749	740	820	71	9	80	25
81		140	258	768	770	845	77	- 2	75	19
82	18/5	140	88	691	675	760	69	16	85	-
83		140	138	723	715	790	67	8	75	-
84		140	188	748	740	820	72	8	80	-
85		140	258	773	770	845	72	8	80	-
86	18/6	180	138	723	700	770	47	23	70	50
87		180	188	748	748	835	87	- 2	85	40
88		180	321	792	785	865	73	7	80	47
89	18/7	200	138	723	685	775	52	38	90	-
90		200	248	770	-	850	80	-	80	-
91	18/8	200	188	748	720	810	62	28	90	48

TEST RESULTS STATIC SODIUM BOILING

TABLE II

vertical tube.

Ref. No.	Test No.	Flux w/cm^2	Press m.m.Hg	Sat. Temp. ^oC	Bulk Temp. ^oC	Wall Temp. ^oC	Super Heat ^oC	$(\theta_w - \theta_B)$ ^oC	Relative Acoustic Intensity at 3.5 Kc/s
92	1	150	145	730	680	730	zero	50	12
93	2	150	145	730	680	725	- 5	45	30
94	3	150	145	730	-	745	15	-	-
95	4	160	145	730	715	755	25	40	15
96	5	165	145	730	695	730	zero	35	14
97	6	165	145	730	690	725	- 5	35	32
98	7	165	145	730	700	740	10	40	55
99	8	165	145	730	690	725	- 5	35	32
100	9	165	145	730	645	740	10	45	25
101	9A	165	145	730	705	750	20	45	-
102	10	165	145	730	710	755	25	45	20
103	10A	165	145	730	715	765	35	50	-
104	11	165	145	730	700	745	15	45	42
105	12	165	145	725	700	735	11	35	36
106	13	165	145	730	685	725	- 5	40	-
107	14	165	96	695	650	680	-15	30	-
108	15	165	96	695	690	730	35	40	-
109	16	165	96	695	760	700	5	40	36
110	17	165	96	695	645	680	-15	35	-
111	18	165	130	719	687	725	6	38	-
112	19	zero	70	675	680	685	10	5	-
113	20	165	96	695	650	690	- 5	40	-
114	21	165	96	695	655	690	- 5	35	-
115	21A	165	96	695	685	730	35	45	-
116	22	165	96	695	680	715	20	35	-
117	23	165	96	695	685	720	25	35	-
118	24	165	96	695	685	723	28	38	-

ITEM Nº.	DESCRIPTION.
1.	STD. FUEL TUBE. O/D :- 0·23" I/D :- 0·20"
2	BRIMOR INSULATING COATING. (BRUSHED ON)
3.	COPPER LEAD.
4.	TITANIUM ADAPTOR. (WELDED TO HEATER TUBE.)
5.	HEATER TUBE 1. TITANIUM O/D :- 0·190" 3" LONG 2. S. STEEL O/D :- 0·197" 3" LONG.

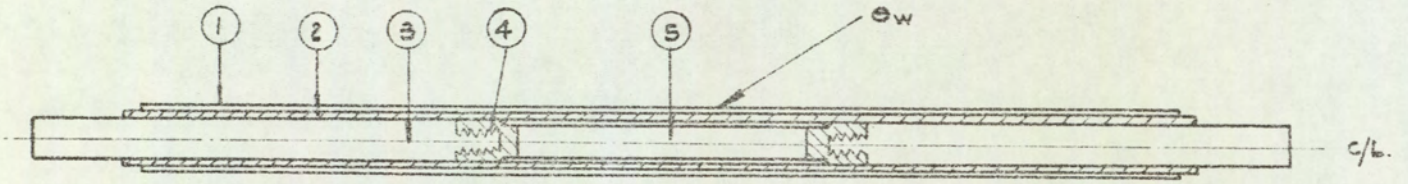

NOTE :- EXPERIMENTAL RATINGS OF 200 WATTS/CM^2 AT Θ_w = 800°C. WITH I = 370 AMPS. V = 7·5 VOLTS.

FIG. 5·1. HEATER ASSEMBLY.

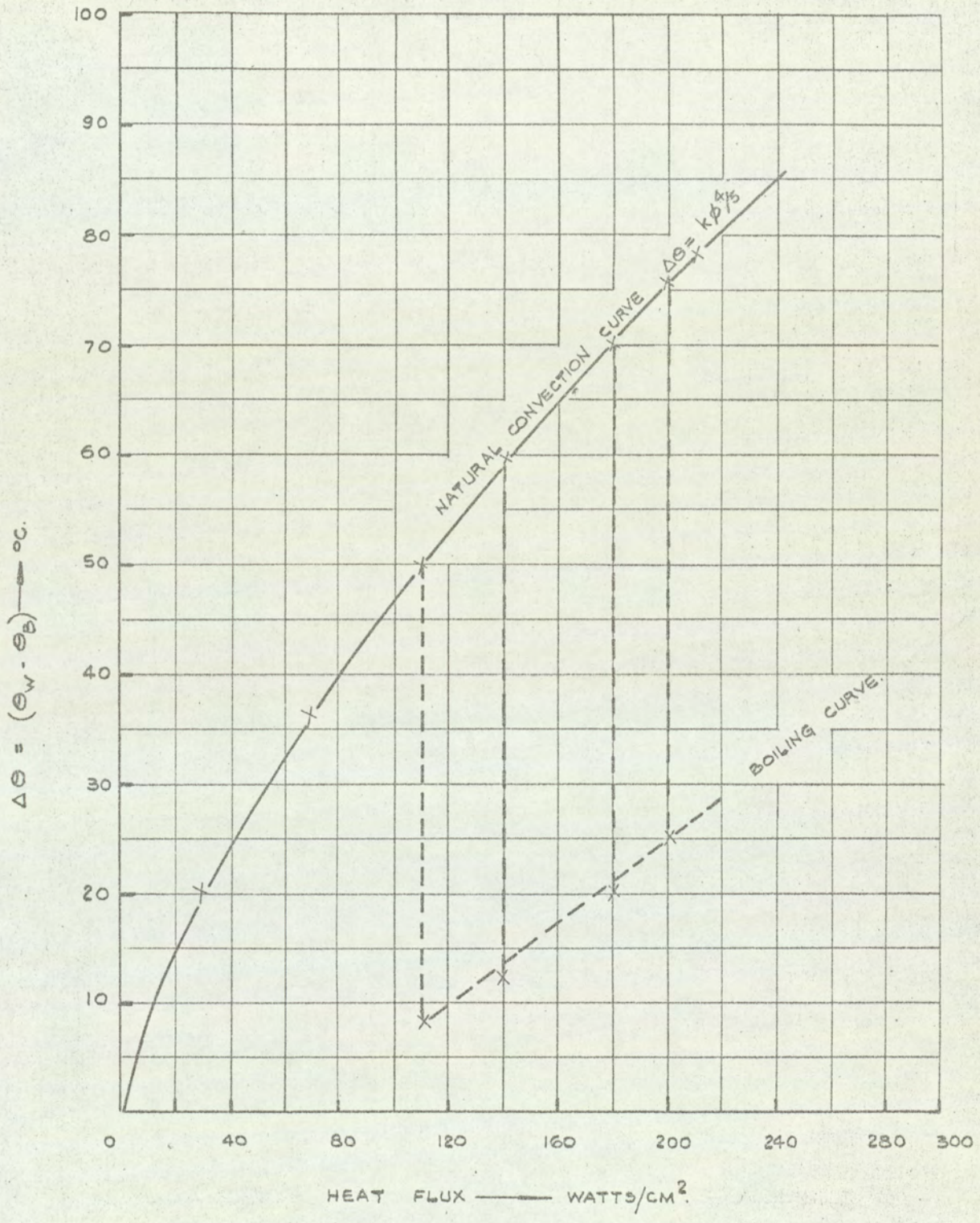

FIG. 5.2 HEAT TRANSFER IN SODIUM — HORIZONTAL TUBE.

FIG 5.2

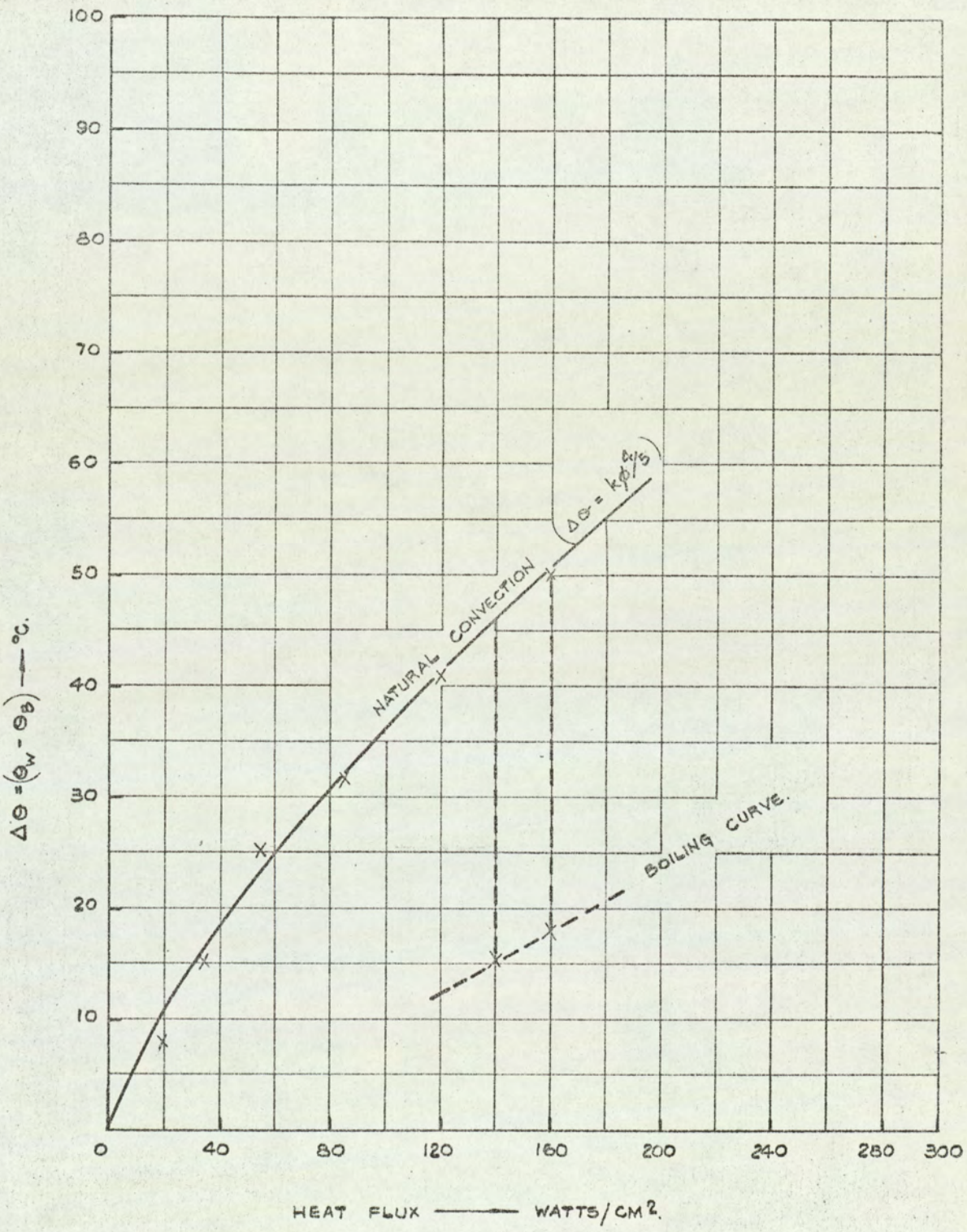

FIG 5.3. HEAT TRANSFER IN SODIUM — VERTICAL TUBE.

FIG. 5.2.

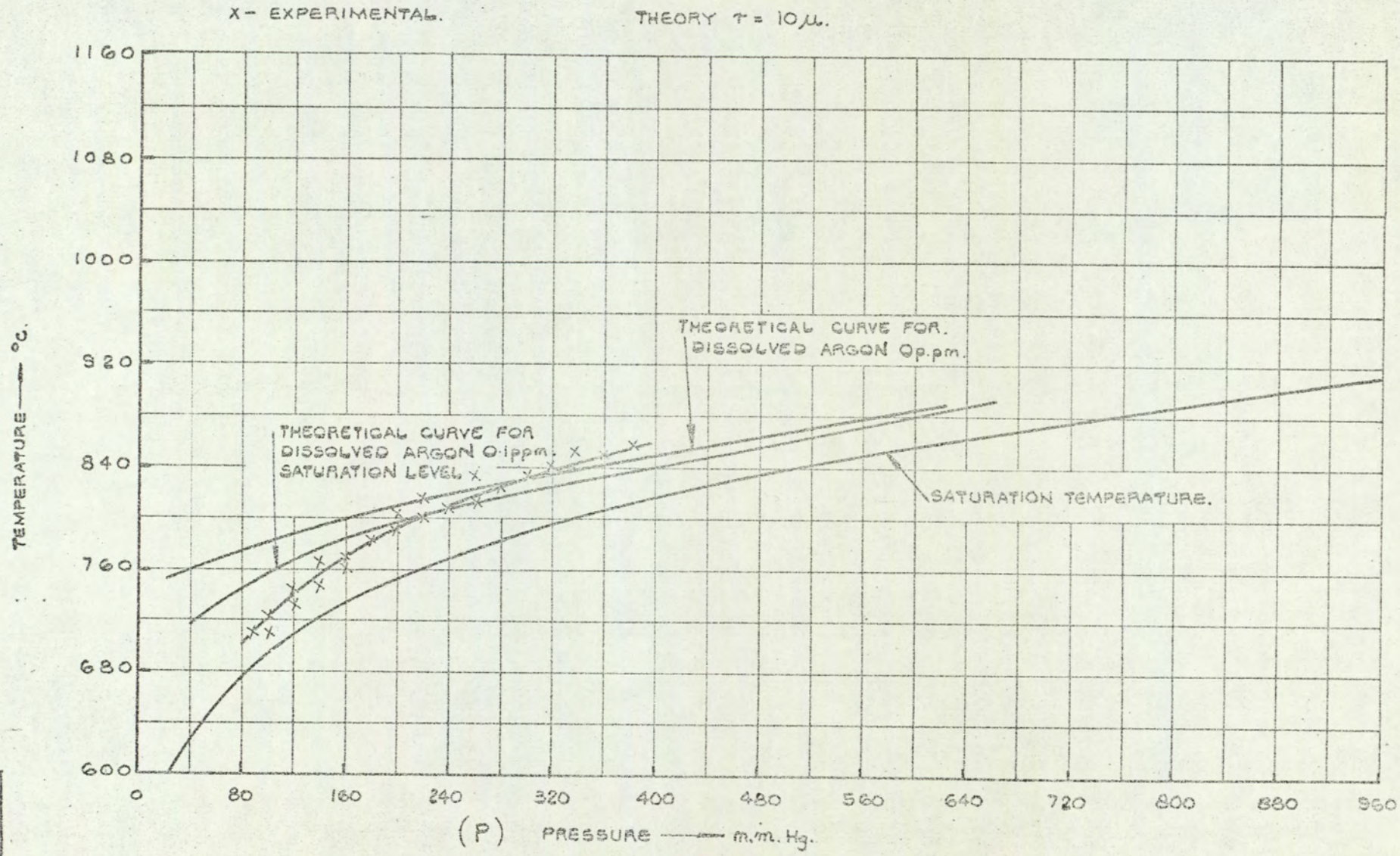

FIG. 5·4

FIG. 5.4 WALL TEMPERATURE NECESSARY FOR THE ONSET OF NUCLEATE BOILING IN SODIUM, horizontal tube,

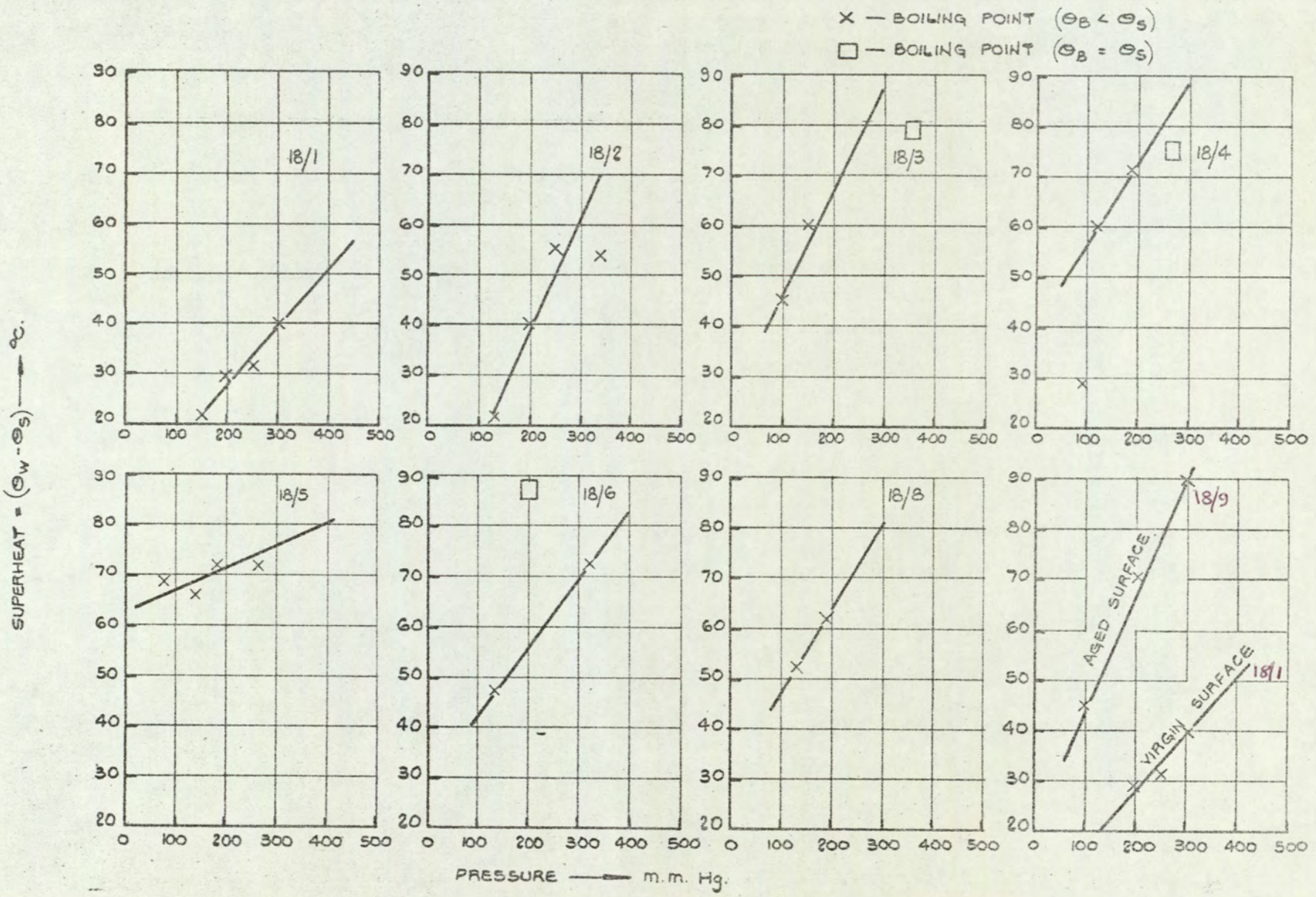

FIG. 5.5 SODIUM SUPERHEAT VALUES FOR HORIZONTAL TUBE.

FIG 5.5

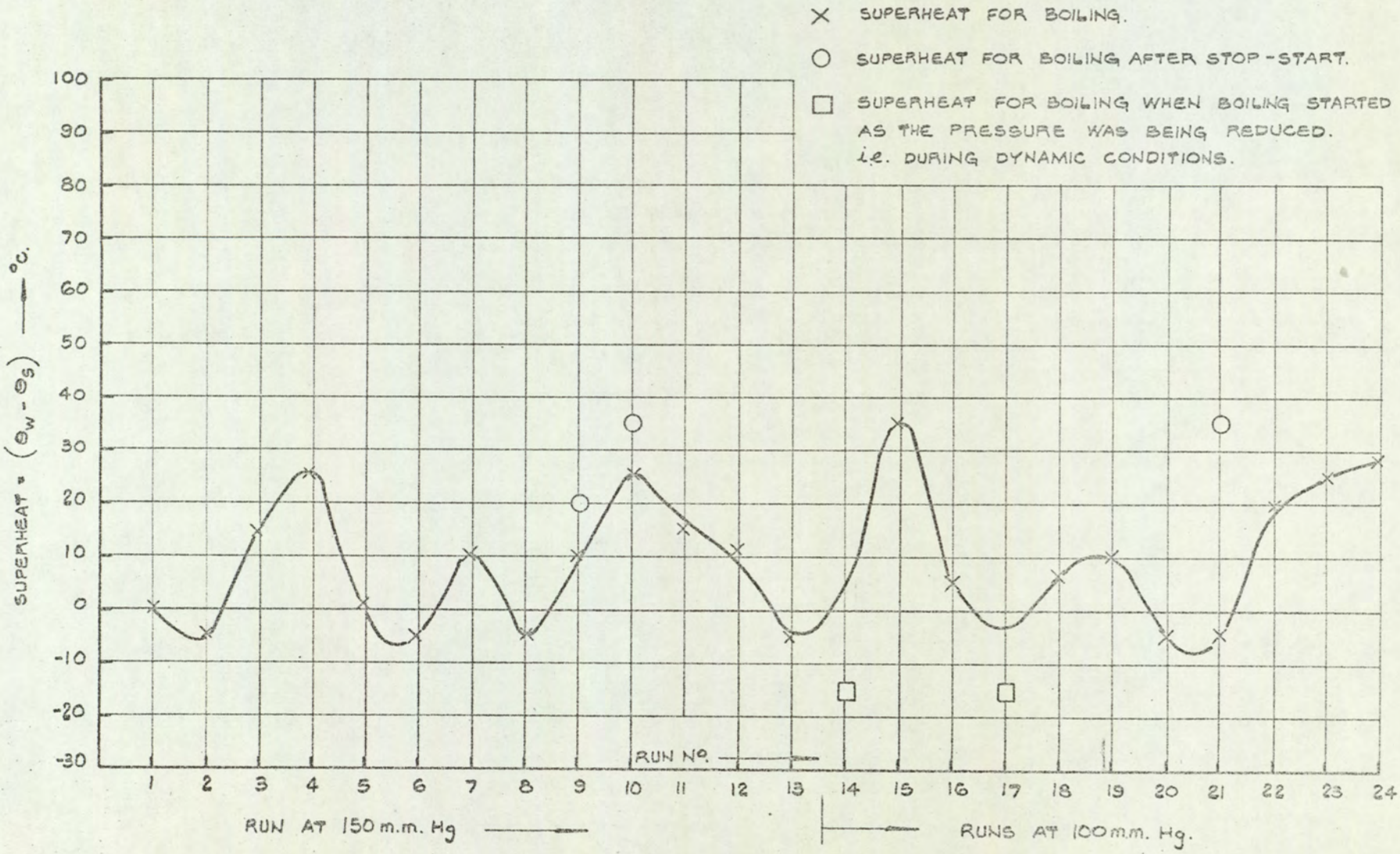

FIG. 5·6

FIG.5·6 TYPICAL VARIATION IN SODIUM SUPERHEAT FOR THE VERTICAL TUBE.

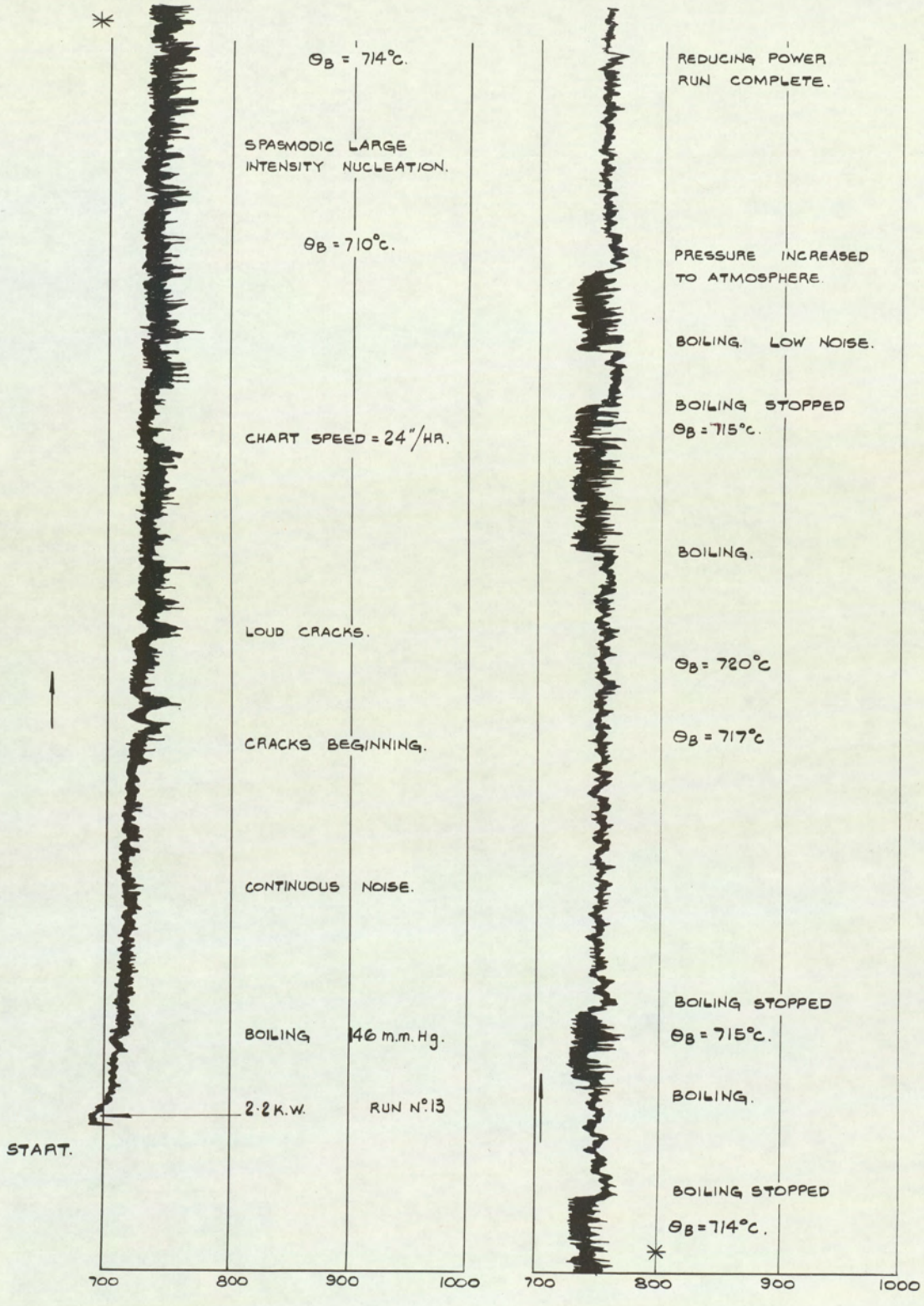

FIG. 5·7. TYPICAL wall TEMPERATURE TIME CHART AT CONSTANT HEAT FLUX AND PRESSURE SHOWING "STOP START" PHENONEMA, CONTINUOUS AND "SPASMODIC" BOILING OF SODIUM. (VERTICAL PIN)

FIG. 5·7

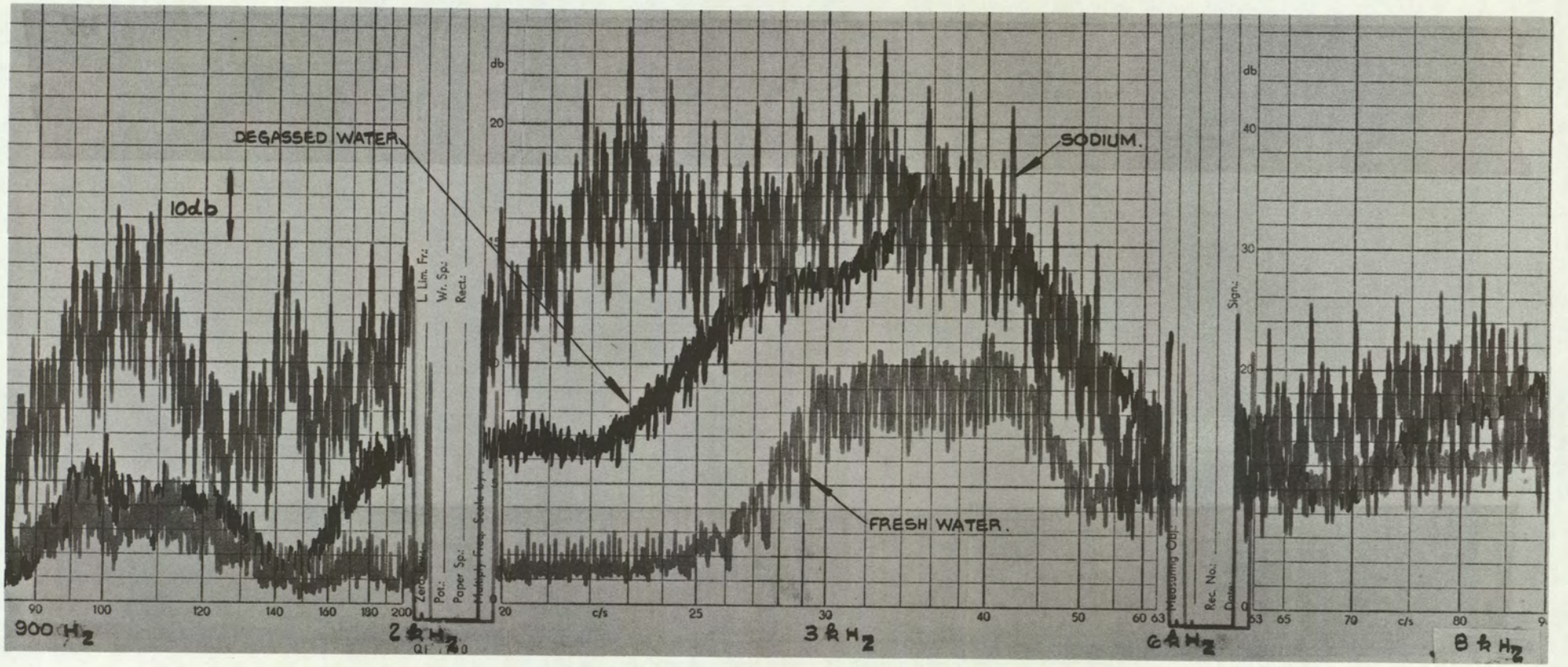

FIG. 5·8. COMPARISON OF THE ACOUSTIC SPECTRA FROM "FRESH" WATER, DEGASSED WATER AND SODIUM AT 40°C. SUB COOLING.

FIG. 5.8

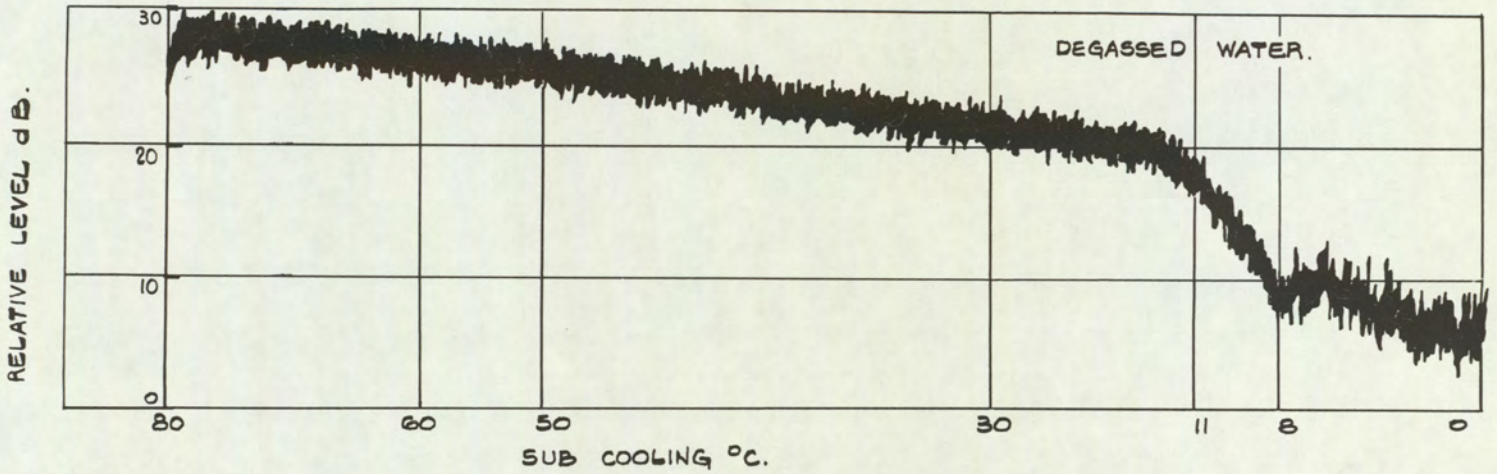

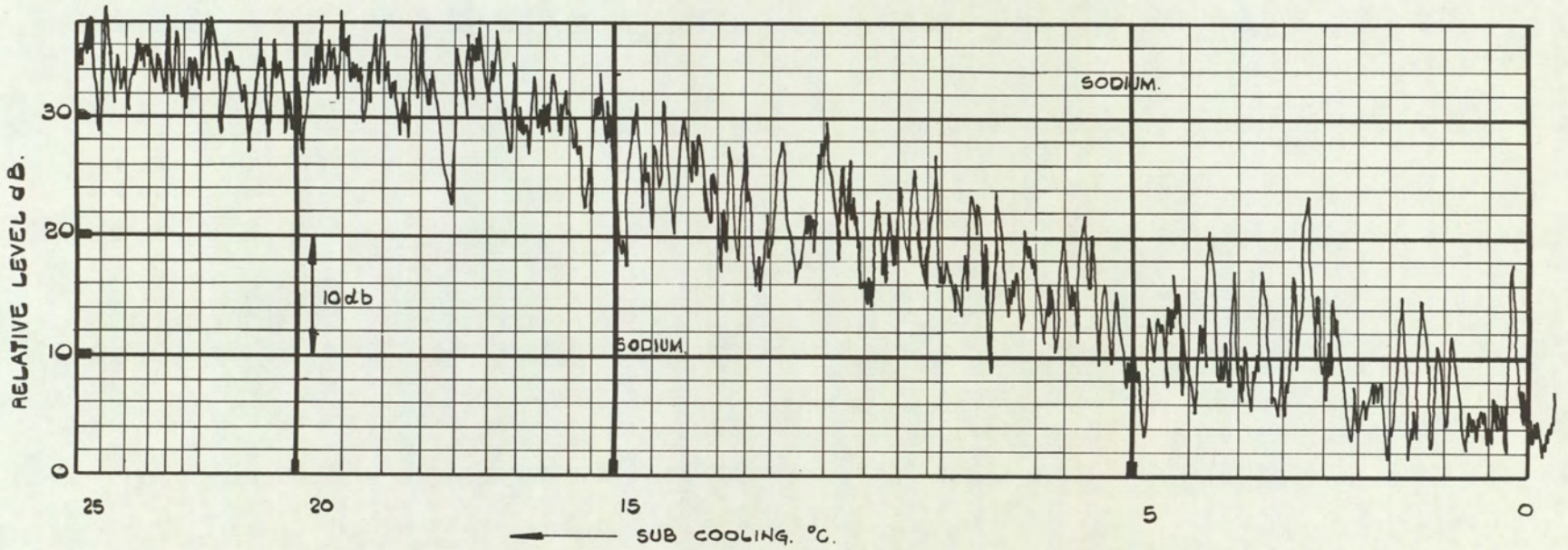

FIG 5.9

FIG. 5.9 COMPARISON OF ACOUSTIC NOISE BETWEEN DEGASSED WATER AND SODIUM AS A FUNCTION OF SUB-COOLING. FREQUENCY APPROX. 3Kc/s.

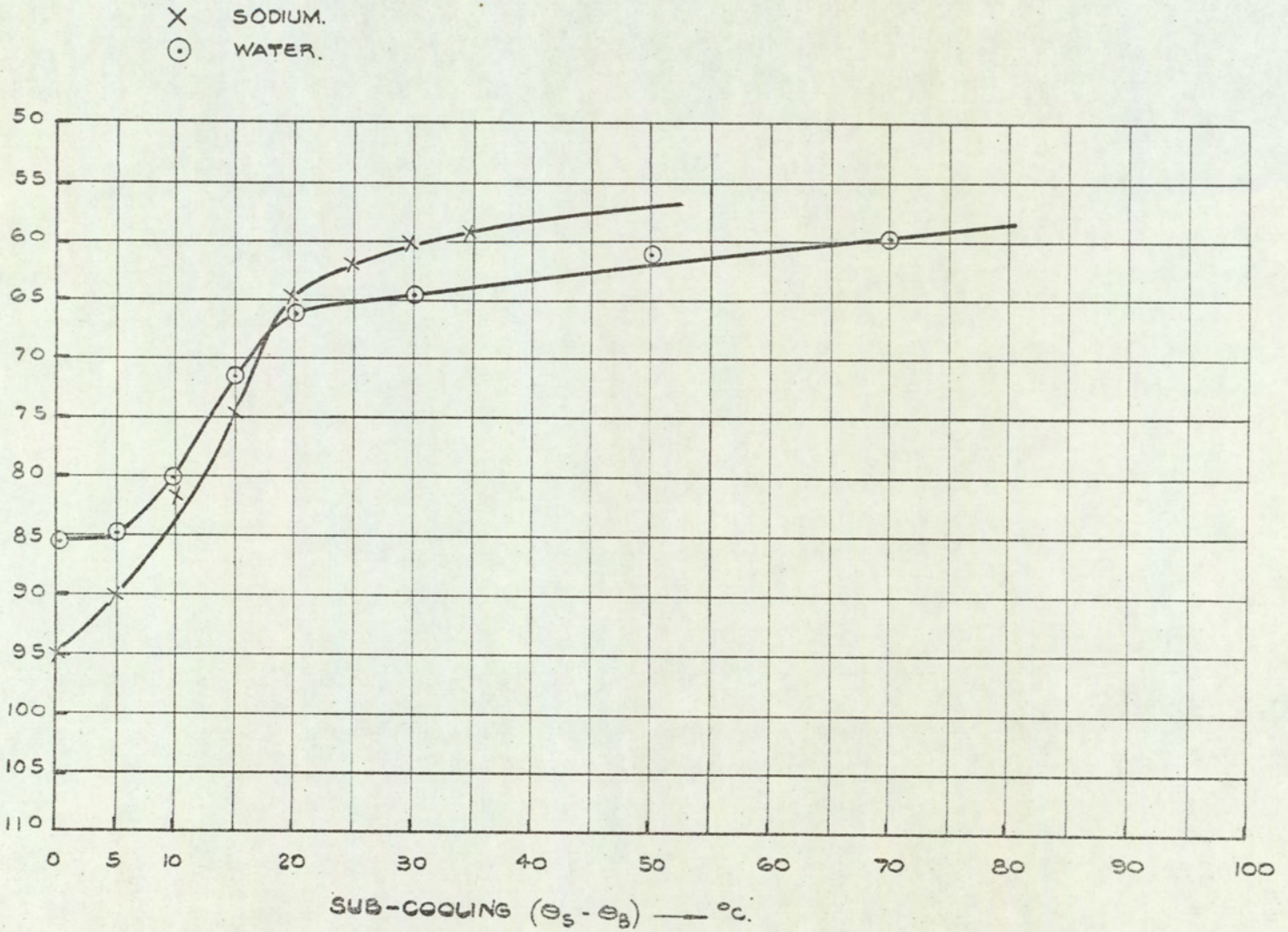

FIG. 5·10

FIG. 5·10. RELATIVE INTENSITY OF WATER TO SODIUM BOILING NOISE AT 3 kc/s.

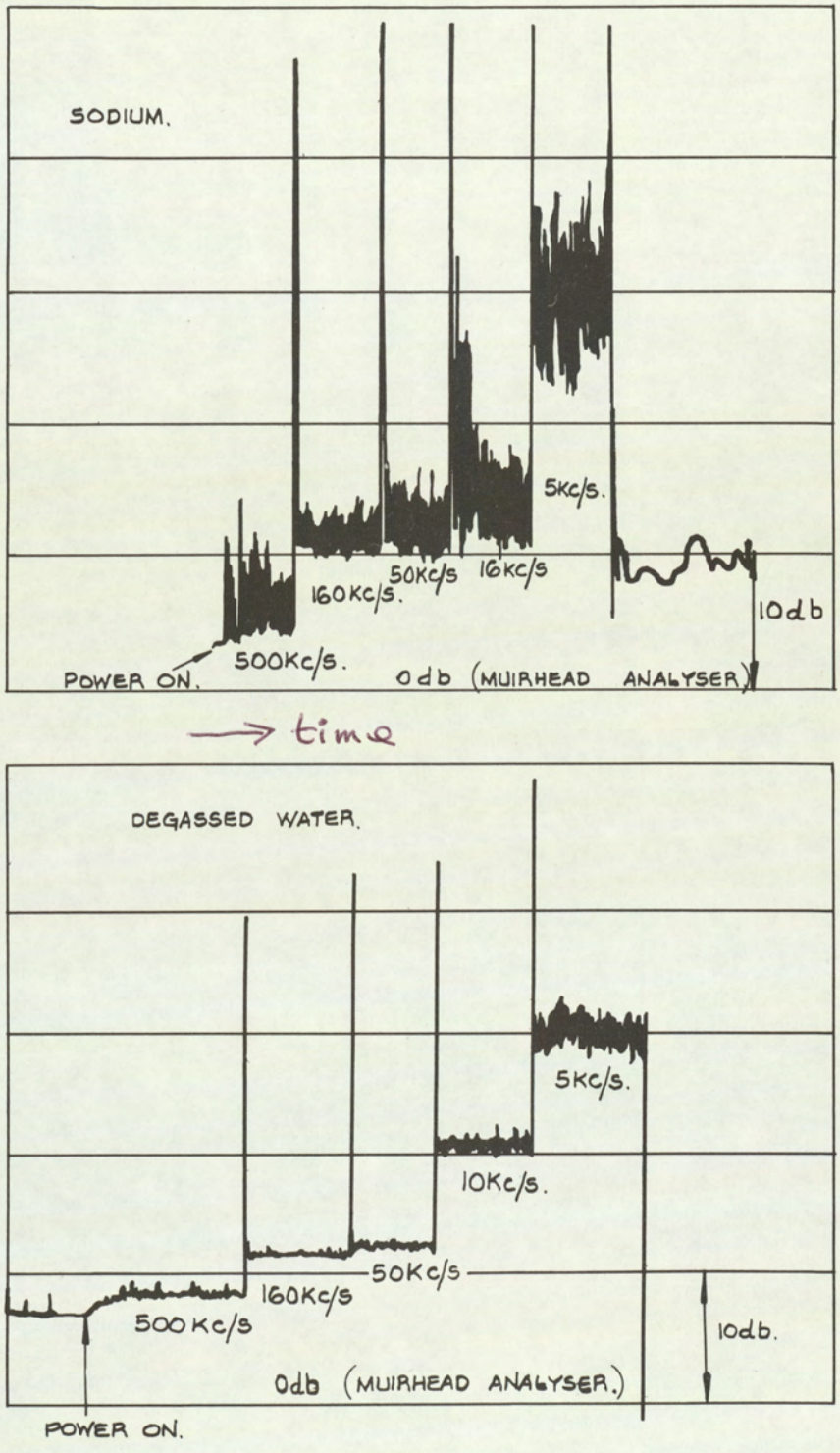

FIG. 5·11. COMPARISON OF ULTRA HIGH FREQUENCY NOISE FROM DEGASSED WATER AND SODIUM AT SAME SUB-COOLING (40°C), GEOMETRY AND HEAT FLUX – (VERTICAL PIN.)

FIG. 5·11.

5.2 Forced Convection Experiments Using Water

In order simultaneously to measure and to assess the effect of superposition of turbulent flow noise on boiling noise and to assess the influence of flow on the boiling process forced convection experiments were carried out, one using water as a coolant. The water experiment is basically simple and is shown in diagrammatic form in Figure 5.12. The acoustic emission was detected using acoustic wave guides following lines along which it is envisaged that wave guides will be used in nuclear reactors. The resulting comparison between flow noise and boiling noise are shown in Figures 5.13 and 5.14. It is interesting to note that the flow noise falls off as the frequency increases whereas the boiling noise tends to increase as the frequency increases. On the basis of this sort of test it would be reasonable to assume that the signal to noise ratio for the detection of boiling in a flowing system is enhanced if the detection is made at a higher end of the frequency spectrum.

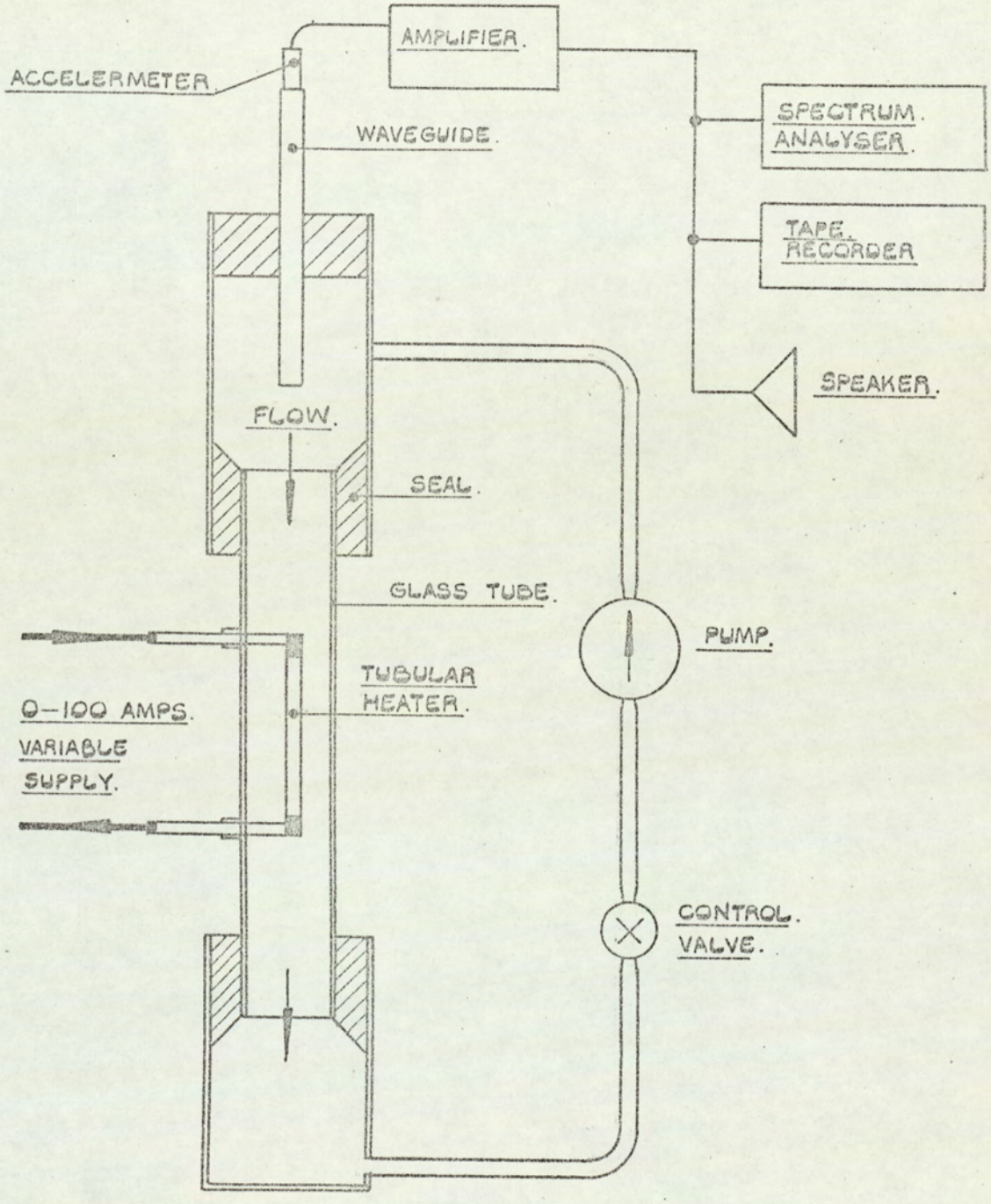

FIG 5·12 BLOCK DIAGRAM OF FORCED CONVECTION WATER EXPERIMENT.

FIG 5·12

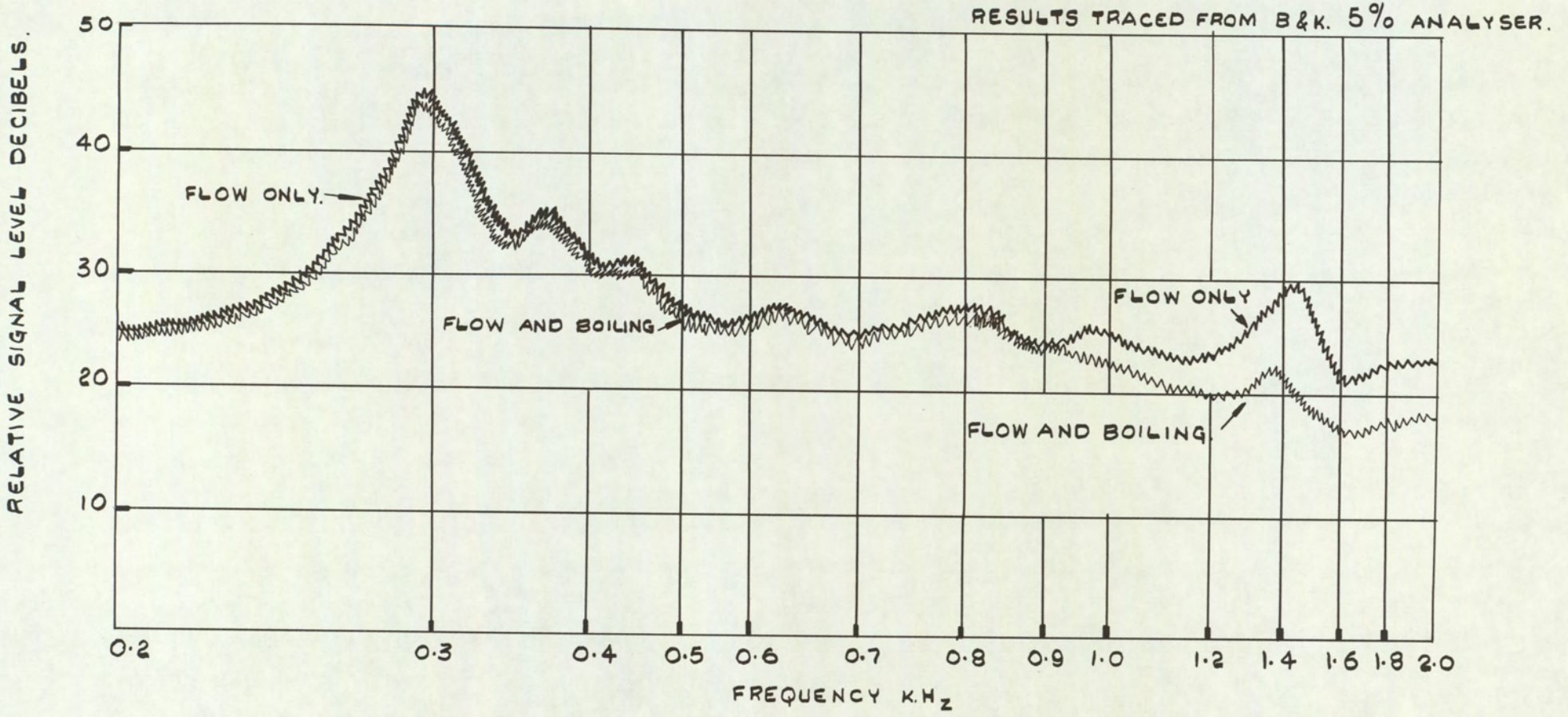

FIG. 5·13 COMPARISON BETWEEN FLOW NOISE AND FLOW AND BOILING NOISE IN A WATER LOOP.

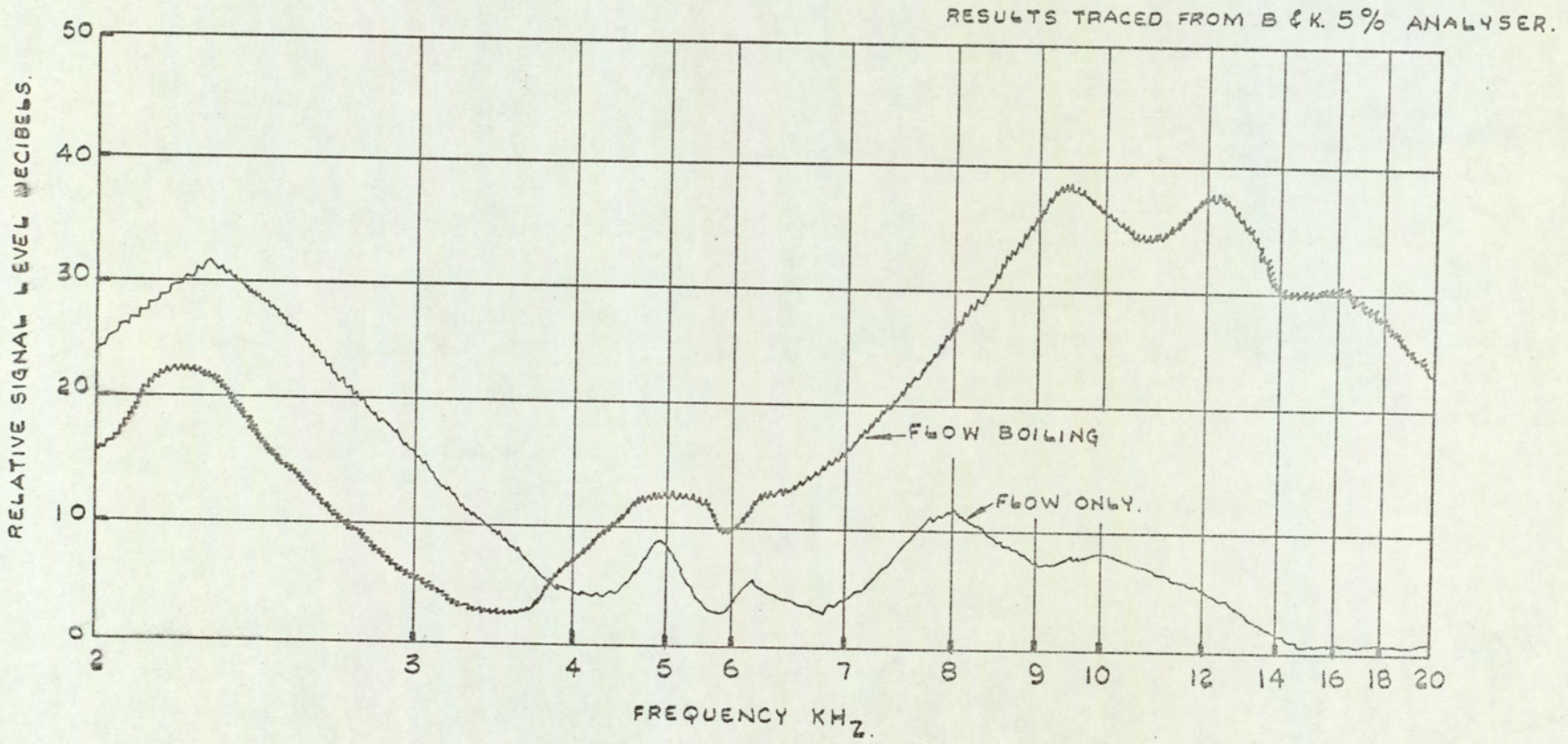

FIG 5·14. COMPARISON BETWEEN FLOW NOISE AND FLOW AND BOILING NOISE IN A WATER LOOP.

FIG. 5·14.

5.3 Forced Convection Sodium Experiment

In order to obtain direct experience of the detection of the boiling process in liquid sodium, an experiment was carried out in a pumped sodium loop at the D.E.R.E. laboratories. This loop is known as the 4 inch loop simply because the pipe work is mainly 4 in. in diameter.

5.3 a) Description of Rig

The 4 in. loop at D.E.R.E. is a conventional figure-of-eight liquid metal rig with an electromagnetic pump circulating the metal 70/30 NaK. The specimen chamber is nominally 12 in. inside diameter and can accommodate rigs up to 9 ft. 0 in. long. The method of mounting test rigs in the specimen chamber is to hang the rig from the specimen chamber sealing flange. The experimental sub-assembly was mounted in this manner (see Figure 5.15) but as it is fairly complex it has a sealing flange as an integral part of the assembly.

The working section makes up the bulk of the assembly and consists of a wrapper channel into which are mounted electrical heaters. The wrapper channel which is approximately 48 in. long and 5 in. in diameter is constructed in four sections and manufactured from solid stainless steel. Machining of the wrapper channel is such that when the dummy heaters are mounted in place they form the same flow channels round the nine electrical heaters, representing fuel pins, as exists in a typical fuel pin sub-assembly (see Figure 5.16). The heaters are of the electrical resistance type and their construction is simply concentric stainless steel tubes with magnesium oxide as an insulant. To achieve the 0.23 in. diameter required to simulate fuel rods the heaters were swaged down from standard material. Grids hold the heaters in position relative to one another and to the dummies in the same manner as in the typical fast reactor fuel assemblies. Once clear of the wrapper channel the heaters are joggled and carried through the inlet containment and sealing flange to where the electrical connections can be made.

The inlet containment was fitted to make sure that no by-pass existed on the inlet to the assembly. To achieve this everything passing through the top flange has to be sealed. This was done by fitting stainless steel olives and clamp nuts.

As the specimen chamber sealing flange is the container for the liquid metal and gas blanket, all joints at this level as far as possible were welded. The exceptions were thermocouples which were brought through the standard type of stainless steel olive gland. As well as the thermocouples, there is mounted on the assembly pressure transducers, monitoring the inlet and outlet pressure of the wrapper channel, and accelerometers for picking up the signal produced by boiling.

5.2 b) Experimental Procedure

The control of the power input to the dummy sub-assembly is via nine thyristors, three in parallel on each of the three phase systems. The power can be smoothly controlled over the range zero to about 120 kw. The upper limit is set by the heat rejection capabilities of the rig.

The experiment was carried out by setting the power to a fixed value (18 kw) and gradually reducing the flow noting the outlet temperature profile as measured by the thermocouples whose position is shown in Figure 5.17. When it was clear that the results obtained from the thermocouples agreed with a simple heat balance calculation it was assumed that the rig was functioning correctly. The power was then increased to 36 KW, and the procedure repeated and again heat balance calculations indicated satisfactory performance of the rig.

The rig was now judged to be in a reliable state of operation and it was decided to try to produce coolant boiling. The power was set to zero and the flow through the assembly set constant at 2 gallons/min. The power was then smoothly increased until the sound of boiling was clearly heard over the monitoring system. The temperature indications were also consistent with the hypothesis that coolant boiling was taking place. The power was kept constant at the level necessary to maintain

boiling. This level was about 89 kW. Recordings were then taken from the installed instrumentation for subsequent analysis.

Instrumentation

The instrumentation used in this experiment is shown schematically in Figure 5.18. The pressure transducers were conventional unbonded strain gauge types manufactured by Solartron. The accelerometers used were piezo-electric type manufactured by Bruel and Kjaar. The low frequency accelerometer had a natural frequency of about 35 kHz and a sensitivity of 50 mV/g. The high frequency accelerometer, which was mounted on an acoustic waveguide, had a natural frequency of 125 kHz and a sensitivity of 10 mV/g. The acoustic waveguide was suspended from the top flange by an antivibration mounting and was bent so that the bottom end entered the specimen chamber at the end of the heated pin outlets, a position at which boiling was most likely to be initiated.

The acoustic signals were recorded on an Ampe type 1300 and Ferrograph tape recorders as well as being analysed on line by a Muirhead and Bruel and Kjaer spectrum analysers.

Void fraction measurement at the channel outlet was determined by a gamma attenuation system using a cobalt 60 source and a scintilation counter as a detector.

Temperature measurement inside the heated channel was made by 48 ½ mm dia. chromel-alumel stainless sheathed thermocouples. The outputs of these thermocouples were displayed on 3 x 16 point recorders, whilst the most important of these (outlet position) were also fed into a 16 channel tape recorder.

Experimental Results

The results of this experiment are shown in tabular form in Table I and Figures 5.19, 5.20, 5.21 and 5.22.

Discussion of Results

Table I shows the relationship between input power and outlet temperature is effectively summarised in Figure 5.19. The temperature distribution immediately flattens as boiling commences; this is thought to be due to the increased heat transfer rates when nucleate boiling starts. Further, this temperature is the limit above which the temperature can not rise and as power is increased the effect is simply to bring the edge channels closer to saturation conditions thereby flattening the profile still more.

The maximum temperature at which boiling was initiated was immeasurably different from the normal saturation temperature indicating a total lack of superheat. This was thought to be due to the existence of small gas bubbles continually entrained from the gas blanket by the flow.

The acoustic data presented in Figures 5.20, 5.21 and 5.22 show a marked increase in the signal to noise ratio as the measurement frequency increases. Figure 5.20 in particular shows the existence of measurable frequencies up to 200 kHz, the limit of measurement. The fall of signal at frequencies in excess of about 50 kHz is probably due to the accelerometer response

Conclusions

This experiment suggests that entrained gas bubbles act as nucleation sites and as a superheat inhibitor. It is thought to be most likely that small entrained gas bubbles will exist in a practical reactor system.

The enhancement of the signal to noise measurement at high frequencies is not inconsistent with the observations made with single heated tubes in water. The existence of these high frequencies is consistent with the results obtained from the static sodium boiling experiments reported previously.

SUB-ASSEMBLY OUTLET TEMPERATURES ^{o}C vs POWER AND FLOW

TABLE I

Power K.W.	Flow G.P.M.	Thermocouple Identification Numbers													
		1	2	3	4	5	6	7	8	9	10	11	12	14	15
0	6	383	383	383	383	383	383	383	383	383	383	383	383	383	383
18	6	405	408	426	435	438	426	425	440	426	417	410	435	423	423
18	5	410	413	435	443	445	432	431	445	433	421	415	442	430	430
18	4	415	420	443	455	458	440	440	458	442	430	421	455	438	438
18	3	425	430	460	475	478	455	475	475	460	441	433	473	451	451
18	2	450	450	492	510	512	478	478	507	492	465	455	506	475	475
18	1.33	469	477	527	550	550	508	508	542	525	491	480	542	505	505
18	1	487	497	550	575	575	530	530	566	556	516	505	562	528	526
18	0.67	508	520	580	610	602	555	555	595	590	547	530	588	552	550
18	0.33	518	533	595	621	600	568	568	598	605	563	548	591	565	560
36	6	432	436	467	480	485	466	465	490	472	450	437	485	458	458
36	5	440	446	482	495	503	480	479	507	487	461	447	500	471	471
36	4	452	460	500	518	528	498	497	530	507	475	460	522	486	486
36	3	471	478	530	555	565	523	523	565	537	498	481	555	510	510
36	2	500	513	584	620	625	562	563	615	592	538	517	605	550	550
36	1.33	545	556	638	683	681	613	613	670	666	590	565	658	600	595
36	1	575	590	685	730	727	655	655	720	720	630	603	680	635	630
36	0.67	612	630	735	790	791	710	714	788	788	685	655	727	682	675
0	2	435	435	435	435	435	435	435	435	435	435	435	435	435	435
17	2	490	490	517	537	546	521	517	544	530	508	496	535	515	515
36	2	545	550	606	650	668	610	605	675	645	585	563	648	605	606
53	2	585	595	676	741	748	680	674	774	730	631	602	721	668	666
63	2	610	623	720	795	797	717	710	810	795	678	639	777	715	710
71	2	635	646	754	830	847	764	760	845	834	705	660	800	725	721
89	2	720	735	890	902	910	894	890	907	902	811	745	900	888	877

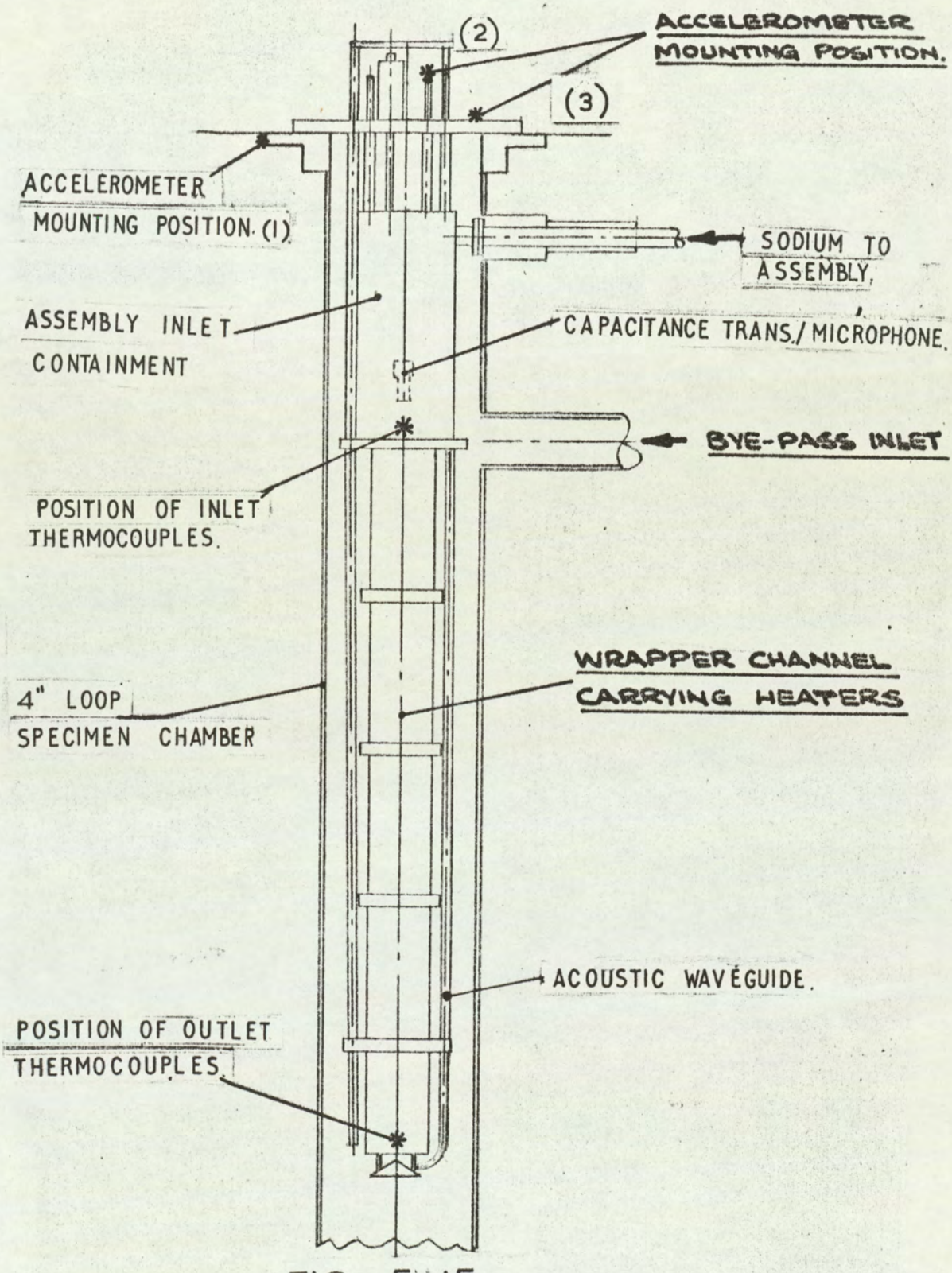

FIG. 5·15.

SKETCH SHOWING 9-PIN SUB ASSEMBLY MOUNTED IN 4"-LOOP SPECIMEN CHAMBER

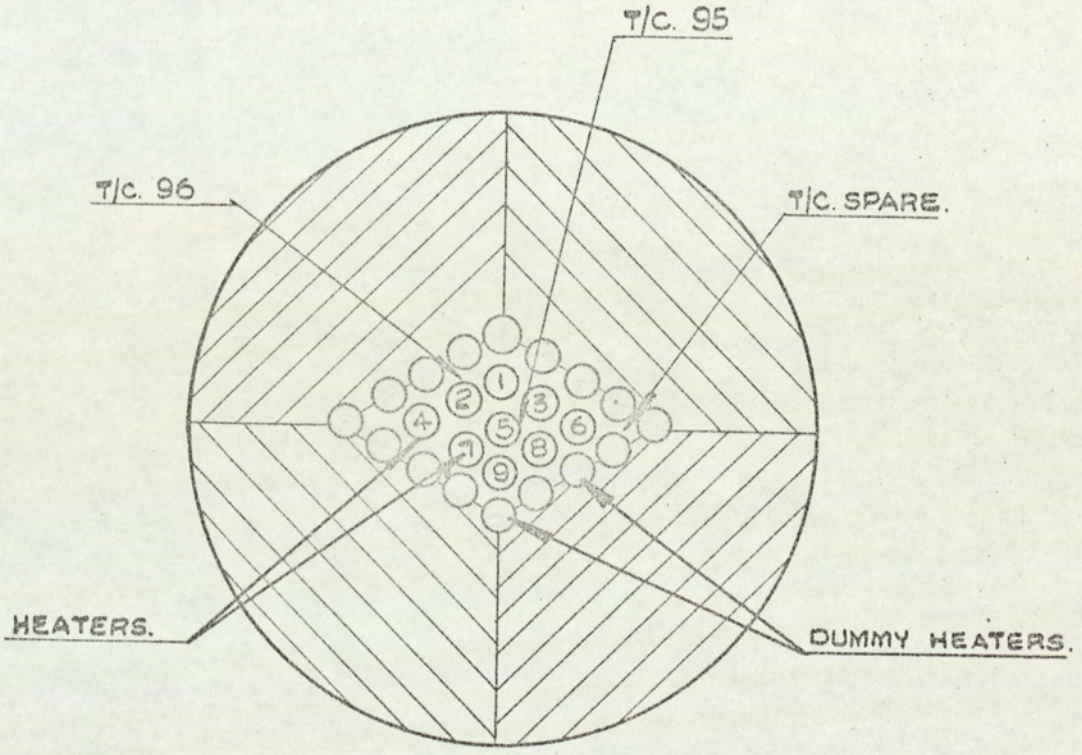

FIG. 5·16 SECTION THROUGH WRAPPER CHANNEL SHOWING RELATIVE POSITION OF OUTLET THERMOCOUPLES.

FIG. 5·16.

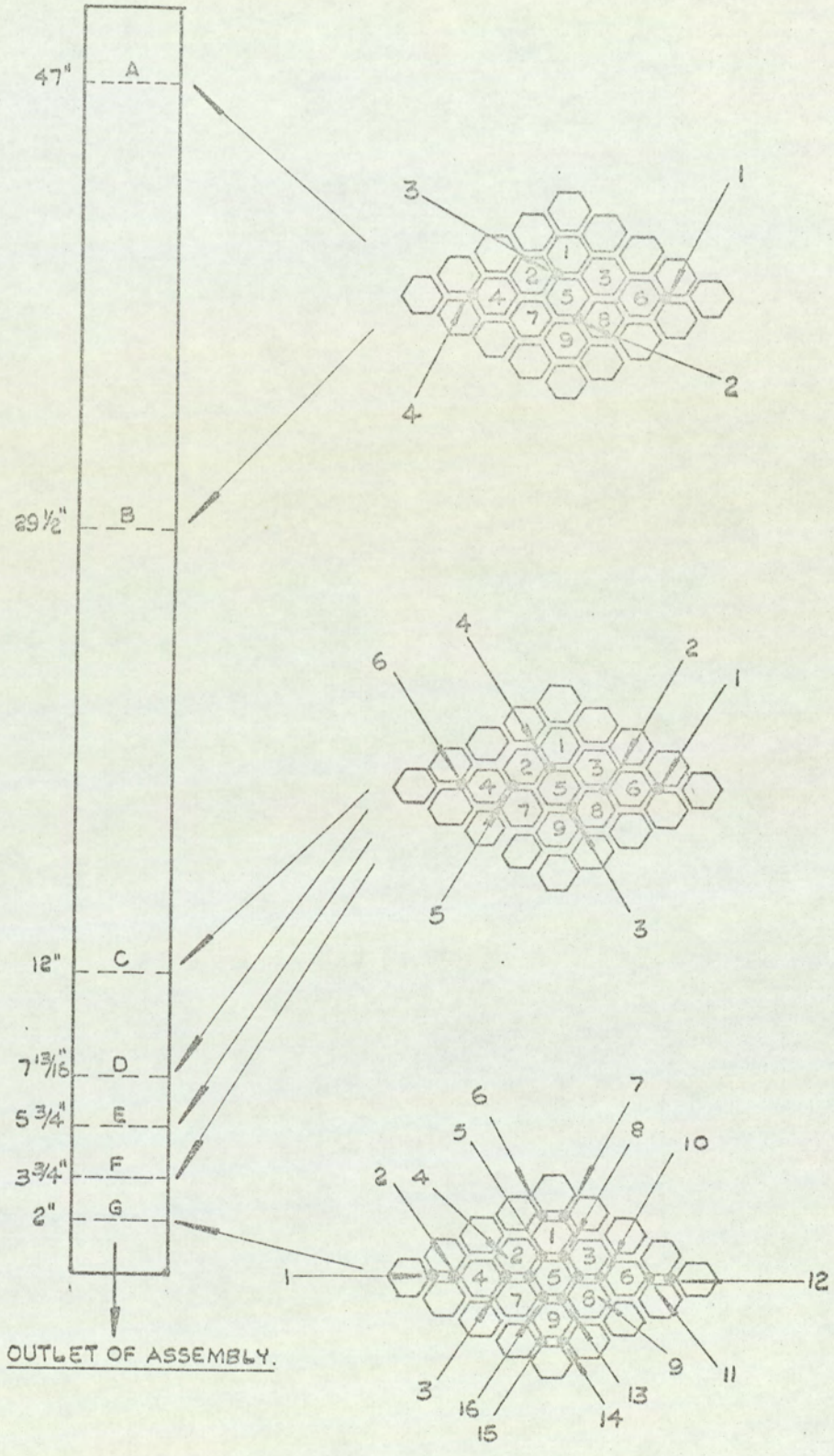

FIG. 5·17 ARRANGEMENT OF 9-PIN SUB-ASSEMBLY WRAPPER CHANNEL THERMOCOUPLES.

FIG. 5·17.

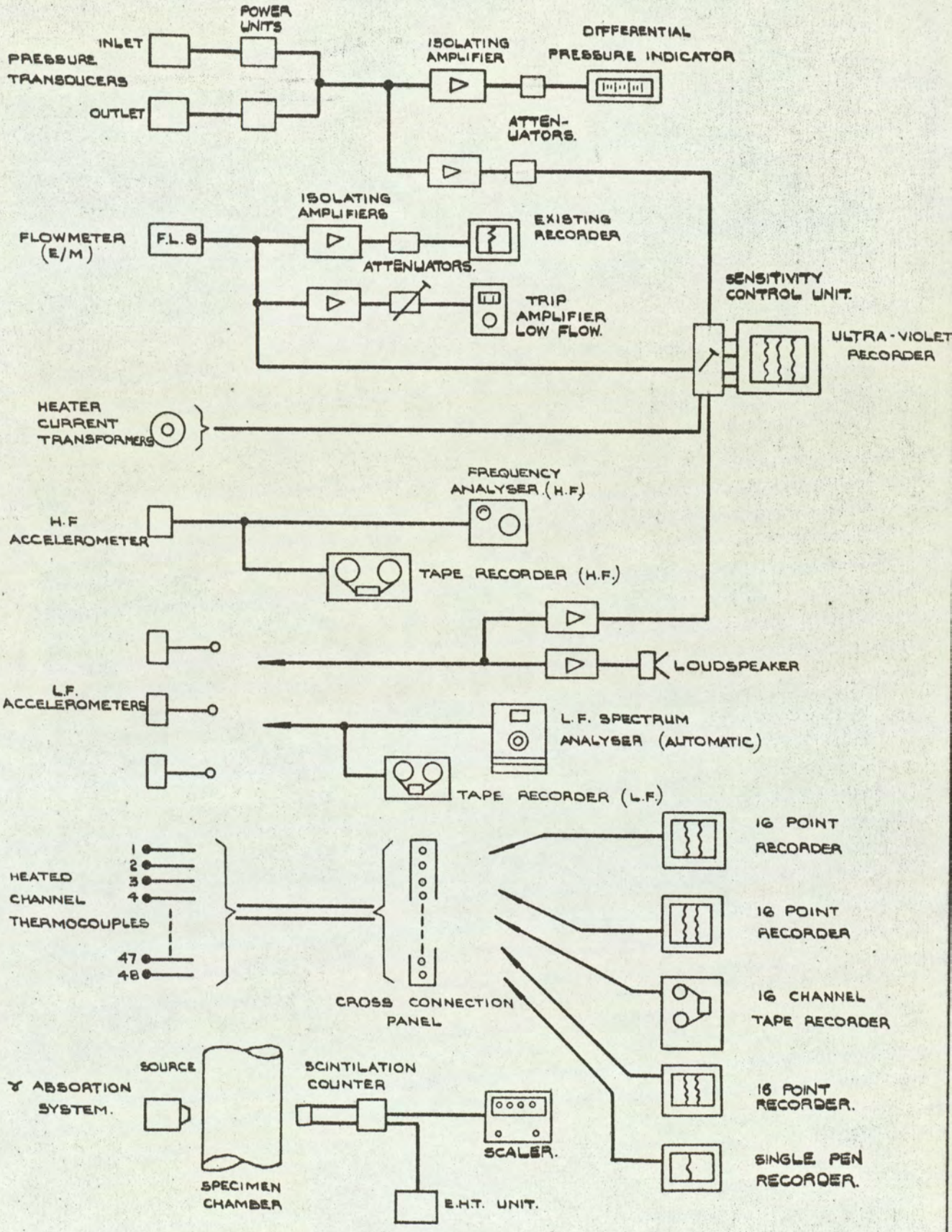

FIG. 5.18. SCHEMATIC LAYOUT OF INSTRUMENTATION.

FIG. 5.18.

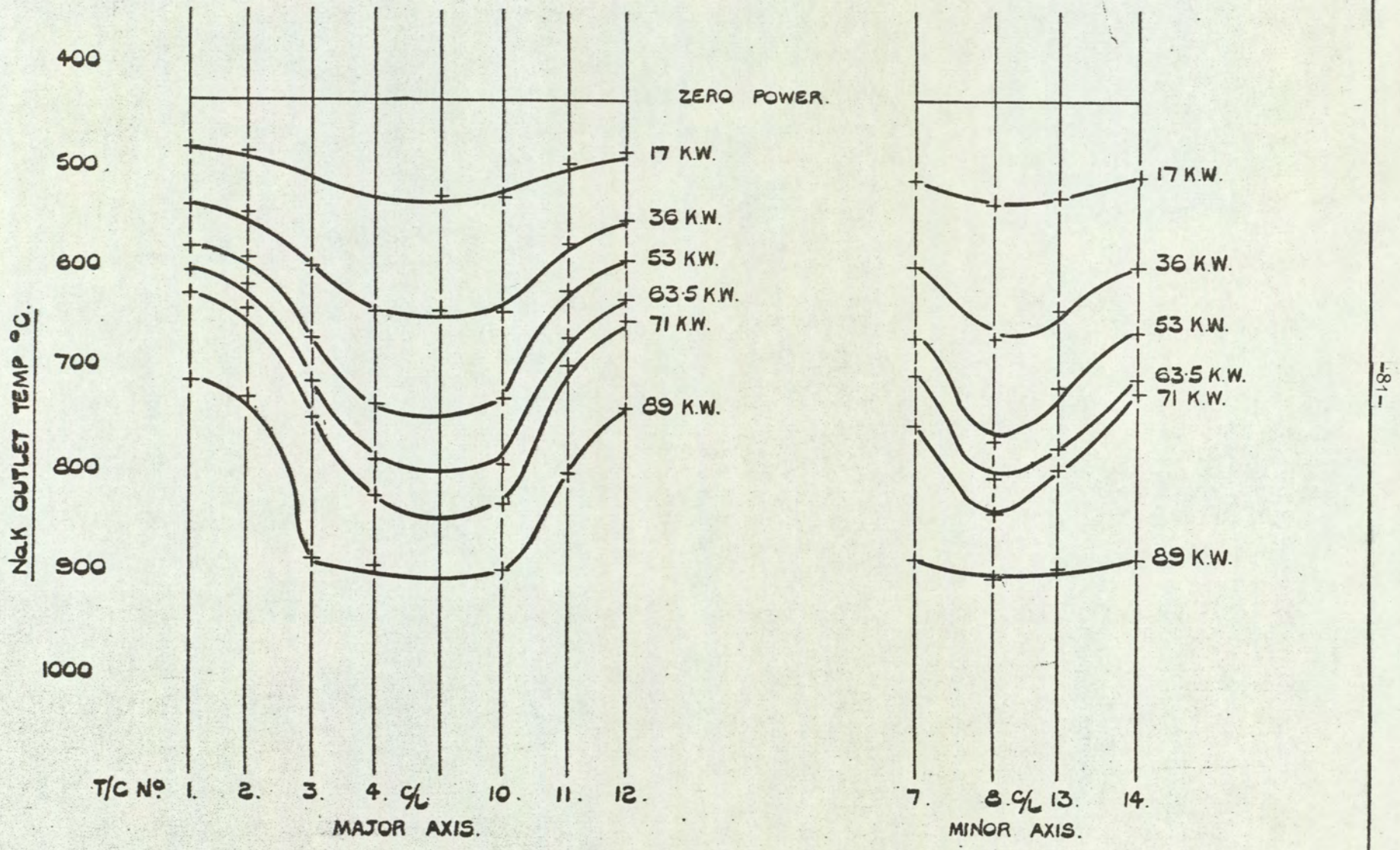

FIG 5·19 OUTLET TEMPERATURE PROFILES BOILING RUN FLOW 2 G.P.M.

FIG. 5·19

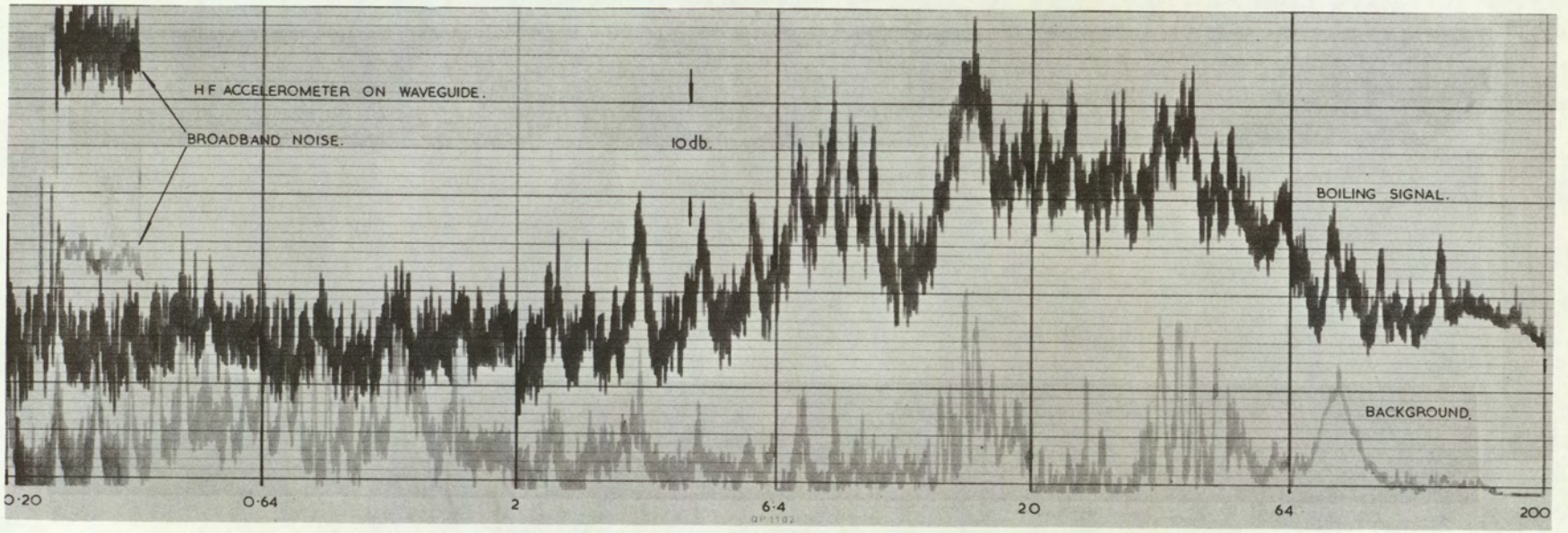

FIG. 5·20

FIG 5·20 COMPARISON OF BOILING AND BACKGROUND SIGNALS Nº 3 TEST 4" LOOP.

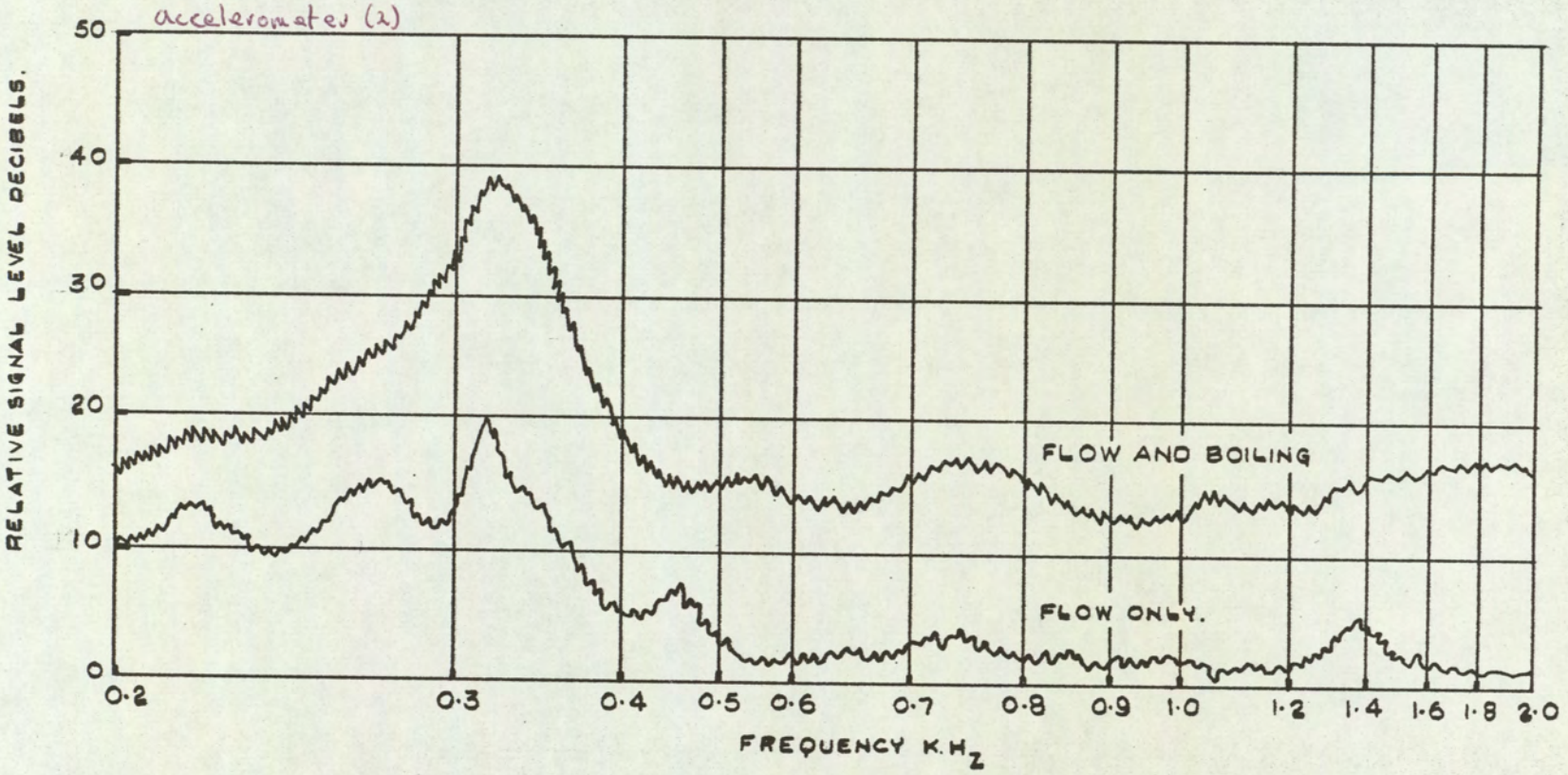

FIG. 5·21. COMPARISON BETWEEN FLOW NOISE AND FLOW AND BOILING NOISE IN A FORCED SODIUM LOOP TEST N° 1.

FIG. 5·21.

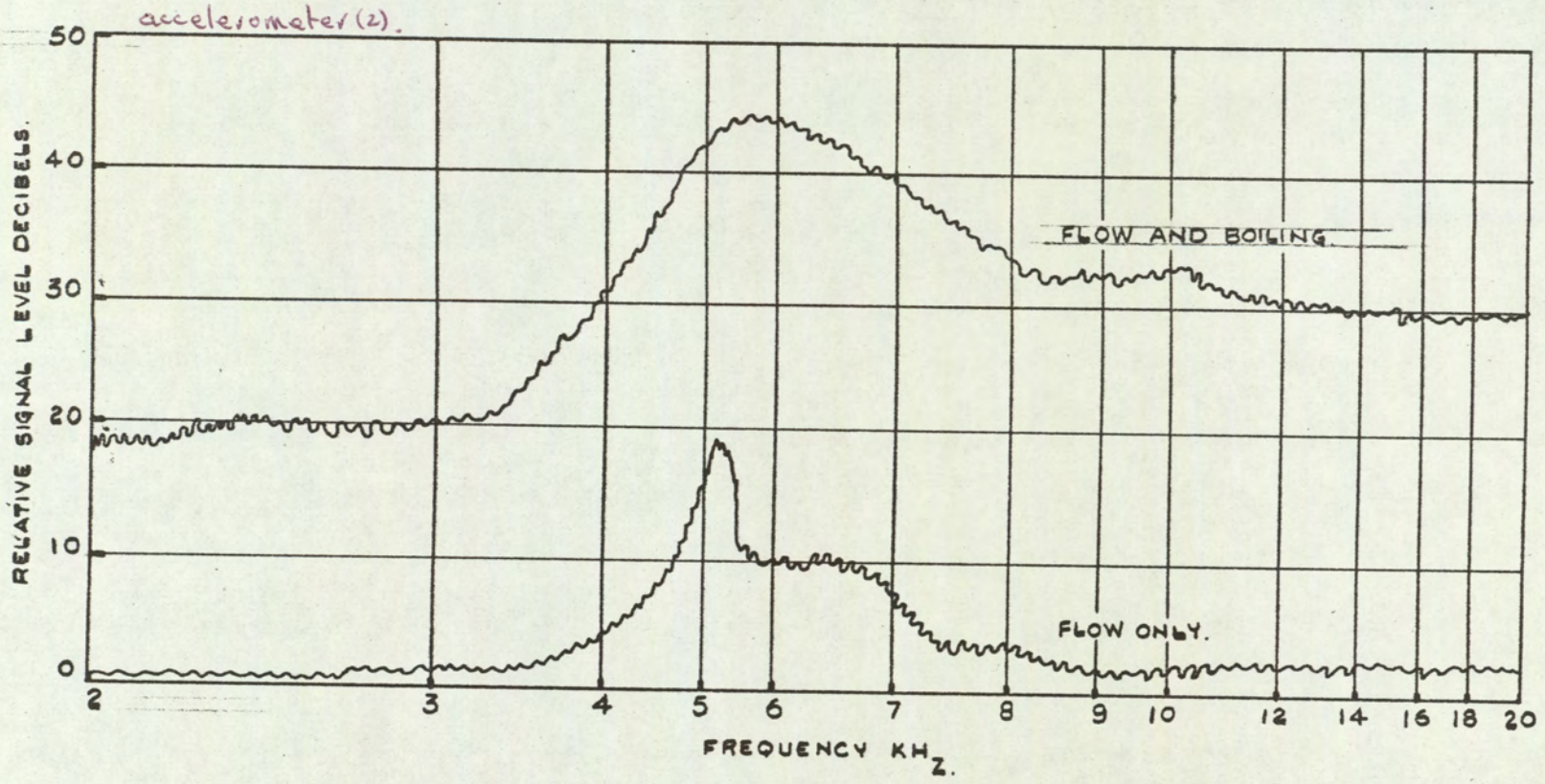

FIG.5·22 COMPARISON BETWEEN FLOW NOISE AND FLOW AND BOILING NOISE IN A FORCED CONVECTION SODIUM LOOP TEST N° 1.

FIG. 5·22.

5.4 Experiments Carried Out in Dounreay Fast Reactor

In order to assess the performance of a proposed instrumentation system to be used to detect the abnormal operation of the fast reactor an experiment was carried out in the D.F.R., firstly to measure the prevailing background noises against which any system would have to complete and secondly, by producing some local boiling within the reactor environment to assess the signal to noise ratio that would exist under fault conditions.

a) Evaluation of the Acoustic Noise System

The monitoring of the "background noise" was a straightforward test, but as the system developed it became increasingly clear that a positive demonstration was required of the waveguides detecting a fault condition, should over-heating and thus nucleate boiling occur. The simulation of a fault condition in the reactor would, therefore, have to be produced.

This simulation was achieved by the introduction of an encapsulated electrical resistance heater through the central hole in the 9 in. charge plug. This meant that the heater capsule, when in position, had the waveguides equispaced round it, and because of the geometry of the reactor core it was possible to lower the capsule to a level below that of the waveguides.

b) Object of the Experiment

(a) To produce nucleate boiling conditions in the capsule and to detect its presence by means of the waveguides.

(b) Once having established that these conditions exist, to show by means of the instrumentation situated in the reactor sphere and control room, that the signal to noise ratio is sufficient to operate the reactor alarm system.

c) Description of the Rig and Instrumentation

The boiling rig was in the form of a thimble with a capsule assembly

at the bottom end. Figure 5.23 shows the assembly of the capsule which consisted of a 0.23 in. diameter resistance heater of equivalent length 5 in. mounted centrally in an inner and outer stainless steel sheath with a gas space between acting as a thermal shield. Three small holes were drilled in the capsule to enable the reactor coolant to enter and also to allow the acoustic "noise" produced to get out. Two thermocouples were fitted inside the capsule, one to monitor the heater sheath temperature, and the other to monitor the bulk liquid temperature in the capsule. There is no outlet for the coolant at the bottom of the capsule thus minimising the convection losses.

The relative position of the capsule to the waveguides and the reactor core is shown in Figure 5.24, as is the equipment required for the loading procedure.

The instrumentation used is shown diagrammatically in Figure 5.25 and consists of a main cable connecting the three waveguides to a selector and amplification rack in the reactor sphere, three leads feeding from the sphere rack to the control room rack which has filter units designed for the frequency range 3-5 Kc/s, signal level meter, signal level recorder, and a two-out-of three alarm unit connected to the reactor alarm system.

Experimental results

The sub-cooling which was present prior to increasing to full power, i.e. at 2.5 kW 115 watts/cm^2, was approximately 125^{o}C. This fell to approximately 25^{o}C when full power, 4 kW (180 watts/cm^2) was reached. Nucleate boiling was heard once the temperature rose to the 850^{o}C mark and continued, though much more spasmodically, until the heater burnt out after the power had been increased to 4.5 kW (200 watts/cm^2). Figure 5.26 shows the "background" noise obtained from a waveguide at reactor shutdown conditions (i.e. 15% flow) superimposed on the "boiling"

noise obtained from the same waveguide. This chart and the chart from the level recorder in the control room showed:

"Background noise" level at 15% flow = -130 dB/3 μV

"Boiling noise" level = -110 dB/30 μV

Therefore Signal level "Boiling/Signal level background = 10:1.

All values are taken for the frequency range 3-5 Kc/s and where necessary the correlation for the use of tape-recorder technique is made; the frequency analyser used 0 dB = 10 V.

Conclusions

The first objective, i.e. to produce nucleate boiling, was achieved, and the detection of the boiling by means of the waveguides was also very successful. The signal received was amplified through a loudspeaker while the experiment was in progress and was clearly audible. A permanent record was also obtained by means of a tape-recorder for analysis, but an attempt to obtain an on-line spectrum was not successful because of the spasmodic nature of the signal.

These records give, for the first time since the programme was started, an insight into the signal levels that could be expected with fault conditions in D.F.R. Although an increase in signal level of 20 dB is very satisfactory, the geometrical conditions prevailing must have attenuated the signal considerably, and an even larger signal/noise ratio could be expected under reactor fault conditions.

5.5 Measurements of Temperature Fluctuations at the Inlet to The D.F.R. Core

It was not possible in the in pile boiling experiment to mount temperature fluctuation detectors downstream of the boiling noise source. As temperature fluctuation cannot possible propagate against the stream the only information that has to date been possible to be obtained in the reactor environment is that of the temperature fluctuations at the inlet of the

reactor system. These fluctuations are, however, very interesting and can provide some means by which the overall performance of thermal noise detection systems may be evaluated. Comparison between the observed frequency spectra as measured by the eddy current detectors and that measured by thermocouples may be made at the low end ~~of the end~~ of the frequency spectrum. Any other comparisons have to be made in out of pile experiments mainly carried on by other workers using such fluids as water, glycerine, mercury, etc. and theoretical predictions as to the shape of the frequency spectrum mainly produced by Bachelor and others.

Figure 4.6 shows the eddy current detector that has been inserted into the inlet stream of the D.F.R., the large one in the photograph being the one used. The impedance fluctuations from this device were detected using the system shown in block diagram form in Figure 6.14. A whole series of measurements under various reactor conditions were made. The results (Figure 5.27) presented in the form of power density as a function of frequency and it was noted that the total RMS fluctuation of temperature is not inconsistent with what has been previously observed by other workers using thermocouples as a detection element. It may further by observed that the limiting slope of the power spectral density curve is approximately that given theoretically by Bachelor and observed experimentally by others. It seems to suggest, therefore, that because the shape of the spectrum is very similar to what has been experimentally observed both in water and mercury that the main source of temperature noise is due mainly to turbulent fluctuations and is less influenced by the eddy diffusivity of the high conductivity sodium.

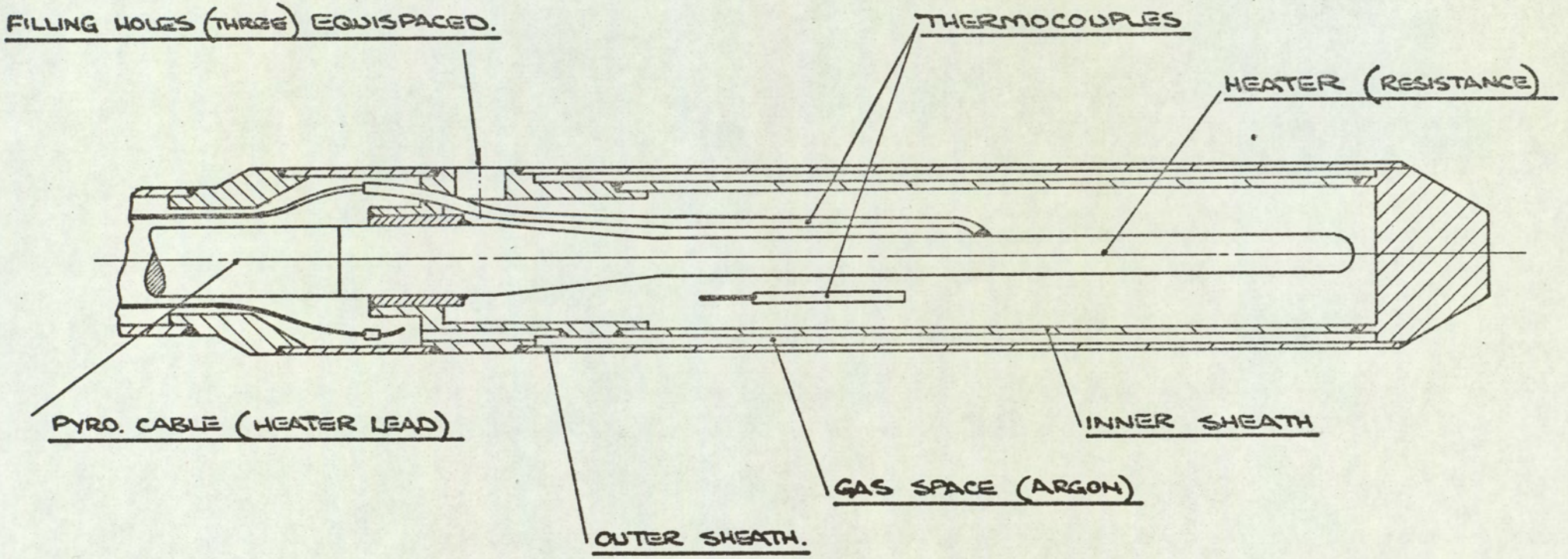

FIG. 5 : 23. SIMULATION OF NUCLEATE BOILING.
HEATER CAPSULE.

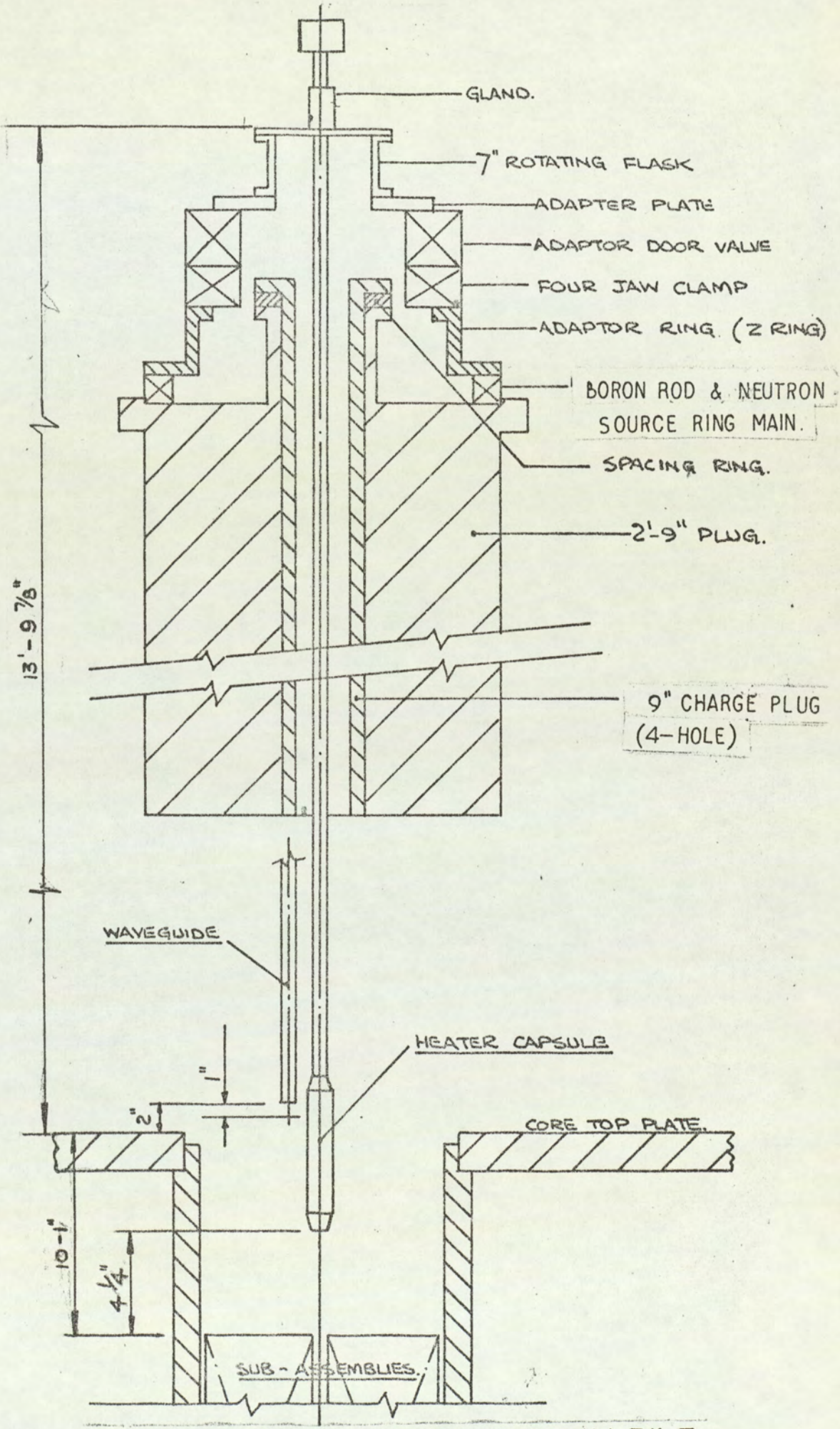

FIG. 5.2.4 ARRANGEMENT OF IN-PILE BOILING NOISE EXPERIMENT.

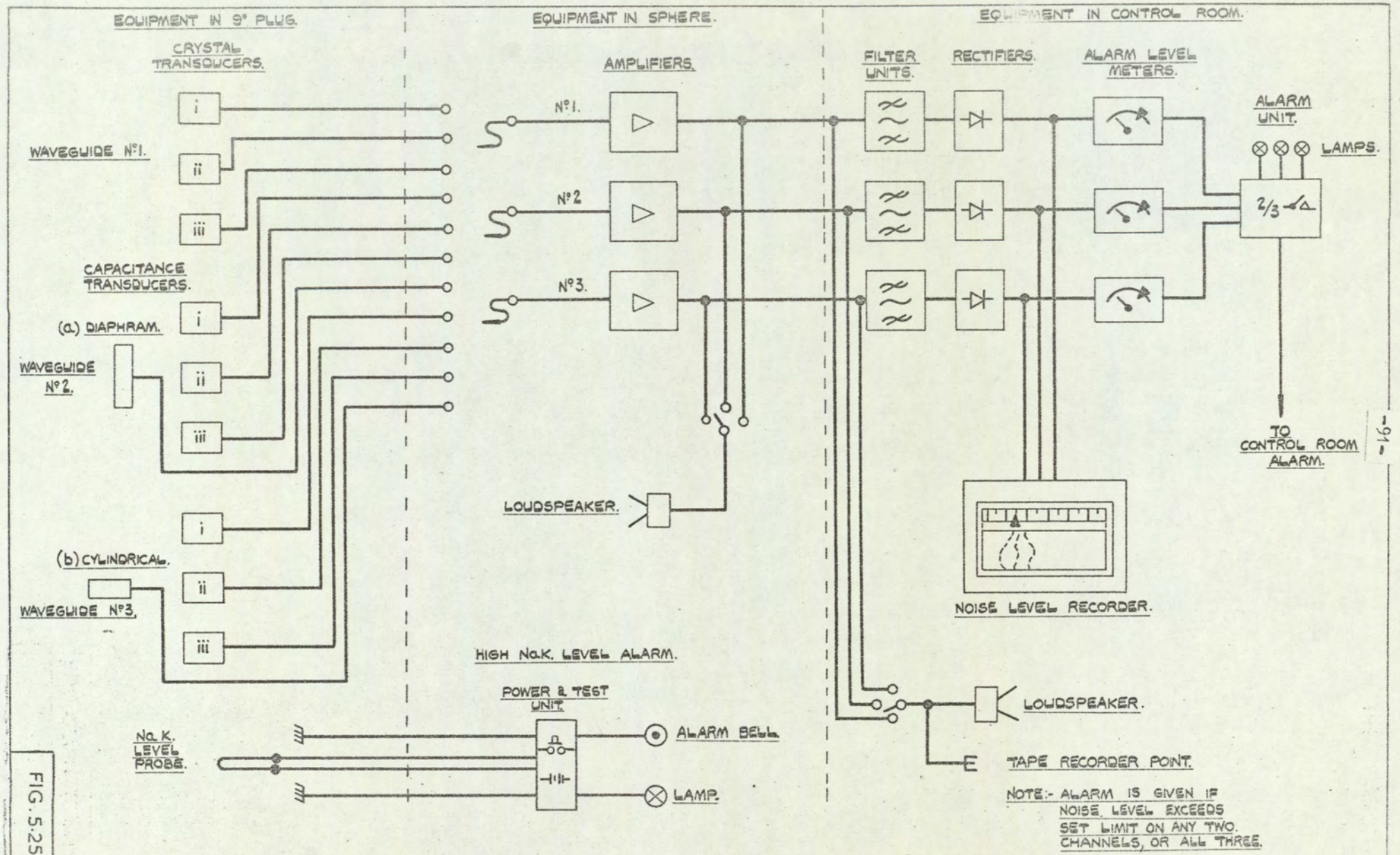

FIG. 5.25.

FIG. 5.25. INSTRUMENTED DIAGRAM FOR BOILING NOISE EXPERIMENT IN D.F.R.

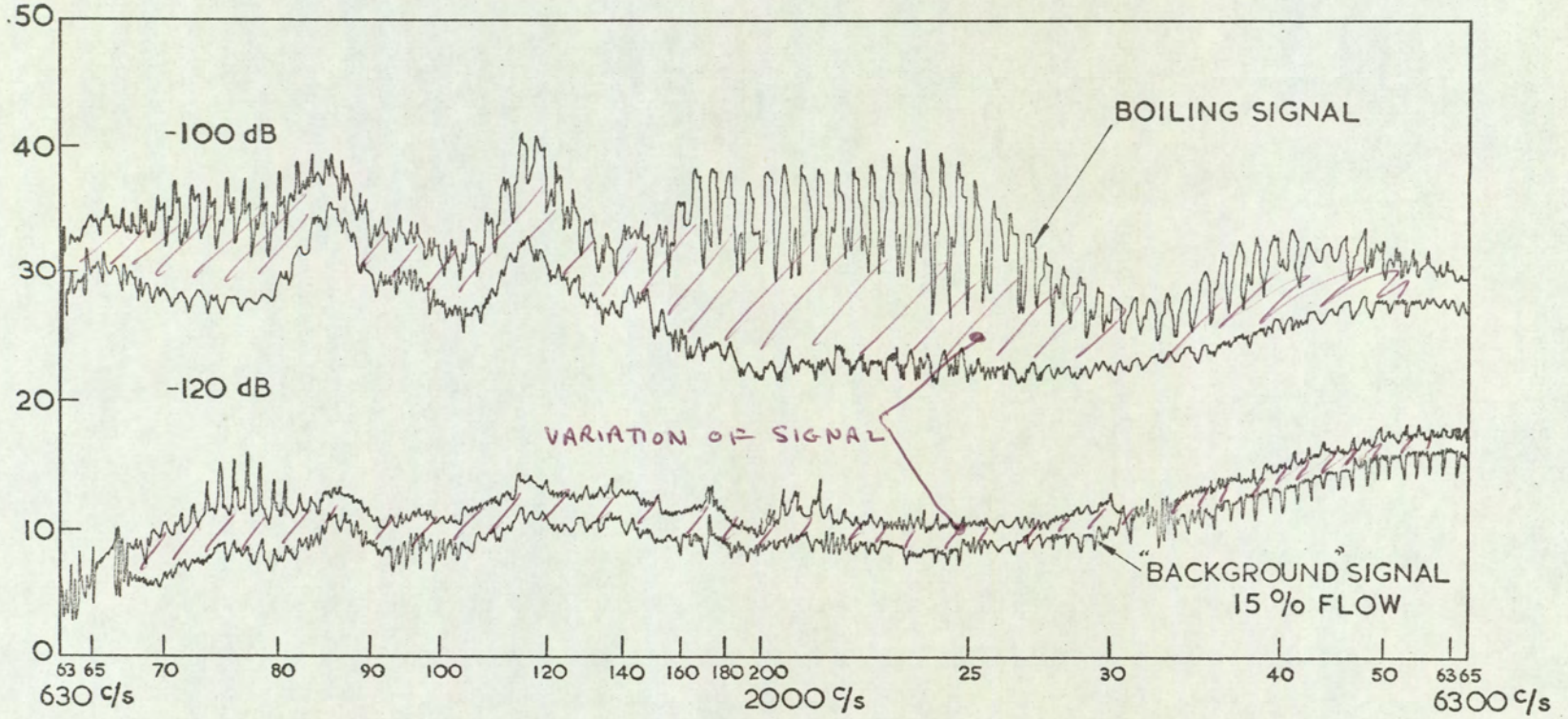

FIG. 5·26. COMPARISON OF D.F.R. HYDRODYNAMIC NOISE & AN 'IN PILE' BOILING EXPERIMENT.

FIG. 5·26.

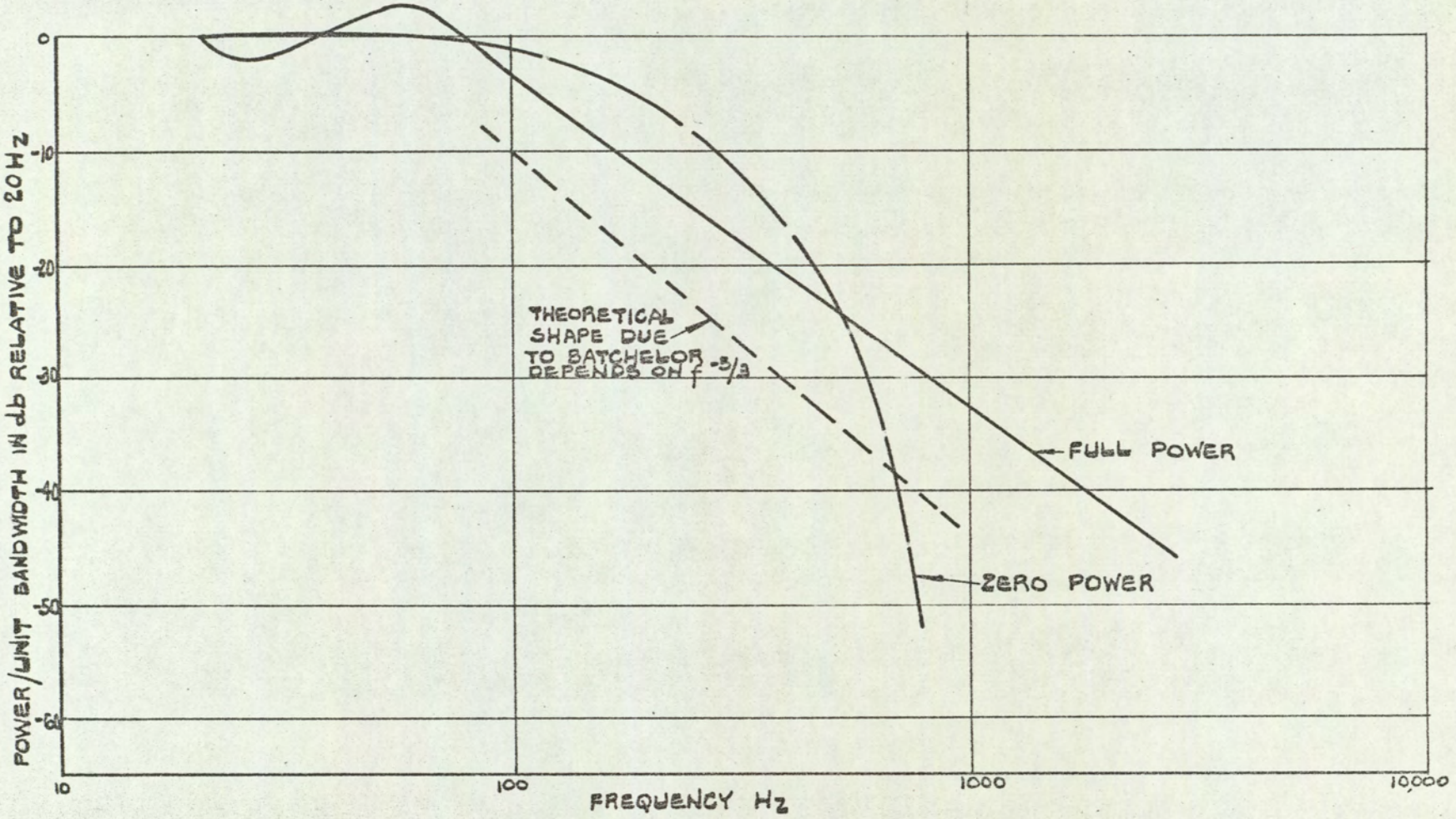

FIG 5·27 TYPICAL THERMAL NOISE SPECTRUM OBTAINED BY EDDY CURRENT PROBE AT THE INLET TO THE D.F.R. CORE.

FIG. 5·27.

CHAPTER 6

PRESENTATION OF THE INFORMATION DERIVED FROM RANDOM SIGNALS TO THE SYSTEM OPERATORS

6.1 General

In order that the information deriving from both the acoustic and thermal emmissions in any practical system may be put to the most use then the results must be analysed, processed and presented in such a fashion as to be easily and unambiguously interpreted by the operators of the system, in this case the reactor operators. It is probably well worthwhile to reiterate some of the fundamental ideas of the analysis of random signals and these are summarised below.

6.2 Some Fundamental Ideas on Random Signal Analysis

The existance of random processes in nature is evident in everyday events, for example the wind velocity will not be constant in any particular direction, but fluctuate about some mean value. If a number of different records of any particular random process is taken for a fixed period of time then the results may have a form similar to the records shown below with time progressing left to right.

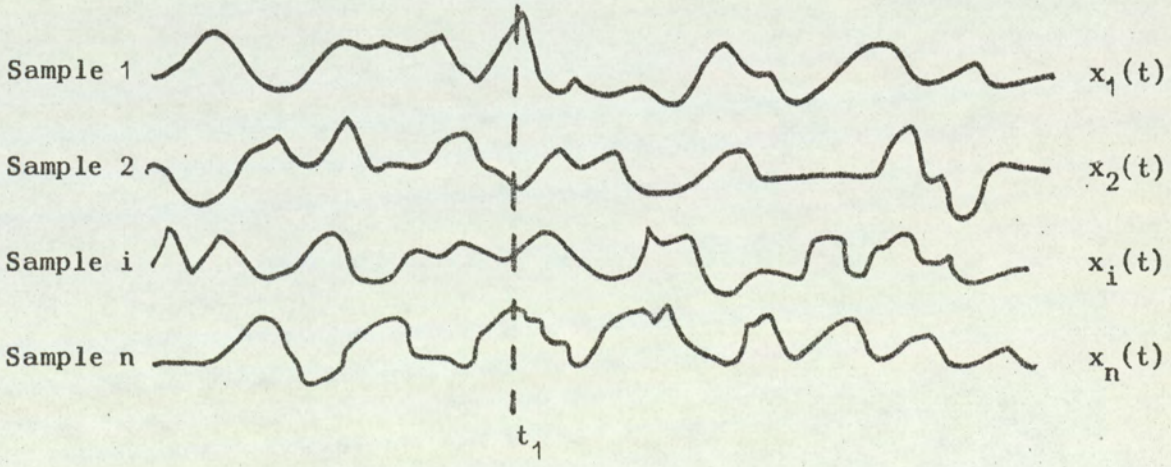

The set $x_i(t)$ is called the ensemble and each $x_i(t)$ is a member of the ensemble.

If we take the average at any particular time t_1 from the start of each record we obtain the ensemble average = $\frac{\sum_n x_i(t_1)}{n}$ which is clearly a function of t_1.

If the ensemble average is independent of t_1 i.e.

$$\frac{\sum_n x_i(t_1+t)}{n} = \frac{\sum_n x_i(t)}{n}$$ for all values of t then the process is said to be stationary.

Further if the time average of any particular record

$$\overline{x_i(t)} = \frac{1}{T}\int_0^T x_i(t)\,dt$$ is equal to the ensemble average then the process is stationary and ergodic. This implies that the statistical properties of the signal are invariant with time and that ensemble properties may be deduced from measurements in time. It is clear that all ergodic processes are stationary but the inverse is not necessarily true. The description of random signals by means of methods used to describe deterministic signals is of little use. The normal method of description of random signals is to use the amplitude probability functions, the mean square value of the signal and either the auto-correlation function or the power spectral density.

The probability density function is obtained by considering the proportion of time a signal spends between two finite limits. This idea is shown diagramatically in Figure 6.1.

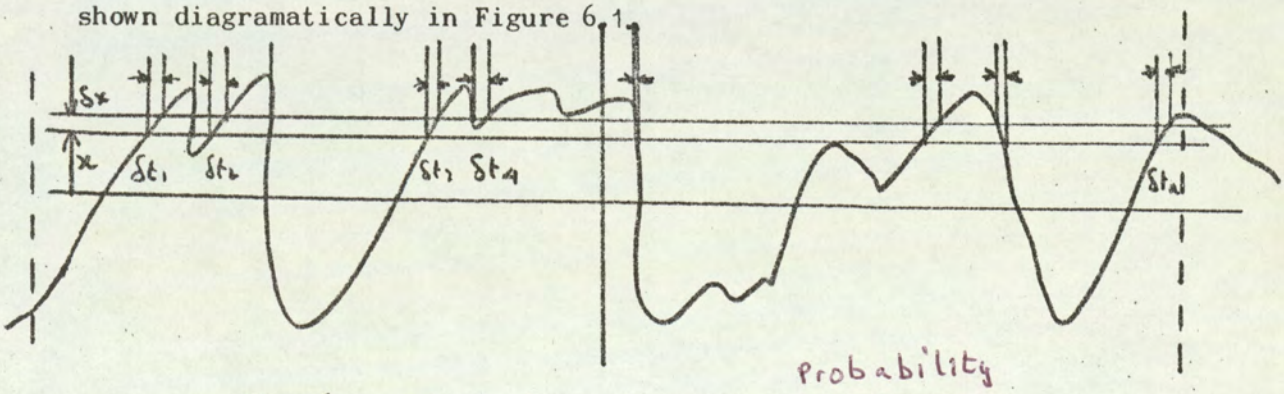

Fig. 6.1 Basic Idea of Amplitude Probability Density Function

The probability that the signal lies in the interval δx in a record of length 2T is simply $\frac{\delta t_1+\delta t_2+\delta t_3 \text{ ------ } \delta tn}{2T}$

i.e. $P(x) = \frac{\Sigma \delta t_i}{2T}$ (1)

and the probability density is $p(x_i) = \frac{1}{2T} \frac{\delta t_i}{\delta x}$ (2)

and is a function of x_i

it is obvious that $\int_{-\infty}^{\infty} p(x)\ dx = 1$ (3)

A probability density function of tremendous practical value, in that most engineering random process obey it is the normal or Gaussian given by $p(x) = \frac{1}{\sigma\sqrt{2\pi}} \exp\left[-\frac{(x-\bar{x})^2}{2\sigma^2}\right]$ (4)

where σ^2 is the variance of the signal.

The time average of a random signal is defined as

$$\bar{x} = \lim_{T \to \infty} \frac{1}{2T} \int_{-T}^{T} x(t)\ dt \quad (5)$$

and the relationship between the instantaneous value and the probability density function follows from (2).

i.e. $dt = 2T\ p(x)\ dx$

$$x(t)\ dt = 2T\ x(t)\ p(x)\ d(x)$$

$$\therefore \int_{-T}^{T} x(t)\ dt = 2T \int_{-\infty}^{+\infty} x(t)\ p(x)\ dx$$

Using (5) we have

$$\bar{x} = \int_{-\infty}^{\infty} x(t)\ p(x)\ dx \quad (6)$$

Correlation Functions

The probability density function outlined above gives information only regarding the amplitude of the signal in a similar manner to the amplitude description of a deterministic function. We seek some way by which a description in the time domain may be given. One such way is the autocorrelation function defined as

$$Rxx\ (\lambda) = \lim_{T \to \infty} \frac{1}{2T} \int_{-T}^{T} x(t)\ x(t+\lambda)\ dt$$

and clearly Rxx(0) is simply the mean square of the signal and is an even function of λ.

The autocorrelation function is very useful in displaying any periodic components in a signal as the parameter is varied. In fact this function used to be called the periodogram, a very descriptive title.

The cross-correlation function is a measure of how one signal y(t) depends on another x(t) and is defined as

$$Rxy(\lambda) = \underset{T \to \infty}{\text{Limit}} \frac{1}{2T} \int_{-T}^{T} x(t)\, y(t+\lambda)\, dt$$

Rxy(λ) degenerates into the autocorrelation function if x(t) and y(t) are equal.

One very useful application of Rxy(λ) is in determining the delay and degree of correlation between a pair of signals.

Some properties of the cross correlation function are given below.

Rxy(λ) is not necessarily an even function of λ.

$Rxy(\lambda) = Ryx(-\lambda)$

If $Rxy(\lambda) = 0$ for all λ then x(t) and y(t) are uncorrelated.

Rxy(λ) is not necessarily a maximum for $\lambda = 0$.

Frequency Description

It is sometimes very convenient to describe the random signals in the frequency domain and this is done by defining the Fourier transform of x(t) as follows:

$$F(j\omega) = \int_{-\infty}^{\infty} x(t)\, e^{-j\omega t}\, dt$$

$F(j\omega)$ is in general complex and $= P(\omega) + jQ(\omega)$

$$= A(\omega)\, e^{j\phi(\omega)}$$

$A(\omega)$ is called the Fourier spectrum of x(t) and $\phi(\omega)$ the phase angle of x(t).

x(t) may be recovered from $F(j\omega)$ by the inverse Fourier transform

$$x(t) = \frac{1}{2\pi} \int_{-\infty}^{\infty} F(j\omega)\, e^{j\omega t}\, d\omega$$

The power density spectrum function measures how the energy in a

random function is distributed as a function of frequency and is defined as $Sxx(\omega) = F(j\omega)F^*(j\omega)$.

where $F^*(j\omega)$ is the complex conjugate of $F(j\omega)$.

As one would expect the information content in this frequency description is the same as that in the time domain. The autocorrelation function and the power density spectrum function are related as a pair of Fourier transforms.

$$Sxx(\omega) = \int_{-\infty}^{\infty} Rxx(\lambda) e^{-j\omega\lambda} d\lambda$$

$$Rxx(\lambda) = \frac{1}{2\pi}\int_{-\infty}^{\infty} Sxx(\omega) e^{j\omega\lambda} d\omega$$

The power in any particular band say ω_1 to ω_2 is given simply by

$$\frac{1}{2\pi}\int_{\omega_1}^{\omega_2} Sxx(\omega)\, d\omega$$

and $\frac{1}{2\pi}\int_{-\infty}^{\infty} Sxx(\omega) d\omega$ is the total power i.e. the mean square of the signal

The cross spectral density is the Fourier transform of the cross correlation function defined as follows

$$Sxy(\omega) = \frac{1}{2\pi}\int_{-\infty}^{\infty} Rxy(\lambda) e^{-j\omega\lambda} d\omega$$

and measuresthe relationship between a pair of signals displayedin the frequency domain.

$Sxy(\omega)$ may also be writen as

$$Sxy(\omega) = F\overset{*}{x}(j\omega)\, Fy(j\omega)$$

where $Fx(j\omega)$ and $Fy(j\omega)$ are the Fourier transform of $x(t)$ and $y(t)$ respectively and the star denotes the complex conjugate.

Relationship Between Input and Output of a System

It is important to understand the way in which random signals are modified on passing through any typical linear system. Consider for example the system shown below.

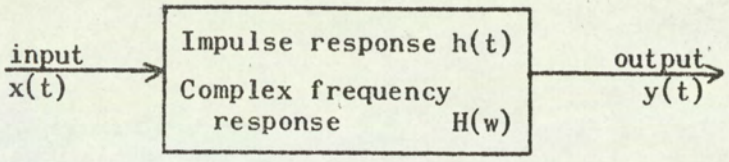

If we regard the input x(t) to be composed of a number of "delta" functions then we may obtain y(t) by the convolution integral

$$y(t) = \int_{-\infty}^{t} x(\lambda)\ h(t-\lambda)\ d\lambda \qquad (1)$$

where λ is the time from the present time t to the point in time at which one of the delta functions is assumed to exist.

The impulse response h(t) and the complex frequency response H(w) form a Fourier transform pair as follows

$$H(w) = \int_{-\infty}^{\infty} h(t)\ e^{-jwt} dt \qquad (2)$$

$$h(t) = \frac{1}{2\pi} \int_{-\infty}^{\infty} H(w)\ e^{jwt} dw \qquad (3)$$

The relationship between the input and output power spectra is obtained on the assumption of a stationary ergodic process and gives

$$Syy(w) = |H(w)|^2\ Sxx(w) \qquad (4)$$

which simply states that the output power spectrum is the product of the input power spectrum and the square of the moduli of the complex frequency response of the system.

An interesting result follows if we consider the cross correlation function between input and output

$$Rxy(\lambda) = \lim_{T\to\infty} \frac{1}{2T} \int_{-T}^{T} x(t)\ y(t+\lambda)\ dt$$

substituting for y(t) from (1) above with a simple change of variable we have

$$Rxy(\lambda) = \lim_{T\to\infty} \frac{1}{2T} \int_{-T}^{T} x(t) \int_{-\infty}^{t+\lambda} x(t-\zeta)\ h(t)\ d\zeta\ dt$$

On assuming that the integrals can be rearranged we see that:-

$$Rxy(\lambda) = \int_{-\infty}^{t} \lim_{T\to\infty} \frac{1}{2T} \int_{-T}^{T} x(t)\, x(t-\zeta)\, d\xi\, h(\lambda)\, dt$$

The inner integral is the autocorrelation function $Rxx(\xi)$. Further if $Rxx(\xi) = \delta(\xi)$ (an impulse function) then we obtain $Rxx(\zeta) = h(\zeta)$. That is if the condition exists that the autocorrelation function of an input signal is a delta function the impulse response is obtained directly as the cross correlation function between input and output.

White noise has the above property as also do many artificial functions which are now finding application in system recognition analysis.

6.4 Some Experiments on the Analysis of Random Signals

Spectral Analysis

The analysis of the preceeding section was based on the use of infinite integration times and extremely narrow bandwidths. The true power spectral density in a band B ~~was~~ is written as:

$$\lim_{\substack{T\to\infty \\ B\to 0}} \frac{1}{T} \int_{0}^{T} \frac{x^2(t)}{B}\, dt$$

In practice the above mathematical ideals cannot be met and it is interesting to examine the effect of varying the product BT. In fact it can be shown (6.1) that the number of degrees of freedom in a statistical sense is K = 2BT. Using the assumed form of the amplitude probability function it is possible to estimate within specified confidence limits the variance of the spectral density measurement. The results presented here an empirical approach using the two commercial spectrum analysers used in the work reported in this thesis.

The experiments which were basically very simple consisted of feeding a wide band random signal into either the Muirhead analyser or the Bruel and Kjaer, the former having a 2% bandwidth and the latter a 5%. Each analyser was tuned to 1KHz giving effective bandwidths of 20Hz and 50Hz respectively. The outputs from these analysers were fed in turn to

a logarithmic recorder which could be operated at a range of effective averaging times from 10 millisecs to 2½ secs. The effective averaging time of each system was determined by switching a 1 KHz pure tone into each analyser in turn and observing the exponential build-up of the trace on the recorder.

The results are presented in the Figures 6.2 and 6.3 and clearly show the effect of increasing the bandwidth integration time product. On the basis of these elementary tests the use of a bandwidth - integration time product of about 50 will give results which are acceptable from a practical engineering point of view.

It is clear from the above discussion that the statistical quality of the measurement improves as the integration time and bandwidth of the detector are increased. However, the analysis time suffers and the resolution diminishes under these conditions and clearly some compromise is necessary. Paradoxically this compromise cannot in fact be made unless the results of the analysis are known before the analysis starts. It is customary therefore to carry out a "quick look" analysis to obtain a rough idea of the spectrum and choose the bandwidth to resolve the peaks in the spectrum. An integration time compatible with the statistical degrees of freedom is then chosen; this also is the minimum record length required for a satisfactory analysis.

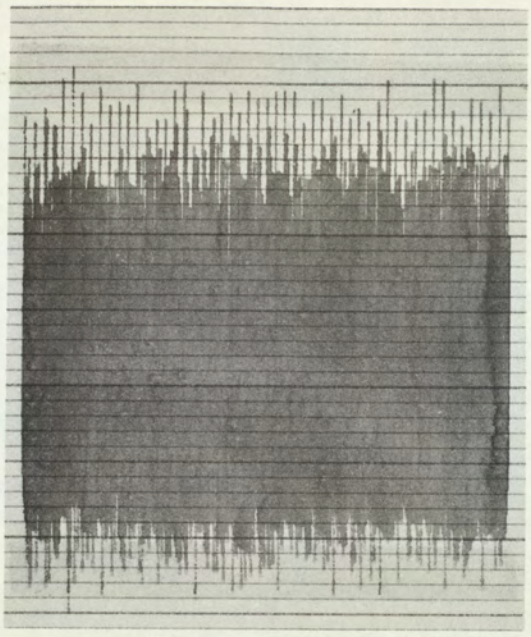

4.5 millisecs

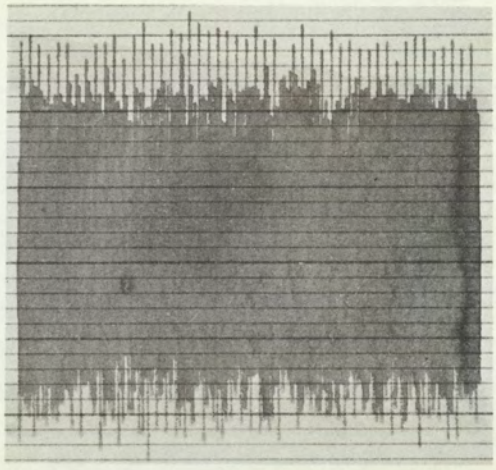

5.6 millisecs

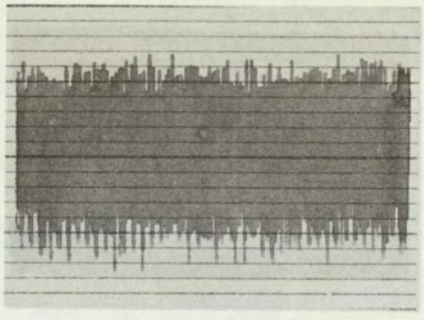

18 millisecs

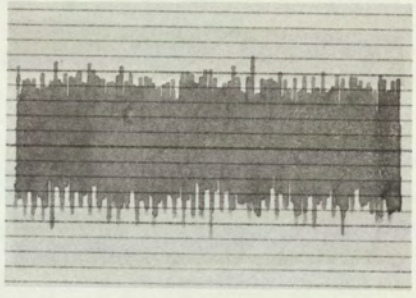

25.4 millisecs

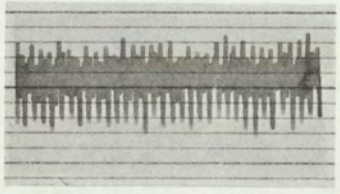

112 millisecs

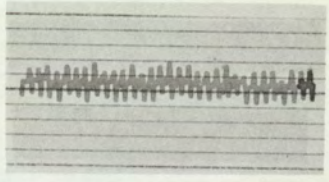

254 millisecs

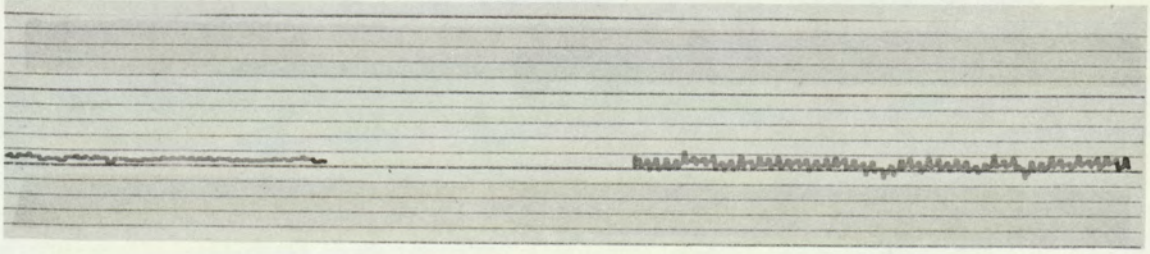

1.125 secs

0.562 secs

Effect of varying the averaging time on a random signal passed through a 20 Hz wide filter.

Fig. 6.2

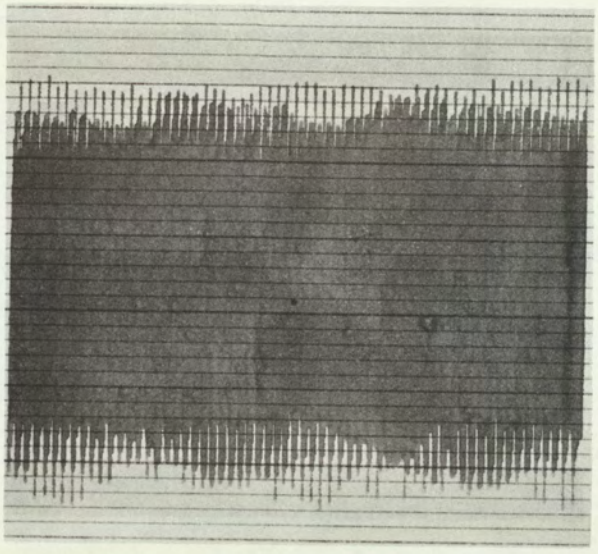

4.5 millisecs

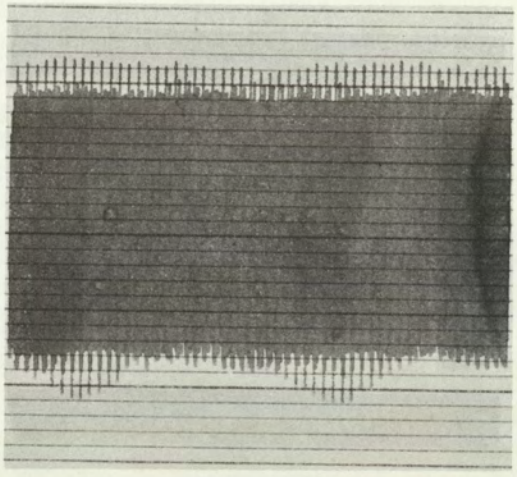

5.6 millisecs

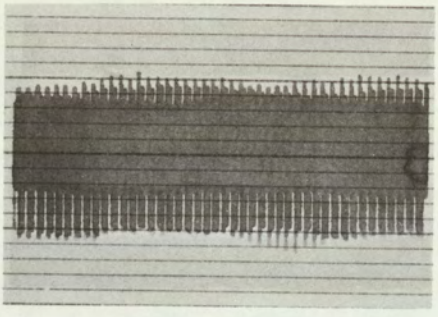

18 millisecs

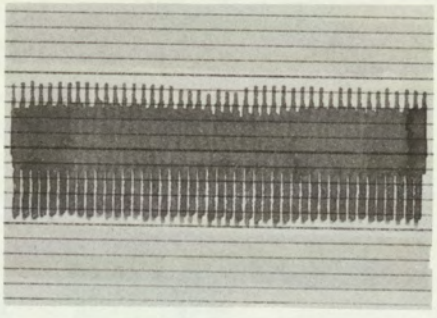

25.4 millisecs

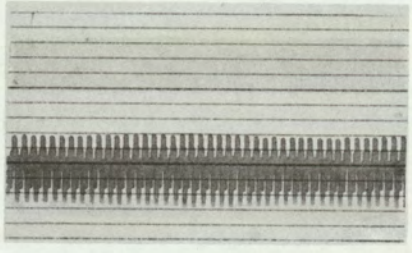

112 millisecs

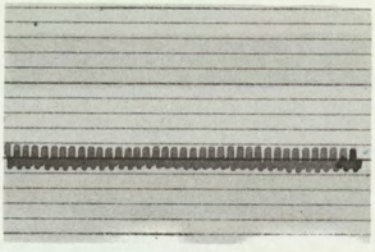

254 millisecs

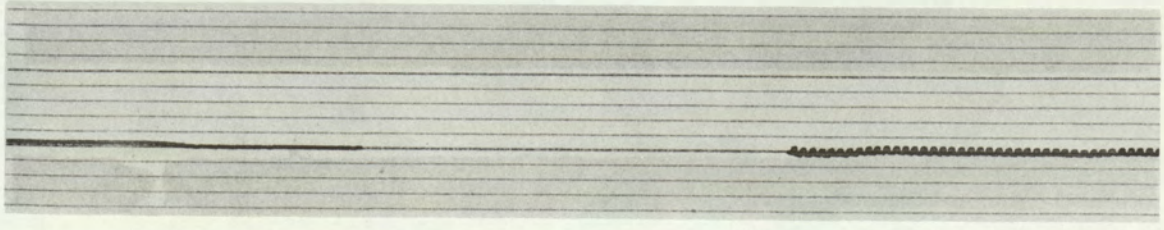

1.125 secs

0.562 secs

Effect of varying the averaging time on a random signal passed through a 50 Hz wide filter.

Fig. 6.3

Correlation Analysis

The use of correlation analysis, particularly the application of cross-correlation requires great care. This is especially true if the ensemble to be analysed exists in a dispersive medium. The effect of such a medium is to change the power spectral density of the signal as it travels. Suppose that a component of the signal at one point may be A sin wt, and at a second point B sin $(w+\delta w)t+\phi$ illustrating a small change in amplitude and frequency. We wish to obtain ϕ, the effective phase angle, by correlation analysis. Proceeding to compute the cross correlation function we have:

$$R_{AB}(\lambda) = AB \lim_{T\to\infty} \frac{1}{T} \int_0^T \sin wt \, \sin[(w+\delta w)t+\phi+\lambda]\, dt$$

This integral becomes, on neglecting δw compared to w,

$$R_{AB}(\lambda) = \frac{AB}{2}\left[\frac{\sin wT}{\delta wT}\cos(\phi+\lambda) + \frac{\cos wt}{\delta wt}\sin(\phi+\lambda) - \frac{\sin(\phi+\lambda)}{\delta w}\right]$$

If δw is zero as in non dispersive medium then integral reduces to

$$R_{AB} = \frac{AB}{2}\cos(\phi+\lambda)$$ from which the unknown phase ϕ may be obtained from the known delay.

However if δw is finite then as T is increased in the interests of statistical accuracy then the cross correlation function reduces to:

$$R_{AB}(\lambda) = \frac{AB}{2}\,\frac{\sin\delta wT}{\delta wT}\cos(\phi+\lambda)$$

This function is dominated by the behaviour of a function of the form sin x/x and very quickly dies away to zero. For example if δw = 1 cps and T = 4.5 secs then the correlation function is reduced to $1/9\pi$ of its "true" value and under normal circumstances would be unobservable.

This effect was clearly demonstrated by using the simple arrangement shown in Figure 6.4. The acoustic wave in the tube was produced by a small mechanical buzzer attached to the pipe. The detection was by conventional piezo-electric accelerometers. The outputs of the two

accelerometers were displayed on a double beam oscilloscope and referring to Figure 6.5 a clear delay between the two signals was apparent. The result of cross correlating the two signals by use of the Hewlett Packard correlator is shown in Figure 6.5 and shows a complete lack of any observable correlation, broadly confirming the analysis above.

A substantial improvement in the ability to measure the delay between the signals is shown in Figures 6.6 and 6.7 in which both pre-filtering of each signal and/or envelope detection was carried out prior to correlating. The most easily interpreted results were obtained by envelope detection before correlating, in fact the envelope detection/correlation of the unfiltered signal gave slightly sharper results than the envelope detected filtered signals, Fig 6.8. This slight difference between filtered and unfiltered is probably due to slight differences in the setting of the two analysers used as narrow band filters.

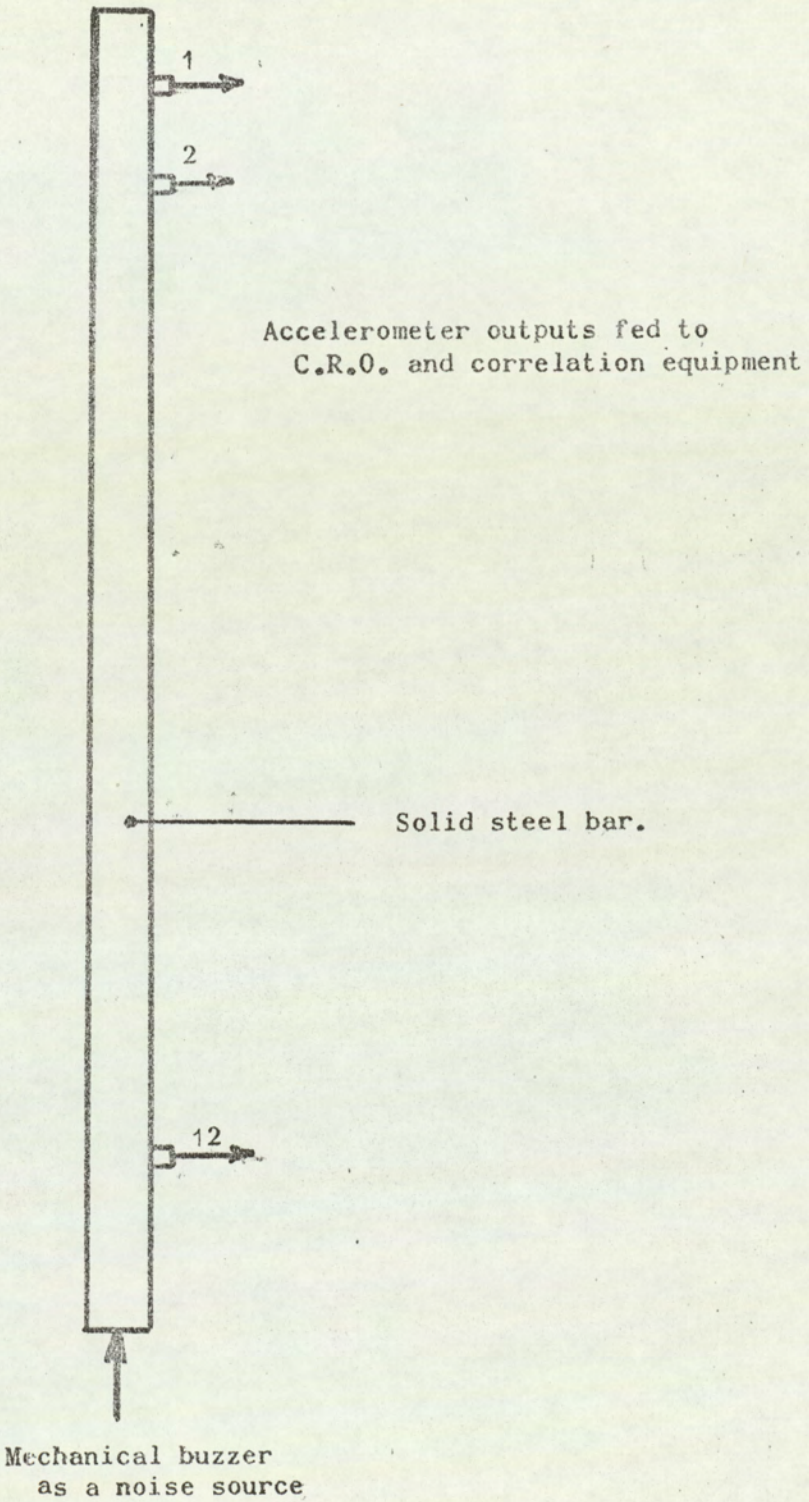

Arrangement of apparatus for correlation experiments.

Fig 6.4

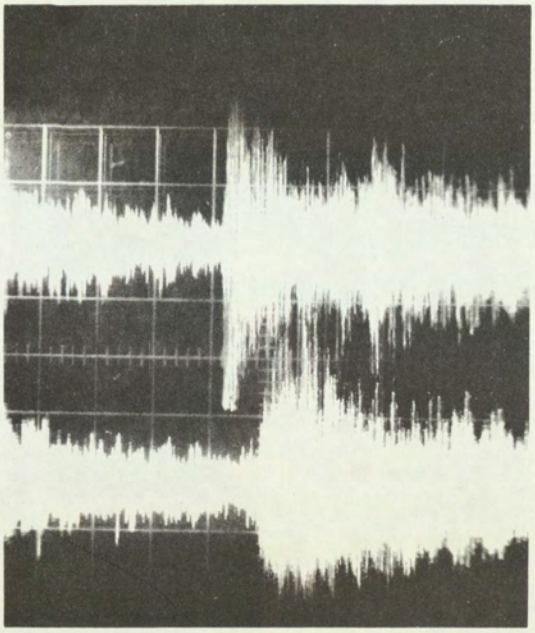

Unfiltered signals from transducers 1 and 12:

T = 2m secs/cms: V = 10V/cms

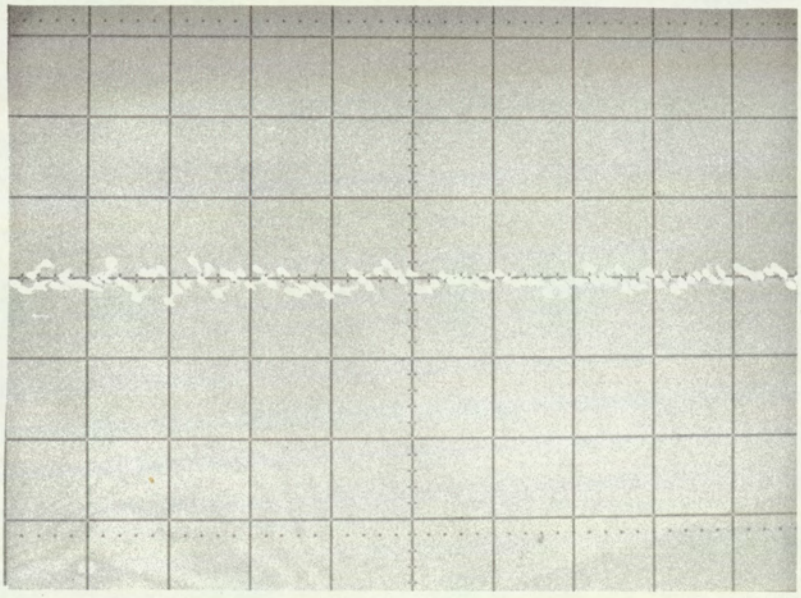

Result of cross correlating the unprocessed signals shown above:

T = 1m sec/~~sec~~ cm

Fig 6.5

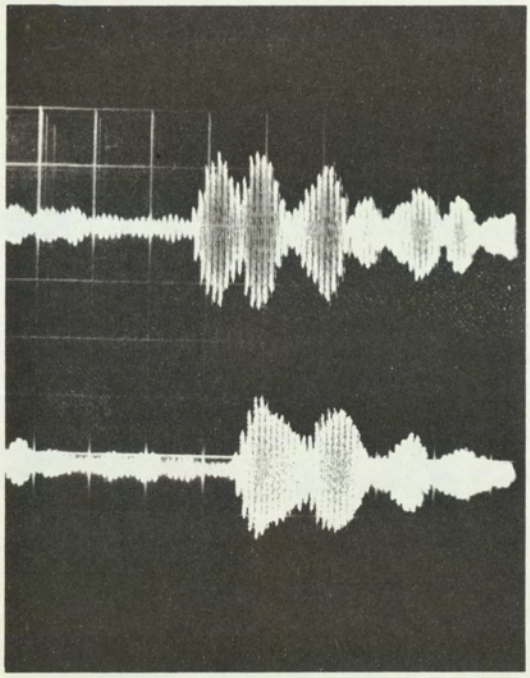

Signals from transducers 1 and 12 passed through 5% 4.6 KHz filters:
T = 2m sec/cm V = 1V/cms

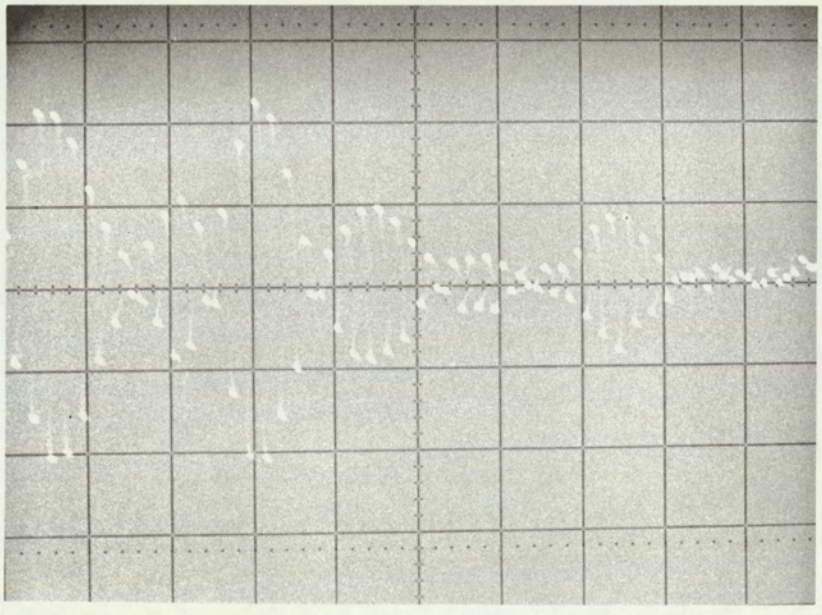

Result of cross-correlating signals shown above:
T = 1m sec/cms

Fig 6.6

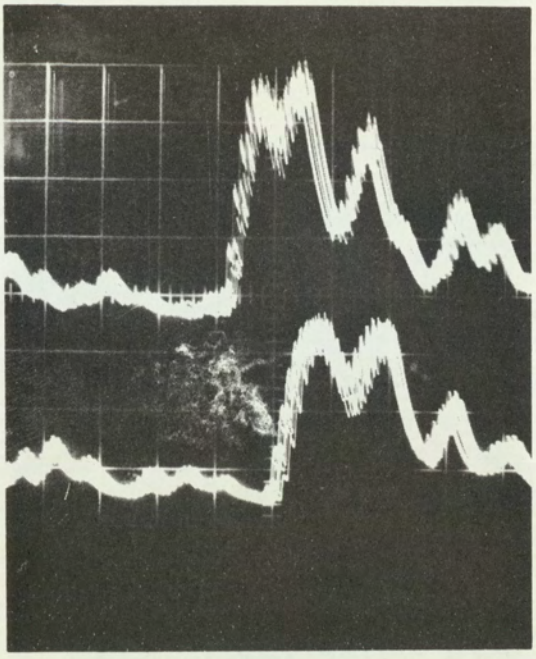

Envelope detection of filtered signals from transducers 1 and 12:
T = 2m secs/cms V = 1 volt/cms

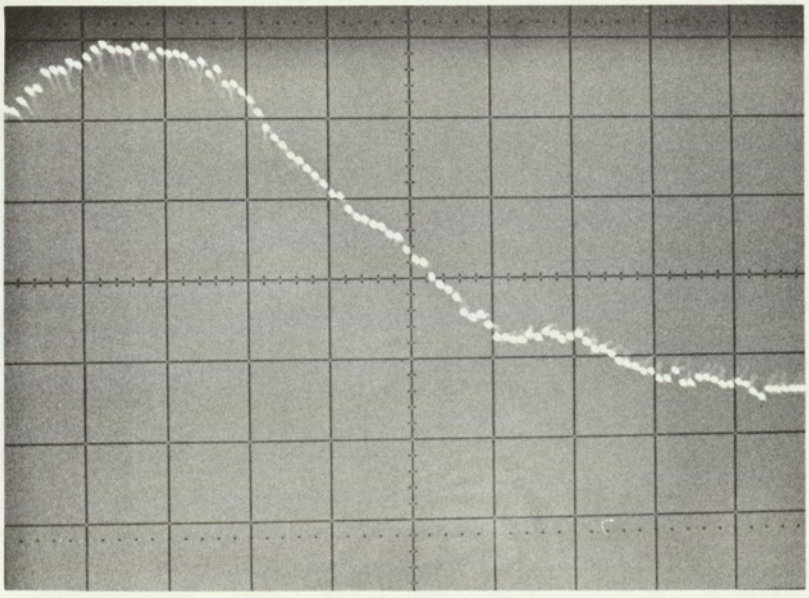

Result of cross-correlating signals shown above:
T = 1m secs/cms

Fig 6.7

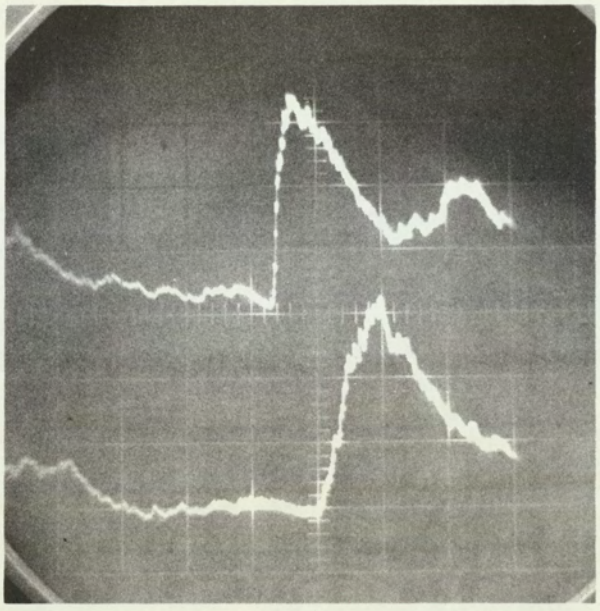

Envelope detection of unfiltered signals from 1 and 12:
T = 2m secs/cms V = 1 volt/cms

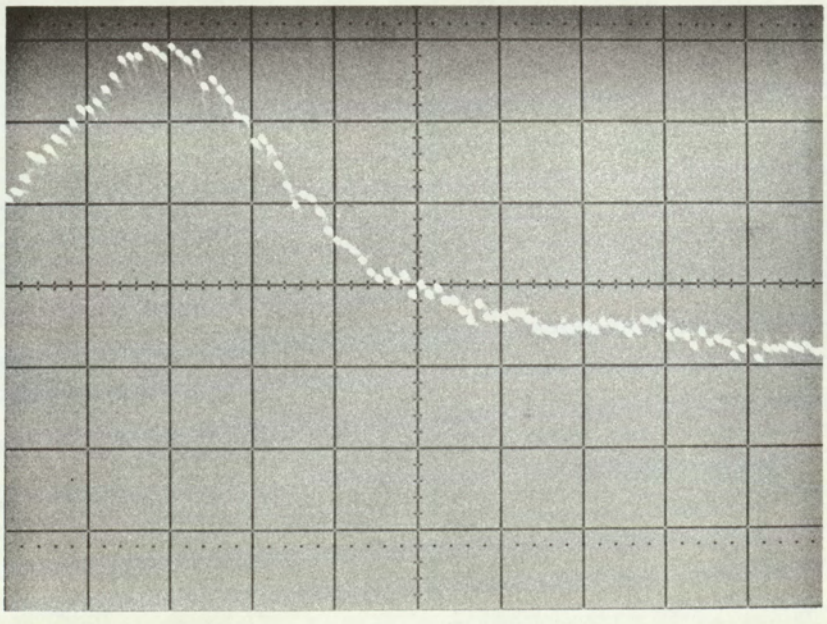

Result of cross-correlating signals shown above:
T = 1m secs/cms

Fig 6.8

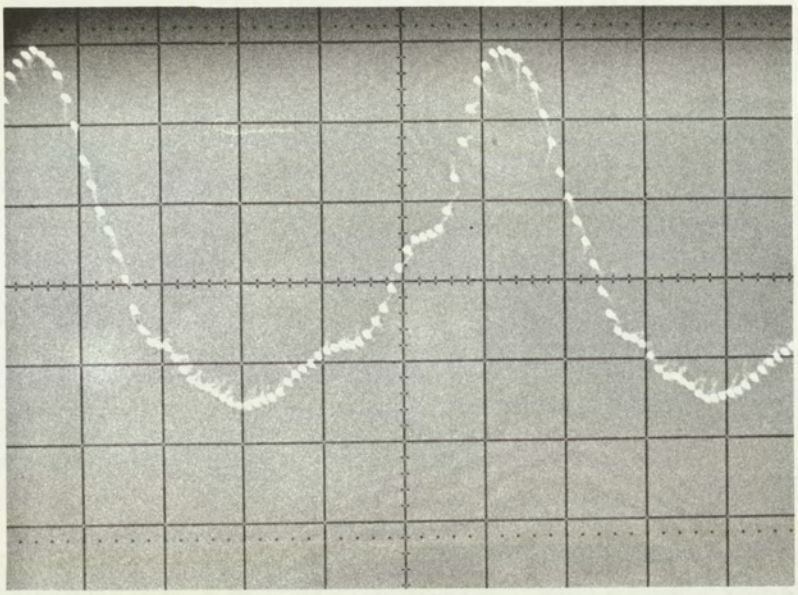

Cross-correlation of demodulated filtered signals:

T = 3.3m secs/cms

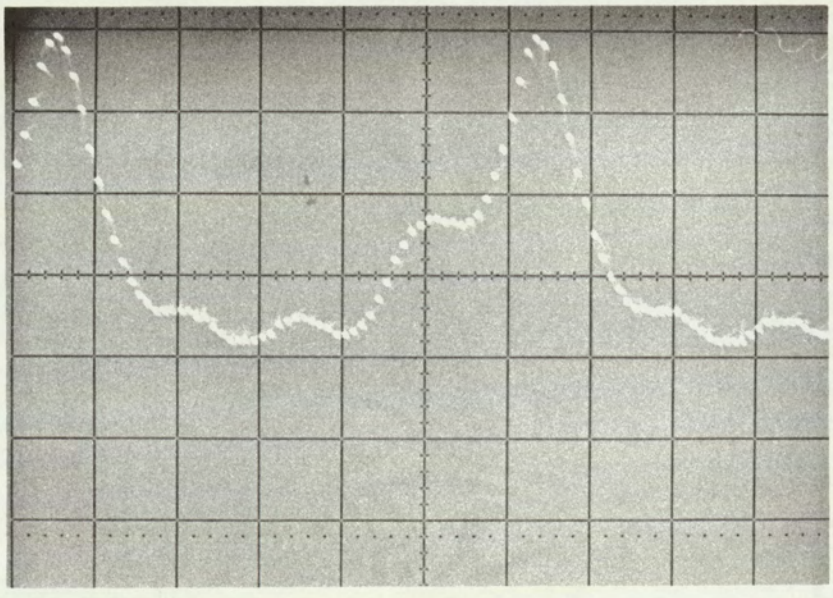

Cross-correlation of demodulated unfiltered signals:

T = 3.3m secs/cms

Range of correlator increased to show repetitive nature of the signals

Fig 6.9

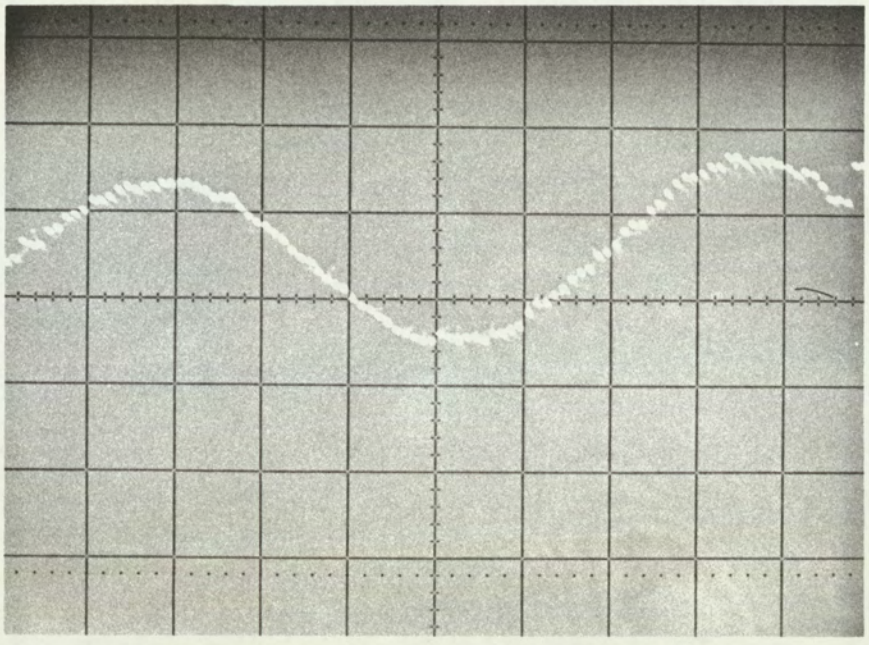

Cross-correlation between transducers 1 and 12:

T = 33.3μ sec/cms

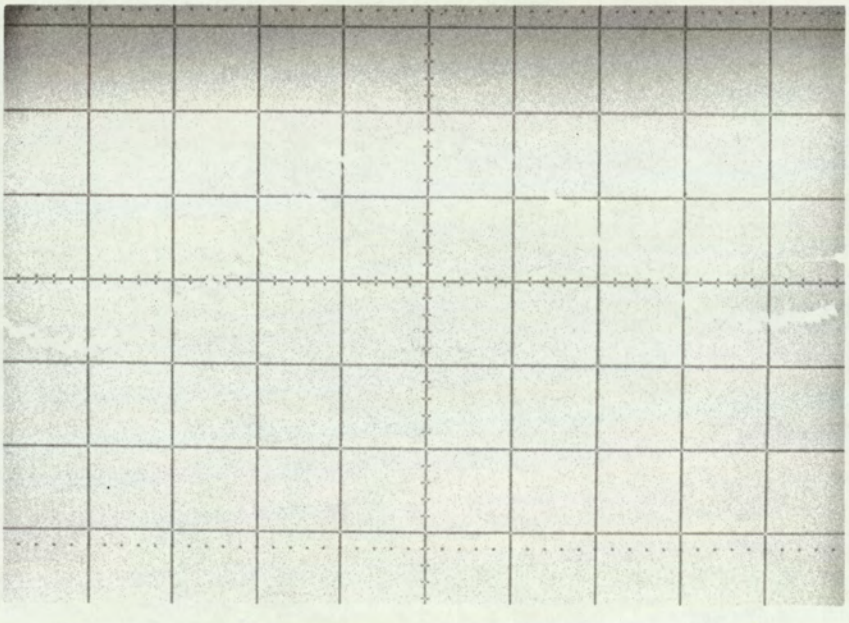

Cross-correlation between transducers 3 and 12:

T = 33.3μ sec/cms

Result of correlating signals from a near pure tone source - shows phase change only

Fig 6.10

6.3 Techniques Used to Analyses Random Signals

Wherever possible the signal source was connected via low noise amplifiers direct to the analysers. The analysers used in this work are described below.

Spectrum Analysis

(i) Bruel and Kjaer type 2107 frequency analyser which has a frequency range 20 Hz to 20KHz. This analyser is a constant percentage type of 5% bandwidth.

(ii) Muirhead type 988 frequency analyser again a constant percentage type of approximately 2% bandwidth.

These analysers suffer from that fact that because they are constant percentage types the results have to be processed in order to present the results in terms of power density. For the majority of experiments however the relative levels only were of interest and in these cases the unprocessed records from the analysers are perfectly satisfactory.

Time Delay Correlation

(i) Honeywell type 940 which has a range of delays from zero to 17 millisecs.

(ii) Hewlett Packard type. The author was particularly fortunate in being able to use a prototype on-line digital correlator on a short term loan from the manufacturers. This correlator is a parallel input type and has the clear advantage that information is processed at a very fast rate in real time. When direct on-line recording was not possible or desirable because of the expected short duration of the signal, the information was recorded on a tape recorder and the tape was subsequently cut into a closed loop form and played back in a cyclic manner. The analysis was then carried out with the serial mode analysers taking care that the time scale of the information on the loop was compatable with the integration time and bandwidth of the analyser.

6.5 Signal to Noise Enhancement

It is desirable to carry out as much signal to noise enhancement as possible in order that the desired information may be presented to the reactor operator in an unambiguous manner. The probability of spurious reactor trips will in general be reduced by carrying out signal to noise enhancement. This reduction in spurious trips will be seen to result in a longer time before the processing system can decide on the validity of the information with which it is presented.

We consider the case in which the amplitude time description of the signal is $f_1(t)$, random in time with an average occurrence γ_1 per unit time. A disturbing unwanted signal is $f_2(t)$, again random in time with an average occurrence of γ_2 per unit time.

We assume $\left[f_2(t)\right]_{max} >> \left[f_1(t)\right]_{max}$

$$\gamma_1(t) >> \gamma_2(t)$$

This is known to be the case when it is desired to detect the collapse of vapour bubbles in the presence of mechanical impacts.

One very simple way in which the signal to noise ratio may be increased is by averaging the signal over a finite time.

$$\text{Now average signal} = \frac{1}{T}\int_o^T \left\{f_1(t) + f_1(t-\lambda_1) + f_2(t-\lambda_2)\ dt\right\}$$

$$+ \frac{1}{T}\int_o^T \left\{f_2(t) + f_2(t-\mu_1) + f_2(t-\mu_2)\ dt\right\}$$

where the λ's and the μ's represent random time increments.

Following Rice (3.17) we may write:-

$$\text{Average measured signal} = \gamma_1 \int_o^{\tau_1} f_1(t)dt + \gamma_2 \int_o^{\tau_2} f_2(t)dt$$

where τ_1 is the life time of $f_1(t)$ and τ_2 is the life time of $f_2(t)$.

Now the average pulse repetition frequency of the signal $f_1(t)$ is $\frac{1}{\gamma_1}$ and the average pulse repetition frequency of $f_2(t)$ is $\frac{1}{\gamma_2}$; this is illustrated in the Fig. overleaf.

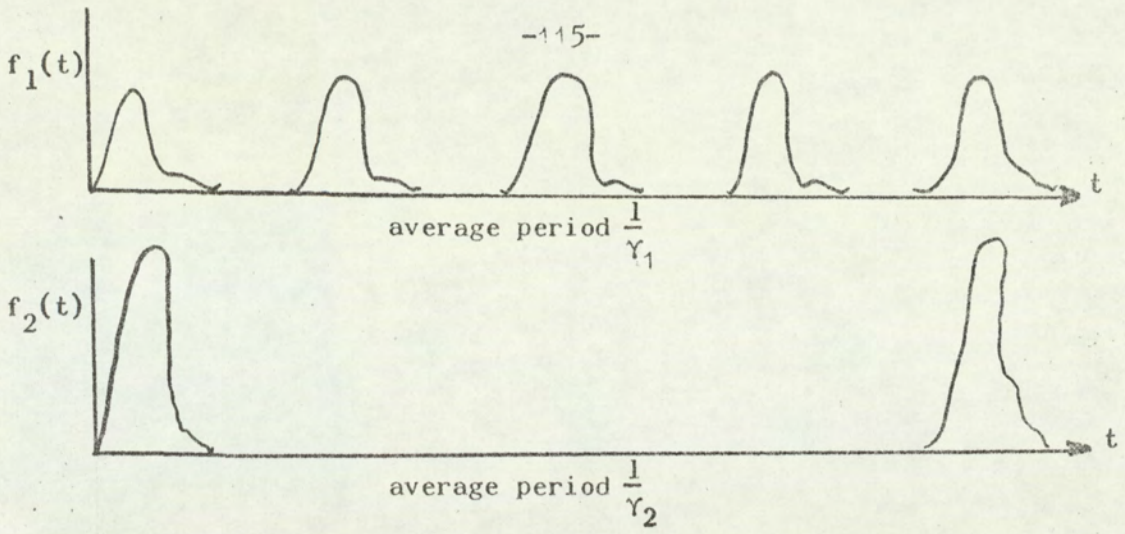

Fig. 6.11 Typical Signals

It is clear from the figure that the average of the signal over T containing n_1 signal pulses is:

$$\frac{n_1}{T} \int_0^{\tau_1} f_1(t)\, dt \tag{1}$$

and the average of the disturbance over the same period is:

$$\frac{1}{T} \int_0^{\tau_2} f_2(t)\, dt \tag{2}$$

providing $T < \frac{1}{\tau_2}$

The signal to noise ratio is therefore:-

$$\frac{\frac{n_1}{T} \int_0^{\tau_1} f_1(t)\, dt}{\frac{1}{T} \int_0^{\tau_2} f_2(t)\, dt} = n_1 \left\{ \frac{\int_0^{\tau_1} f_1(t)\, dt}{\int_0^{\tau_2} f_2(t)\, dt} \right\} \tag{3}$$

which clearly depends on n_1 and is a maximum when the averaging time is $\frac{1}{\gamma_2}$ and then the signal to noise ratio is $\frac{\gamma_1}{\gamma_2} \left\{ \frac{\int_0^{\tau_1} f_1(t)\, dt}{\int_0^{\tau_2} f_2(t)\, dt} \right\}$ (4)

$$\log S/N = \log \frac{\gamma_1}{\gamma_2} + \log \int_0^{\tau_1} f_1(t)\, dt - \log \int_0^{\tau_2} f_2(t)\, dt \tag{5}$$

The first term on the right hand side represents the signal to noise enhancement.

As a simple example consider the signal to be a series of delta functions $\delta(t)$ at a repetition frequency of 100 Hz and the disturbing source to be 10 $\delta(t)$ at a repetition of 1 Hz; $\int_{-\infty}^{\infty} \delta(t) = 1$.

Then we may form the following table.

Averaging Time Secs	Signal to Noise Ratio dB
0	-20 dB
0.1	0 dB
1	+20 dB

showing a signal to noise enhancement of + 40 dB which is consistent with $20 \log \frac{\gamma_1}{\gamma_2} = 20 \log \frac{100}{1} = 40$ dB.

Again considering the case of low frequency high amplitude disturbance superimposed on a relatively high frequency low amplitude signal, it is clear that an immediate improvement results from some limiting process applied to the incoming signals. This simply reduces $\int_0^{\tau} f_2(t)\, dt$ in equation (5) and a resulting increase in signal to noise ratio follows.

The major disadvantage of using a limiting method, particularly in acoustically derived signals, is the possible loss of the top end of some signals. The dynamic range necessary to record and present the acoustic data referred to in this thesis is about 50 dB. Alternatively to preserve this dynamic range the limiting level would have to be set above the required dynamic range and disturbing signals below this level would not be effected by this process.

A technique which overcomes the above mentioned disadvantages is logarithmic weighting. This is readily realized using conventional logarithmic amplifiers. In this process the signals are first passed through a logarithmic amplifier and then averaged as described previously. The averaging time being over the whole period of the low frequency disturbing signal.

The averaged signal then becomes $\gamma_1 \int_0^{\tau_1} \log f_1(t)\, dt$

and the averaged disturbance becomes $\gamma_2 \int_0^{\tau_2} \log f_2(t)\, dt$

It should be noticed that integration and taking the logarithms are not commutable. The signal-to-noise ratio under this condition is therefore:

$$\frac{\gamma_1}{\gamma_2} \int_0^{\tau_1} \log f_1(t)\, dt / \int_0^{\tau_2} \log f_2(t)\, dt$$

The significance of the above equation is illustrated in the following example using two trains of rectangular pulses for ease of arithmetic manipulation.

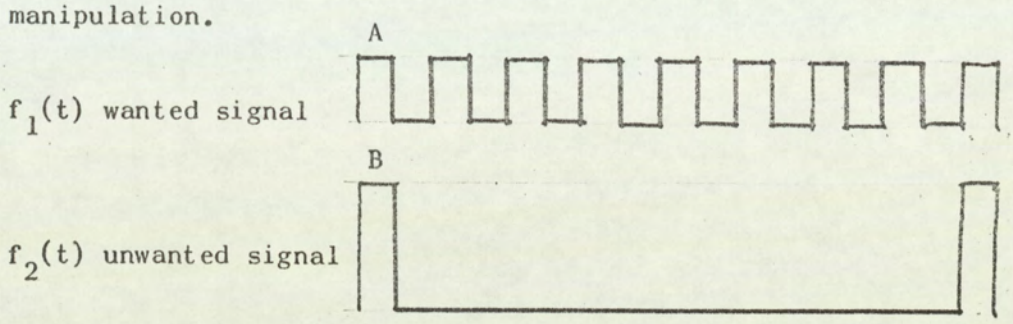

Fig. 6.12 Idealized Signals

then average of $f_1(t)$ over period of $f_2(t) = \gamma_1 A$

and average $f_2(t)$ over period of $f_2(t) = \gamma_2 B$

then signal to noise ratio $= \frac{\gamma_1}{\gamma_2} \frac{A}{B}$ (6)

If we repeat the above averaging process but first take the logarithm of each function we obtain:

average of $\log f_1(t)$ over the period of $f_2(t) = \gamma_1 \log A$

average of $\log f_2(t)$ over the period of $f_2(t) = \gamma_2 \log B$

signal to noise ratio is now $= \frac{\gamma_1}{\gamma_2} \frac{\log A}{\log B}$ (7)

which is clearly an improvement over (6) providing that $B > A$. It may be seen the two are identical if $A = B$.

If $B < A$ then the logarithmic weighting process actually reduces the signal to noise ratio, compared to the average of the linear functions.

The relationship between the signal to noise enhancement and the ratio of A to B is shown in Fig6.13. both for linear and logarithmic averaging.

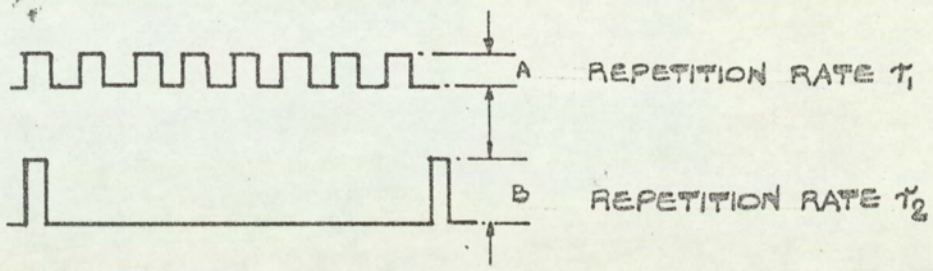

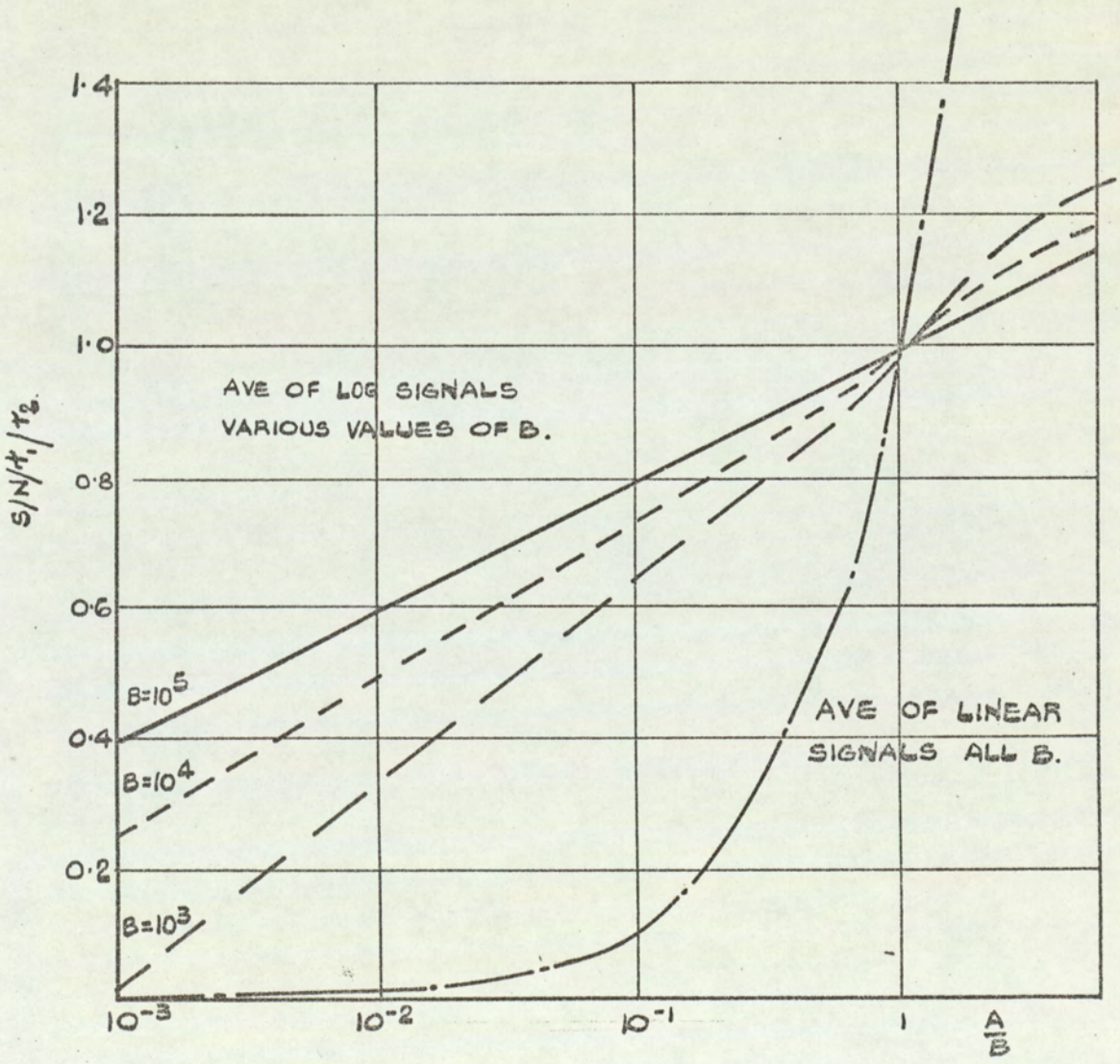

FIG 6·13 ILLUSTRATION OF SIGNAL TO NOISE ENHANCEMENT.

FIG.6·13

6.6 Description of a Proposed Reactor Instrumentation Scheme for the Detection of Local Overheating

The basic problem discussed in this section is that of the presentation of the intrinsic thermal and acoustic information to the reactor operator. It is also important that some permanent record be available for diagnostic purposes if and when required. The system described in this section consists of two parts, namely the instrumentation required to present thermal noise fluctuations and that required for presentation of acoustic noise.

The transducers recommended for the detection of thermal fluctuations are of the type discussed in section 4.3.b and would normally be installed at the outlet of channels about which information was desired. It has been possible to test these devices in pile in the Dounreay Fast Reactor only in the inlet to heated channels and hence any comment on the ultimate sensitivity regarding these devices must await further evaluation work.

A simple block diagram showing the instrumentation required for a thermal noise monitor is shown in Fig. 6.14. The non-active winding on the transducer gives primary temperature compensation and the simplified block diagram shows a system which is adequate for short term use. If the system is required to operate over long periods then a form of secondary temperature compensation is required. In principle it is possible to take the output from the bridge balance unit and accept the information above a certain frequency, say 0.1 Hz, as representing true thermal fluctuations in the liquid sodium coolant and regard low frequency disturbances as long term unwanted drift. A proposed system is therefore to pass the output of the bridge through low pass filters and use this in the correct phase as a feed back signal to a tertiary winding on the transformer bridge to keep the system balanced. Work on such a system is currently being carried out at the Dounreay Establishment by Hughes and the system shows the potential of being able

to maintain a bridge balance of 1 part in 10^0 over a temperature range of 200^oC.

A simplified block diagram of a single acoustic channel is shown in Fig. 6.15. and shows the route of the signal from the reactor coolant to the display and record facilities in the control room. In D.F.R. there are in fact three waveguides and three such instrumentation channels. The audio listening channel and the on-line spectrum analyser are capable of being switched to any line.

The band pass filter was chosen as a result of the in pile boiling experiment discussed in 5.4. The logarithmic amplifier is useful in enabling a wide range of amplitude of signals (about 3 decades) to be presented in a readable form on a standard linear pen recorder. As discussed in 6.5 this logarithmic amplifier together with the averaging circuit help to minimise the disturbances due to mechanical rattles occurring in the ~~recorder~~ reactor.

It is found in practice that the audio listening channel is of great value in providing an easily assimilated subjective appreciation of the acoustic noises in the reactor. A little practice is all that is required to be able to distinguish between the various mechanical noises in the reactor and such hydrodynamic sources of acoustic noise as entrained gas bubbles.

The pen recorder provides a qualitative measure of the mean square signal in the selected frequency band. The alarm level on the trip amplifier is set at +30 dB relative to the level at full coolant flow with the power of the reactor at zero.

The three acoustic channels are arranged so that an alarm is sounded only if any two of the three channels exceed the preset alarm level.

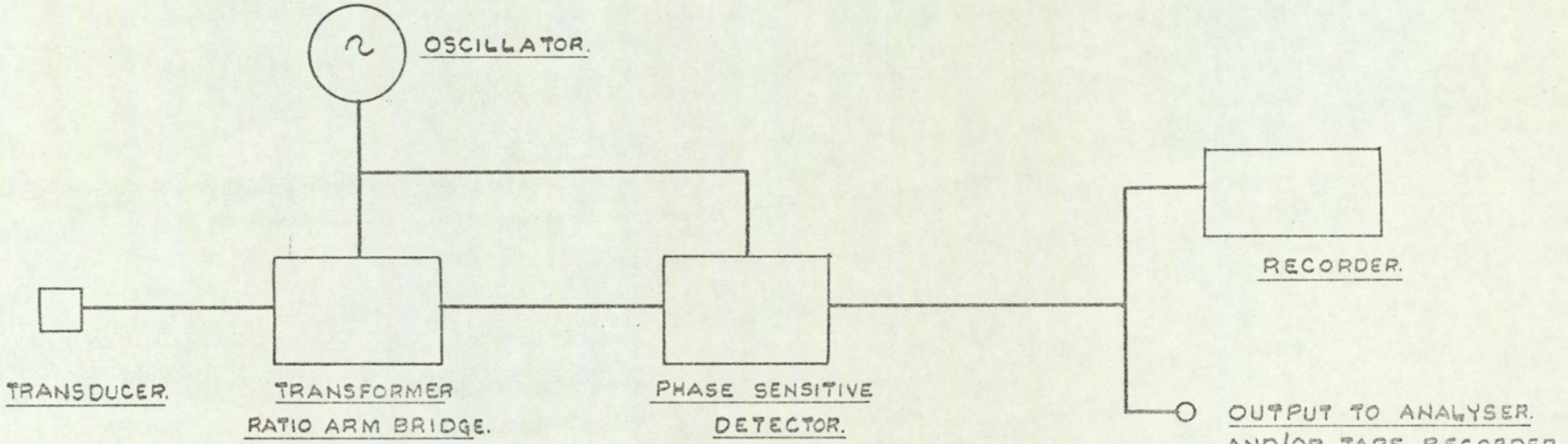

FIG 6·14 SIMPLIFIED BLOCK DIAGRAM OF THERMAL NOISE CHANNEL.

FIG. 6·14.

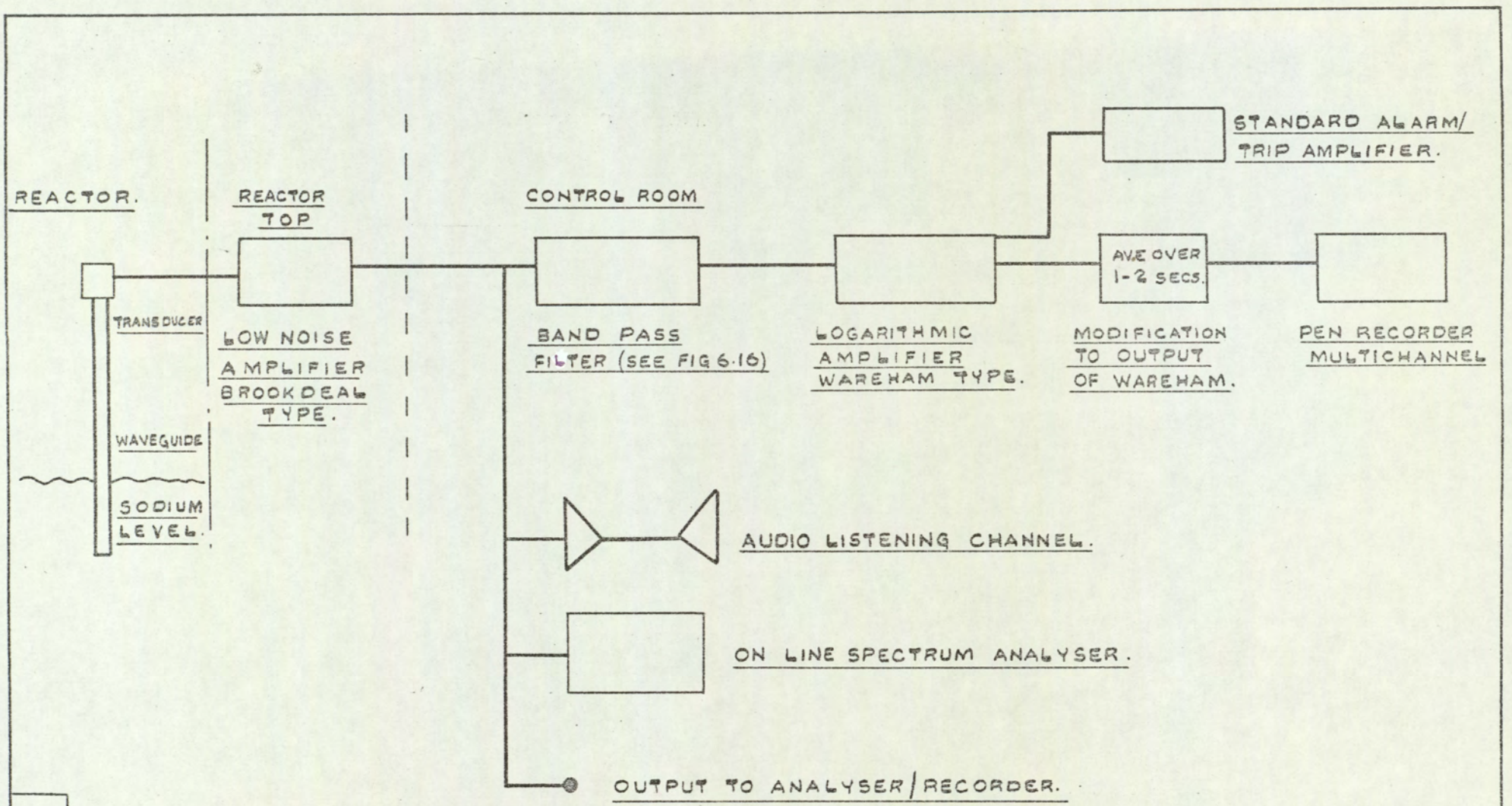

FIG. 6.15.

FIG. 6.15. SIMPLIFIED BLOCK DIAGRAM OF AN ACOUSTIC DETECTION CHANNEL.

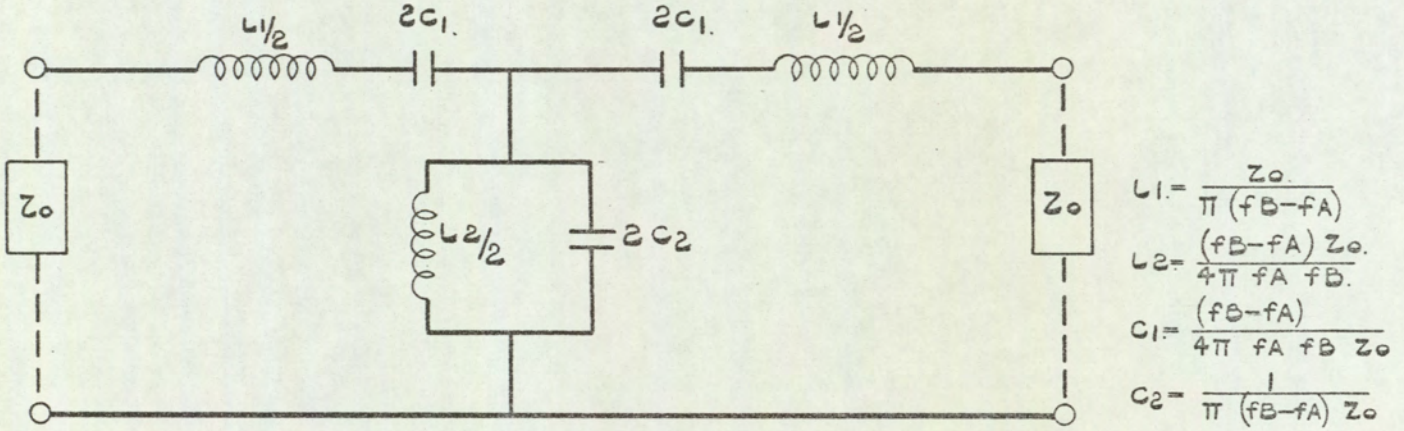

fA AND fB ARE CUT OFF FREQUENCIES OF THE PASS BAND AND. Zo IS THE LOAD IMPEDANCE.

FIG 6·16 DETAIL OF BAND PASS FILTER USED IN THE D.F.R. ACOUSTIC SYSTEM

FIG 6·16

CHAPTER 7

SOME INITIAL OPERATING EXPERIENCE WITH THE PROTOTYPE INSTRUMENTATION SYSTEM IN THE DOUNREAY FAST REACTOR

7.1 General

As the Dounreay Fast Reactor is now largely operating as a material test reactor it has installed at any one time a large number of experimental fuel element assemblies. Some of these fuel assemblies are deliberately designed to be capable of being operated up to the failure point of the assembly. The failure of these elements is safely contained and presents but a small operational inconvenience when failure takes place. Their existance in D.F.R. does however provide a unique oportunity to test out the installed acoustic detection equipment to see if the fuel element failure can be detected by the waveguide installation.

Two such elements have failed in recent months and the results of analysis of the acoustic records is presented in the following sections.

7.2 Results from the Installation under Normal Conditions

Acoustic frequency spectra have been taken every day over the last few months from each of the installed waveguides. Typical results are shown in Fig. 7.1 and show that the acoustic noise is essentially stationary. These records provide a reference against which suspected maloperation records may be compared. Judged from the consistancy of these records a deviation of about 5 dB can be thought to be significant. The actual alarm level corresponds to a deviation of 30 dB.

7.3 Results from the Installation under Fault Conditions

Two recent non crucial failures of experimental elements in D.F.R. have given very useful demonstrations of the viability of the acoustic detection installation.

The first failure gave indications which lasted from 3rd October, 1968 to 1st November, 1968. The second one gave similar indications between 26th February, 1969 and 17th March, 1969. In both cases by comparing the magnitudes of the relative signals from the three waveguides

and examining the loading plan in the reactor for the position of highly rated high burn-up experimental elements the position of the suspected failures was inferred. (7.1) and (7.2).

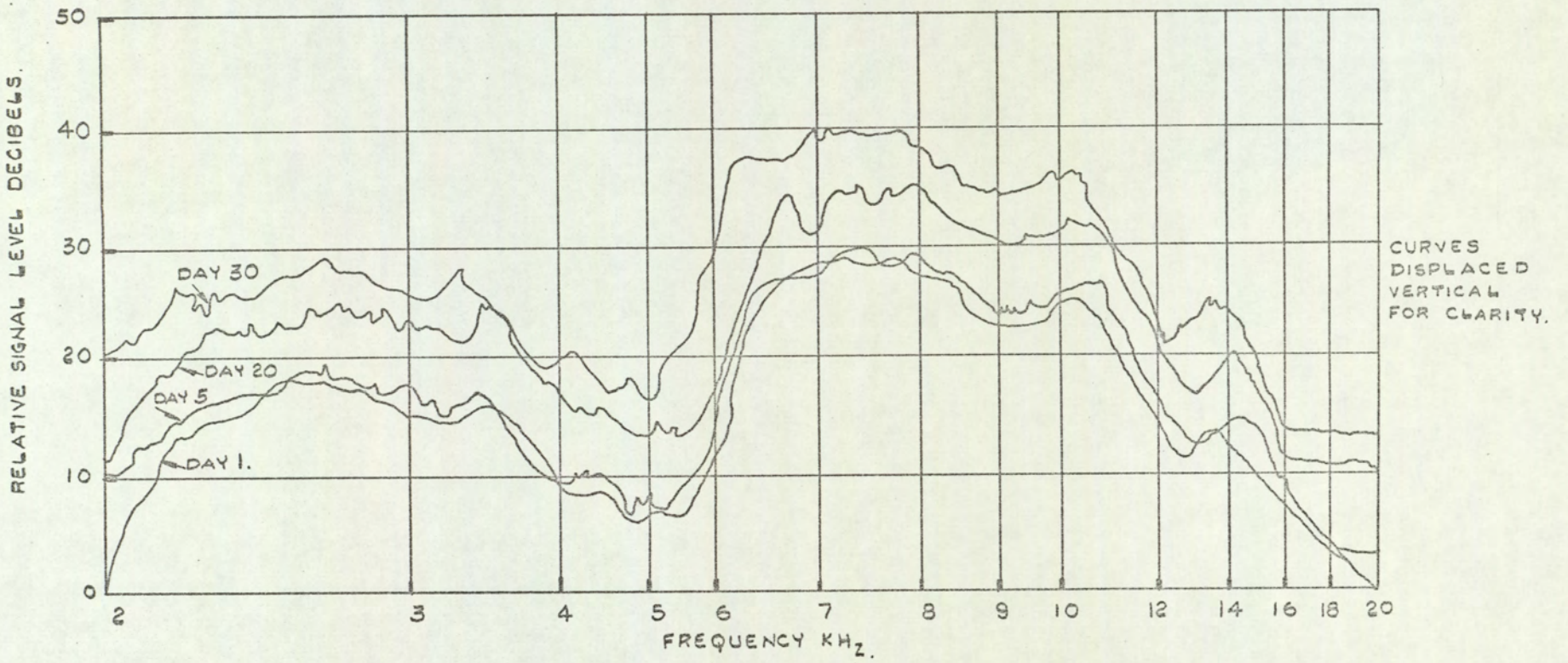

FIG 7·1. TYPICAL FREQUENCY SPECTRA FROM WAVEGUIDES IN D.F.R. SHOWING STATIONARY NATURE OF THE SIGNAL.

FIG. 7·1.

CHAPTER 8

GENERAL CONCLUSIONS

This thesis shows the necessity of drawing together many different scientific and technological disciplines in order to solve a complex problem.

The object of the study detailed in this thesis was to examine the problems involved in detecting local overheating in liquid metal cooled fast neutron reactors. Following a discussion of the underlying fluid mechanical phenomena in liquid coolants and the central problem of detecting local overheating, exploratory studies were conducted on suitable transducers for use in nuclear environments. A series of experiments using static and flowing sodium were carried out culminating in an experiment using an electrical heater in the D.F.R. to simulate a fault condition near the reactor core.

Detailed conclusions have been drawn and are discussed in the body of the thesis under the relevant sections, mainly chapter 5 and chapter 7. It is possible to draw from this work the general conclusion that the detection of local overheating in a nuclear reactor may be possible using the transducers and techniques discussed in this thesis. The limit of detection being set by the background noise existing in the environment in which the detection of fault condition is required. The electro-mechanically pumped D.F.R. system produces relatively little hydrodynamic noise compared to a mechanically pumped system and detection of local boiling in this case has been shown to be possible.

The limit of detection in any particular application, is best arrived at by an in situ calibration of the type discussed in this thesis.

REFERENCES

1.1 Dietrich, J. R. "Efficient Utilisation of Nuclear Fuels" Power Reactor Technology Vol.6 No. 4. 1963

1.2 Fuchs, K. E. "The Promise of Nuclear Power" Kernenergie, June/July 1964.

1.3 Iliffe, C. E. "Economics of Plutonium Breeding etc." TRG Report 1207(R) (Unclassified). July 1966

1.4 Frame, A. G. Matthews R.R. "Fast Breeders on the Line by 1971" Nucleonics September 1966.

2.1 Barclay, F. J. Ledwidge T.J. Cornfield G.C. "On the Velocity of Sound through Two Phase Mixture and the Relation to Critical Flow" To be published at I. Mech. E. Symposium on Two Phase Flow, September 1969.

2.2 Lions, N. "Detection Des Gaz Entraines Dans Le Sodium Aux Surfaces Libres". Paper 85/5. Symposium on Alkali Metals etc. Vienna 28th November - 2nd December 1966.

2.3 Karplus, H. B. "The Propagation of Sound Waves in a Mixture of Water and Steam". Armour Research Foundation 4132-12 January 1961.

2.4 Claxton, K. J. "The Influence of Radiation on the Inception of Boiling Liquid Sodium" A.E.R.E. Harwell Report R 5308. Jan. 1967

3.1 Corrsin, S. "On the Spectrum of Isotropic Temperature Fluctuations in an Isotropic Turbulance" J. Appl. Phys. 22, 469-473 (1951).

3.2 Bachelor, G. K. "Small Scale Variations of Convected Quantities like Temperature in Turbulent Fluid, Part I" J. Fluid Mech. 5, 113-133 (1959).

3.3 Bachelor, G. K. Howells, I. D. Townsend, A. A. "Small Scale Variations of Convected Quantities like Temperature in Turbulent Fluid, Part II" J. Fluid Mech. 5, 134-139 (1959).

3.4 Tanomoto, S. Hanratty, T. J. "Fluid Temperature Fluctuations Accompanying Heat Transfer in a Pipe" Chemical Eng. Sc. 18, 307-311 (1963).

3.5 Rust, J. H. Sesonske, A. "Turbulent Temperature Fluctuations in Mercury and Ethylene Glycolin Pipe Flow" Int. J. Heat Moss Transfer 9, 215-227 (1966).

3.6 Babov, V. P. Ibragimov M. Kh. Subbottin, V. I. "Time Characteristics and Temperature Pulsation Spectrum in the Turbulent Flow of a liquid in a Tube" Teplofiziba Vysokibh Temperature 6, No.1 99-109 (1968).

3.7 Minneart, M. "On Musical Air Bubbles and the Sound of Running Water" Phil. Mag. Vol. 16, No. 7 p.235 (1933).

3.8 Strasberg, M. "Gas Bubbles as Sources of Sound in Liquids" Jour. Acoustical Soc. of America Vol. 28 No. 1 January 1965.

3.9 Dickson, A. N. Silver, R. S. "The Flow of Flashing Water in Conduits" Second European Symposium on Fresh Water from the Sea, May 1967, Athens, Greece, European Federation of Chemical Engineering.

3.10 Din-Yu HSIEH "Some Analytical Aspects of Bubble Dynamics" Transactions of the A.S.M.E. Basic Engineering, Vol. 87 Series D, No. 4. Dec. 1965

3.11 Zwick, S. A. Plesset, M. S. "Note on the Dynamics of Small Vapour Bubbles in Liquids" Calif. Inst. Tech., Hydrodynamics Laboratory. Report No. 26-7, February 1954.

3.12 Ivany, R. D. Hammitt, F. G. "Cavitation Bubble Collapse in Viscous, Compressible Liquids - Numerical Analysis" Transactions of the A.S.M.E. Basic Engineering,

Vol. 87, Series D, No. 4. Dec. 1965

3.13 Florschuety, L. W., Chao. "On the Mechanics of Vapour Bubble Collapse" Report No. ME-TN-106.9-2, Department of Mech. and Indus. Eng., University of Illinois, 1963.

3.14 Ivany, R. D. Hammitt, F. G. Mitchell, T. M. "Cavitation Bubble Collapse Observations in a Venturi," Transactions of the A.S.M.E. Basic Engineering, Vol. 88 Series D, No. 3. Sept. 1966

3.16 Plesset, M. S. Zwick, S. A. "A Non-Steady Heat Diffusion Problem with Spherical Symmetry" Journal of Applied Physics, Vol. 23, 1952.

3.17 Rice, S. O. "Selected Papers on Noise and Stochastic Processes" Dover Publications, Inc., New York 1954.

3.18 Lord Rayleigh "On the Pressure Developed in a Liquid during the Collapse of a Spherical Cavity" Phil. Mag. Vol. 34 P. 94. 1917.

4.1 Hughes G. Thesis. "A high Temperature Transducer for the Detection of rapid temperature transients in Liquid Metals. MSc Thesis, University of Aston in Birmingham. October, 1967.

4.2 Hughes G. Patent. "Patent Application No. 58871/69".

4.3 Ledwidge T.J. Hughes G. I.E.E. Paper "Transducers for the measurement of temperature noise, acoustic noise and gas density in nuclear environments". Joint I.E.E./I.E.R.E. Symposium on Automation Techniques in Industry April, 1968.

6.1 Bendat et al. "The Application of Statistics to the Flight Vehicle Vibration Problem". A.S.D. Technical Report 61-123, Offices of Technical Services, U.S. Dept of Commerce, Washington 25 D.C.

3.15. BARCLAY R J LEDWIDGE T.J CORNFIELD G.C, Contribution to discussion on CAVITATION. Proc I, Mech. E, Jan 1969,

In addition to 3.17 and 6.1 other useful references on the theory of random signals are:-

Blackman & Tukey — "The Measurement of Power Spectra". Bell System Technical Journal, 1958.

Davenport & Roat — "An Introduction to the Theory of Random Signals and Noise". McCraw Hill 1958.

Crandall (Ed) — "Random Vibration". Wiley 1958.

Bendat, J.S. — "Principles and Applications of Random Noise Theory." Wiley, 1958.

7.1 Ledwidge T.J. Hale J.C. — "Analysis of the Acoustic Signals from D.F.R. 3rd October to 1st November, 1968. Internal Report.

7.2 Ledwidge T.J. Hale J.C. — "An Analysis of the acoustic signals from D.F.R. 26th February to 17th March, 1969. Internal Report.

NOMENCLATURE

θ	Temperature
θw	Wall temperature
θ_{sat}	Saturation temperature
r	Bubble radius
λ	Latent heat of vapourisation: Ratio of capacitances: Delay time
G	Universal gas constant
P	Pressure
Pa	Partial pressure due to a gas
σ	Surface tension. Standard deviation
f	Frequency
Re	Reynolds number
Pr	Prandtl number
γ	Ratio of specific heats of a gas: Pulse repetition rate
ρ	Density
R	Radius co-ordinate
t	Time: Thickness of gas gap in transducer
Pv	Vapour pressure
Po	Reference pressure
$\underline{E}$	Electrostatic field: Output voltage: Youngs modulus
ϕ	Electrostatic potential: Heat flux
k	Dielectric constant
τ	Thickness of transducer shell
C	Capacitance
V	Voltage
d	Diameter of transducer
ϵ	Thickness of aluminium oxide on transducer
T	Integration time
ω	Angular frequency
B	Bandwidth

APPENDIX I

Theory of the Operation of the Under-Sodium Microphone

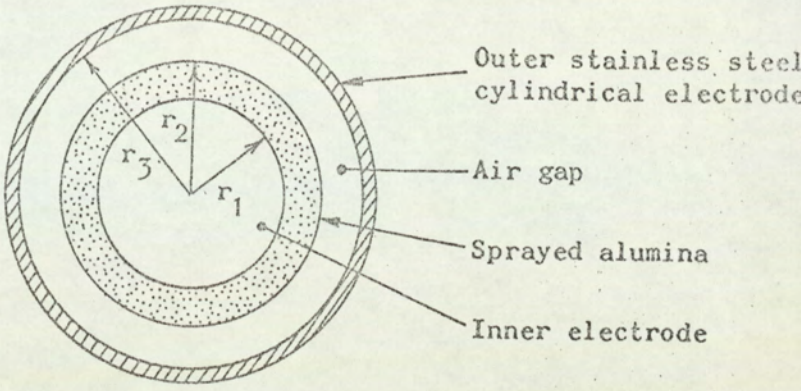

Fig. 4.2

Diagram of the geometry

The transducer is, in effect, a concentric capacitor of composite dielectric; the capacitance can be calculated from

$$\underline{E} = -\nabla\phi$$

where $\underline{E}$ is the electrostatic field and ϕ is the potential.

As, in this case, the field is purely radial

$$\underline{E} = -\frac{\partial\phi}{\partial r} . \qquad \ldots\ldots\ldots\ldots\ldots\ldots (1)$$

From Gauss' divergence theorem we have:

$$\int_{\text{surface}} k\underline{E} \cdot \underline{ds} = 4\pi q$$

where q is the included charge and k the dielectric constant.

Applying this to a general cylinder between r_1 and r_3 we have

$$k\underline{E} \cdot 2\pi r = 4\pi q \qquad \ldots\ldots\ldots\ldots\ldots\ldots (2)$$

therefore

$$\underline{E} = \frac{2q}{kr} .$$

Substituting in equation (1) we have $\frac{2q}{kr} = -\frac{\partial\phi}{\partial r}$

$$\text{or} \quad \frac{2q}{k}\int\frac{dr}{r} = -\int d\phi \;\ldots (3)$$

Solving equation (3) from $r_1 \leq r \leq r_2$

and $r_2 \leq r \leq r_3$

we have

$$\frac{2q}{k_1} \log \frac{r_2}{r_1} = -(\phi_2 - \phi_1) \quad \ldots\ldots\ldots\ldots\ldots\ldots\ldots \quad (4)$$

where k_1 is the dielectric constant for $r_1 \leq r \leq r_2$

and

$$\frac{2q}{k_2} \log \frac{r_3}{r_2} = -(\phi_3 - \phi_2) \quad \ldots\ldots\ldots\ldots\ldots\ldots\ldots \quad (5)$$

where k_2 is the dielectric constant for $r_2 \leq r \leq r_3$.

Adding equations (4) and (5) gives

$$2q \left[\frac{1}{k_1} \log \frac{r_2}{r_1} + \frac{1}{k_2} \log \frac{r_3}{r_2} \right] = -(\phi_3 - \phi_1) = V \quad ..(6)$$

where V is the potential difference between the inner and outer electrodes.

Now with $q = VC$ and in this case we have

$$C = \frac{1}{2 \left[\frac{1}{k_1} \log \frac{r_2}{r_1} + \frac{1}{k_2} \log \frac{r_3}{r_2} \right]} \quad \ldots\ldots\ldots \quad (7)$$

where C is the capacitance.

The only variable due to pressure changes is the radius of the outer cylinder, r_3, and, if $r_3/r_2 \simeq 1.0$ we can write

$$r_3 = r_2 + t$$

where t is the small air gap.

By Maclaurin's theorem

$$\log \frac{r_3}{r_2} = \log \left(1 + \frac{t}{r_2} \right) \simeq \frac{t}{r_2}$$

therefore

$$C = \frac{1}{2 \left[\frac{1}{k_1} \log \frac{r_2}{r_1} + \frac{1}{k_2} \frac{t}{r_2} \right]}$$

where the variable is now t. Therefore

$$\frac{dC}{dt} = -\frac{1}{2\left[\frac{1}{k_1}\log\frac{r_2}{r_1} + \frac{1}{k_2}\frac{t}{r_2}\right]^2}\ \frac{1}{k_2 r_2}$$

i.e.
$$\frac{dC}{C} = \frac{dt}{k_2 r_2\left[\frac{1}{k_1}\log\frac{r_2}{r_1} + \frac{t}{k_2 r_2}\right]} \quad \ldots\ldots\ldots\ldots\ldots (8)$$

Now dt is [illegible] related to the hoop stress by the relations:

(a) $\text{stress} = \frac{Pd}{2\tau}$

where d is the outside diameter of the transducer and τ is the shell thickness.

(b) $\text{strain} = \frac{\delta r_3}{r_3} = \frac{\text{stress}}{E} = \frac{Pd}{2\tau E}$.

But $\delta r_3 = \delta t$ therefore

$$\delta t = \frac{Pdr_3}{2E\tau} \simeq \frac{Pd^2}{4E\tau} \quad \ldots\ldots\ldots\ldots\ldots\ldots\ldots\ldots (9)$$

and by substituting in equation (8) we have

$$\frac{dC}{C} = \frac{Pd^2}{4E\tau\left[\frac{1}{k_1}\log\frac{r_2}{r_1} + \frac{t}{k_2 r_2}\right]k_2 r_2} \quad \ldots\ldots\ldots\ldots (10)$$

Putting $r_2 = r_1 + \epsilon$ then equation (10) simplifies to

$$\frac{dC}{C} = \frac{Pd^2}{4E\tau\left(t + \frac{\epsilon}{k_1}\ k_2\right)} . \quad \ldots\ldots\ldots\ldots\ldots\ldots (11)$$

If the transducer is now "shunted" using a cable of capacitance C_c then the percentage change in C is reduced to

$$\frac{dC}{C} = \frac{1}{(1+\lambda)}\ \frac{Pd^2}{4E\tau\left(t + \frac{k_2\epsilon}{k_1}\right)} \quad \ldots\ldots\ldots\ldots\ldots (12)$$

where $\lambda = \frac{\text{cable capacitance}}{\text{transducer capacitance}}$.

If the transducer-cable circuit is now made one arm of an a.c. bridge energised with V volts r.m.s. the output signal is given by

$$E_s = \frac{1}{4}\ \frac{dC}{C}\ V.$$

In this case

$$E_s = \frac{1}{4} \frac{Pd^2V}{(1+\lambda)4E\tau\left(t + \frac{k_2\epsilon}{k_1}\right)} \quad \ldots\ldots\ldots\ldots (13)$$

Equation (13) dictates the operation of the bridge output which is linearly related to pressure when the other variables have been fixed. Strictly speaking E_s is a function of P and t but the change in P is very great compared with the change in t and thus E_s can be thought of as being a function of pressure only.

We will now examine equation (13) with practical values in mind to determine the minimum value of d for any pressure range. The assumptions made are:

Minimum value of t obtainable = 0.002 in.

Minimum value of ϵ obtainable = 0.010 in.

Minimum value of τ obtainable = 0.010 in.

k_2 = 1.0

k_1 5.0

E = 30×10^6 lb/in^2

Minimum ratio workable $(E_s/V)_{min}$ = 10^{-4}

We can now write the "optimised" equation (13) as

$$10^{-4} = \frac{P(d^2_{min})}{4(1+\lambda)4 \times 30 \times 10^6 (2 + \frac{10}{5}) \times 10^{-3} \times 10 \times 10^{-3}}$$

which reduces to

$$P(d^2_{min}) = 1.925(1+\lambda)$$

or

$$d_{min} \simeq \left[\frac{2(1+\lambda)}{P}\right]^{\frac{1}{2}} \quad \ldots\ldots\ldots\ldots\ldots\ldots (14)$$

It should be noted, however, that the larger the diameter of the transducer, the greater the capacitance per unit length; the value of λ therefore decreases for a given cable run.

Equation (14) will, however, serve to give a rough guide to the principal dimensions.

APPENDIX II

Approximate analysis of the natural frequency of a thin walled cylinder vibrating in the radial mode

Assume that the radius of the cylinder is increased from a to a + x; the circumferential strain is then x/a and the circumferential stress Ex/a for a thin cylinder.

The equivalent increase in pressure to produce this stress is given by

$$\frac{Pa}{\tau} = \frac{Ex}{a}$$

therefore

$$P = \frac{Ex\tau}{a^2} \quad \ldots\ldots\ldots\ldots\ldots\ldots\ldots\ldots\ldots\ldots \quad (15)$$

Consider an arc of length η ; then the mass is given by

$$M = \frac{\eta l \tau \rho}{g}$$

and the restoring force on the element is

$$- P\eta l .$$

The equation of motion is

$$P\eta l = \frac{-\eta l \tau \rho}{g} \cdot \frac{d^2x}{dt^2}$$

giving

$$\frac{d^2x}{dt^2} + \frac{Pg}{\rho\tau} = 0 . \quad \ldots\ldots\ldots\ldots\ldots\ldots\ldots\ldots \quad (16)$$

Substituting for P from equation (15) we have

$$\frac{d^2x}{dt^2} + \frac{Eg}{a^2\rho} x = 0 , \quad \ldots\ldots\ldots\ldots\ldots\ldots \quad (17)$$

i.e. the simple harmonic motion with a frequency of

$$\frac{1}{2\pi a} \left(\frac{Eg}{\rho}\right)^{\frac{1}{2}} .$$